SYNCHROTRON BASED INFRARED MICROSPECTROSCOPY OF CARBONACEOUS CHONDRITES

by

MEHMET YESILTAS
B.S. Ondokuzmayis University, 2007
M.S. Florida State University, 2011

A dissertation submitted in partial fulfillments of the requirements
for the degree of Doctor of Philosophy
in the Department of Physics
in the College of Sciences
at the University of Central Florida
Orlando, Florida

Spring Term
2015

Major Professor; Robert E. Peale

ABSTRACT

Relationships between organic molecules and inorganic minerals are investigated in five carbonaceous chondrites, Northwest Africa 852 (CR2), Tagish Lake (C2-ungroupped), Orgueil (CI1), Sutter's Mill (CM), and Murchison (CM2), with micron spatial resolution using synchrotron-based imaging micro-FTIR spectroscopy. Correlations based on absorption strength for various constituents are determined using statistical correlation analysis. Silicate band is found to be positively correlated with stretching modes of aliphatic hydrocarbons in NWA 852 and Tagish Lake. The former is highly correlated with the hydration band in all meteorites. Negative correlation is observed between water+organics and carbonate bands in all meteorites. Two dimensional infrared maps for NWA 852 and Orgueil show that carbonates are spatially separated from water+organic combination, silicates, OH, and CH distributions. Overlapping of the latter three in NWA 852 and Tagish Lake suggests a possible catalytic role of phyllosilicates in the formation of organics. Additionally, spectroscopic analyses on Sutter's Mill meteorite fragments present multiple distinct mineralogies. Spatial and spectral evidences on this regolith breccia suggest mixing of multiple parent bodies. Ratios of asymmetric CH_2 and CH_3 band strengths for NWA 852, Tagish Lake, and Sutter's Mill are similar to the average ratio of interplanetary dust particles and Wild 2 cometary dust particles, however significantly exceeds that of interstellar medium objects and several aqueously altered carbonaceous chondrites such as Orgueil. This suggests distinct formation regions and/or parent body processing of organics for these meteorites. Our infrared spectro-microtomography measurements on Murchison meteorite, representing the first such measurement on any kind of meteorite, comprise of three-dimensional reconstructions of specific molecular functional groups for understanding the spatial distributions of these groups.

to my mother and grandmother, who valued education above all

TABLE OF CONTENTS

LIST OF FIGURES

LIST OF TABLES

CHAPTER ONE: GENERAL INTRODUCTION

1.1 Meteorites

Meteorites are extraterrestrial samples of the solar system. The great majority of them originate from asteroids. A small fraction comes from comets, Mars, and the Moon. Carbonaceous chondrites are the most primitive meteorites and are probably fragments of either primitive asteroids or comets [1]. Their uniqueness is that they still contain and carry records and signatures of prebiotic chemistry as well as processes occurred during the early solar system [2]. Some carbonaceous chondrites are aqueously altered to a greater or lesser extent (petrologic types 1 and 2, respectively), while others are thermally metamorphosed (types 3 to 6). Nevertheless, they still carry records of presolar materials as well as solar nebula and post-accretional processes. Carbonaceous chondrites are rich in carbon (C), some proportion of which is organic C and the rest is inorganic. This group of meteorites contain up to ~6 wt% C [5], and higher concentrations and varieties of organic molecules than other meteorite types [4].

1.2 Organics

Compositions of carbonaceous chondrites are highly C-rich. Organic carbon content of CI, CM, and CR chondrites amounts to at least ~4 wt% [3]. Organic molecules consist of carbon atoms in rings or long chains, where other atoms (e.g. hydrogen, oxygen, and nitrogen) are attached. Examples include hydrocarbons, polymers, amino acids, aliphatic-, aromatic-, and alicyclic- compounds. The synthesis and provenance of organic molecules are highly relevant to the question of how life arose on Earth. In some cases organic matter of interstellar origin

survived processing and remained intact within meteorite parent bodies [6]. Some species may arise during alterations [7, 8], for example, melting of ices would hydrate simple organic molecules, producing organic compounds of higher complexity. Delivery of these prebiotic organic compounds may have contributed to the origin of life on early Earth [9-15]. Understanding how organic compounds are formed in extraterrestrial matter is therefore important to the question of how life arose on Earth [16]. Relationships between organic matter and mineral species may provide clues to such formation. However, little is known about the spatial distribution and mineralogical relationships of organics in meteorites.

Many species of organic molecules have been identified in interstellar and circumstellar regions in gas phase or condensed on dust, e.g. poly-aromatic hydrocarbons (PAH). Most of the molecules containing more than 4 atoms in such regions include carbon. Simple organic molecules may be formed in dense interstellar clouds directly via gas phase homogeneous reactions. It was suggested that organic molecules in space may form through catalytic reactions on dust grains [17]. In addition, much carbon is found on cosmic dust grains [18], and dust may be considered as a chemical catalyst [19, 20]. Icy mantles form on dust particles by accretion and reaction with the surrounding gas. At the typical 10 K temperatures of interstellar clouds, atoms H, C, O, and N are mobile on grain surfaces and may find reaction partners. Formation of small molecules is aided by the exothermic nature of the required reactions and the absence of formation barriers for those molecules. Abundant CO_2 ice forms on grain surfaces by oxidation of CO, whereas gas-phase CO_2 is rare. Observation of OCN spectra in interstellar regions indicate that acid-base reactions occur on dust grains. Due to reaction barriers, formation of larger molecules, e.g. CH_3OH, requires reaction pathways that must be assisted by UV, cosmic

rays, or elevated temperatures. Such complex and energetic chemistry is clearly possible on dust grains in the interstellar environment.

Collapse of molecular clouds to form stars and protoplanets processed meteorite source material by aqueous alteration, thermal metamorphism, and energetic impacts. Such processing may have combined simple organics into complex ones [21], thus organic species found in meteorites record reactions that occurred in a variety of distinct environments [22]. Aqueous alteration forms second-generation complex organics such as amino acids. For instance, presence of SiC grains in carbonaceous chondrites, and absence in the ISM emphasizes the importance of processing. In addition, PAHs are synthesized by non-aqueous high temperature processes [23], such as combustion.

For a given number of carbon atoms, there is complete structural diversity among classes of organics found in meteorites. Abundance of organics with different numbers of carbon atoms is determined according to growth by addition of individual carbon atoms. This is consistent with formation on cold dust-grain surfaces, where the mobility of atoms is due to tunneling between stable surface sites.

1.3 Mineral – organic connection

Understanding the chemical interaction of organic molecules with minerals in extraterrestrial materials is very important for understanding the origin of life on Earth [24]. Main processes responsible for the formation of organic molecules are Miller-Urey (MUT) type and Fisher-Tropsch (FT) type reactions [25]. The former makes use of energy in the form of UV

and/or electric discharges for reactions, while the latter uses host surfaces (e.g., phyllosilicate surface) for catalytic reactions to concentrate organic molecules. Both of these reaction types are responsible for specific meteoritic compounds. For instance, majority of organic hydrocarbons (aliphatic and aromatic) found in meteorites have been formed through FT type reactions, whereas MU type reactions are responsible for most of the amino acids however fail to produce hydrocarbons [26, and references therein]. Additionally, solar nebula had conditions that are appropriate for FT type reactions but not for MU type reactions [26].

Host surfaces are necessary in FT type reactions for the production of organic matter [10]. Minerals are suggested as providers of the host surfaces [16, 27, 28]. Clay minerals have been experimentally shown to be successful catalysts for FT type reactions [29, 30]. Indeed, among the natural catalysts in the solar nebula is phyllosilicates [26]. On the other hand, the nature and characteristics of mineral surfaces affect reaction rates, so that particular organic molecules may preferentially concentrate on particular mineral surfaces. In other words, selective formation of organics occurs on specific mineral types depending on such mineral surfaces. Therefore, a genetic link between organic matter and mineral products of aqueous alteration such as phyllosilicates is highly possible. Indeed, those carbonaceous chondrites with abundant aqueous alteration product minerals such as CI and CM chondrites have the most organic matter [28]. Although there are laboratory evidences on the relationships between organic matter and mineral species, it has been only poorly understood or indirectly shown for meteorites [2, 28]. Complex organic synthesis has been linked with minerals [16, 28], but the actual types and phases involved are still in question.

Several evidences indicate partial segregation of organic matter among specific minerals in heterogeneous meteorites. The degree to which specific organics can be concentrated by specific minerals depends on factors such as cationic exchange capability, ion-dipole and coordination interactions, hydrogen bonding, and physical forces such as Van der Waals forces [16, 31]. In this context, clays are best candidates and examples for absorbing organic molecules where organic cations replace inorganic cations, thus forming organic-clays [2]. Carbon chains are found to be longer when clays are present during the synthesis of organics in chemical reactions in laboratory experiments [32]. Kaolinite was found to be more effective catalyst than montmorillonite for the production of organic polymers from organic-kaolinite mixtures [33]. Indeed, [34] pointed out the importance of clay minerals in condensation reactions, and they showed that certain organics form in the presence of kaolinite, but not in its absence. Organic C has been found in discreet grains in primitive type 3 carbonaceous chondrites, and chemically altered organics were found suspended in fluid veins of moderately altered meteorites [35]. Carbon of unknown chemical form has been identified preferentially at the surface of metal and troilite grains in ordinary chondrites [36, 37].

Phyllosilicates are hydrated layered silicates produced by the interaction of liquid water and rock-forming minerals. Clays are especially important type of phyllosilicates. Organics may be bound within the layers of clay minerals, increasing the effective surface area for catalyzing the formation of primitive biopolymers [16], and protecting them from destruction by later processing [2, 38]. [39] reported that clay minerals are highly capable of absorbing organic molecules by exchanging cations between organic and inorganic compounds. Adsorption and retention of organics by clay minerals has been studied by several groups [e.g., 16, 27, 28, 40,

41, 42]. Indeed, organics and clay minerals are found together within the chondrule rims in Murchison [28]. [43] experimentally showed that organic molecules were not only synthesized by clay minerals such as smectite and montrmorillonite, but also protected from destructive events. [2] showed that clay minerals in CI chondrites and Tagish Lake meteorite played a catalytic role for the production of meteoritic organic molecules, and additionally protected organic C in Tagish Lake from oxidizing conditions. To date, no correlation between organic matter and sulfide minerals or metals has been found.

During early biological evolution, mineral surfaces played the role of gathering organic compounds [10], but whether specific minerals adsorb only certain types of molecules remains unknown. However there does exist some evidence to support the hypothesis of partial differentiation of organics among specific minerals in heterogeneous meteorites. Very little is known about the spatial distribution and mineralogical relationships of organics in meteorites. Any relationships between minerals and organics should be known to understand the evolution of organic material in early solar system.

1.4 Work in this dissertation

As discussed above, there are evidences to suggest that certain minerals may be associated with, and play a role in the formation of specific organic molecules. Though, conditions in space differ from those in the laboratory, such relationships seem likely in heterogeneous meteorites, for which mineral-organic correlations have been very little investigated to date. Knowing whether the organics exist as separate blobs or coat pre-existing mineral grains, and whether specific organics associate with specific kinds of minerals can

provide clues about which came first and could tell us if the mineral grains played a role in the formation of the organics [Scott Sandford, private communication]. A little work is being done in this area, yet it takes highly advanced analytical instrumentation since we need to search for the organics *in situ* on micron and submicron scales. The experimental approach employed for this work has this unique capability to spectrally interrogate large areas at micron spatial resolution to identify and locate organic molecules simultaneously within the local mineralogy of the sample.

Organic molecules and minerals have characteristic vibrational absorption bands in the mid-infrared between 3 and 15 μm wavelengths, which is an important region for remote characterization of cosmic dust and meteorite source objects [e.g., 44, 45], where interpretation is facilitated by laboratory measurements on both pure phases and heterogeneous meteorites [46]. For the work presented in this dissertation, large amount of spectroscopic data have been acquired from meteorites *in situ* with high spatial resolution. Chapter 2 describes these meteorite samples as well as experimental techniques employed for this research. Chapter 3, 4, and 5 present results for organic – mineral correlations in Northwest Africa 852, Tagish Lake, and Orgueil meteorite grains, respectively. Chapter 6 presents micro-infrared and micro-Raman spectroscopic results of multiple Sutter's Mill meteorite grains, and discusses origin of this meteorite as well as parent body processes. Finally, chapter 7 presents an application of a new experimental technique to meteorites: three-dimensional infrared spectro-microtomography measurements on Murchison.

CHAPTER TWO: SAMPLES AND EXPERIMENTAL DETAILS

2.1 Meteorite samples

Meteorite samples studied in this dissertation are five carbonaceous chondrites, Northwest Africa 852 (CR2), Tagish Lake (C2 ungroupped), Orgueil (CI1), Sutter's Mill (C ungroupped), and Murchison (CM2). All of these meteorites experienced different types of processing at varying degrees on their respective parent bodies, which is evident from their infrared and Raman spectra.

Chips of these samples were ground down to ~10 – 30 micron sized powders with an agate mortar and pestle set. Subsequently, a sparse layer of non-overlapping grains were placed on a diamond window for micro-FTIR transmittance spectroscopy, and on a silicon substrate for micro-Raman measurements. Spectra of individual grains were collected after regions of interest were defined under the optical microscope.

Contamination can affect meteorites and change their spectra [e.g., 56]. It was reported by [57] that storing meteorite samples in containers which include silicone rubber, silicone grease, or adhesive tape contaminated the samples within very short times with volatile organics. These contaminations usually give rise to C-H stretching features between 2800 – 3000 cm^{-1}, which makes the identification of indigenous C-H stretching features difficult. We note that meteorite samples studied here are free of any contamination. After grinding, we stored our meteorite samples in a weighing paper, which is water and air resistant, and no evidence of contamination was observed. In particular, several phyllosilicate-rich carbonaceous chondrites were stored in this way, and their infrared spectra show no C-H stretching features in the region 2800 – 3000 cm^{-1}. Therefore, we conclude that our sample preparation protocol is

contamination-free, and the organic matter observed in our experiments is indigenous to the meteorite samples. Terrestrial weathering might affect infrared spectra of meteorites. For instance, as a result of terrestrial weathering, oxidation may occur in iron-rich meteorites, however iron-oxides have absorption features in the visible region, therefore does not affect our investigations. Additionally, terrestrial weathering seems to have little or no effect on bulk C content of meteorites [58]. NWA 852 itself has experienced very little terrestrial weathering and is classified as weathering grade W1 [1]. Murchison has weathering grade of W1-2. Other samples' weathering grade is currently unknown.

FTIR microspectroscopy and micro-Raman spectroscopy have been considered as nondestructive techniques for *in situ* investigation of meteorite samples [59, 60]. Infrared transmittance spectroscopy requires thin specimens, so that the beam traverses only a few microns of matter to avoid saturating the strongest bands. This is most conveniently achieved by crushing the sample to obtain individual grains. This crushing process does not alter the samples, chemically or physically. Some of the petrographic context may be lost as a result of crushing the sample, i.e. information on chemical and mineral distributions over lengths scales of several mm may be lost. However, we retain it on lengths scales of ~10 microns, and we can preserve it over length scales of several mm by crushing different samples from different portions of the parent meteorite. In fact, not only the two spectroscopy techniques are useful and practical for the investigation of chemical compositions of meteorite samples at a micron and submicron scale, they have significant advantage over other techniques such as chromatography, combustion, TEM, SIMS and ICPMS, all of which alter the chemical composition of samples and are considered to be destructive [e.g., 60].

2.2 Micro-Raman spectroscopy

Microscopic analysis and examination of materials such as minerals and polymers via their vibrational modes were performed as a complementary study by micro-Raman spectroscopy. Micro-Raman spectra of meteorite samples were collected *in situ* at the Material Characterization Facility of University of Central Florida with Renishaw RM 1000 micro-Raman spectrometer coupled to a Leica DMLM microscope, a CCD detector, and Ar ion CW laser excitation at 514.5 nm wavelength. Total laser power of 20 mW was focused to a 4 μm^2 spot, so that the intensity on the sample was 5 $mW/\mu m^2$. Experimental setup is shown in Figure 1. For data collection, small amount of meteorite powders were placed on a silicon substrate, then the substrate was placed under the microscope. A 50X objective was used for collecting spectrum after meteorite grains were located on the substrate using a 5X objective. The spectrometer was calibrated using a silicon substrate with a well characterized Raman band at 521 cm^{-1}. All grains were measured 3 times with an integration time of 30 seconds between 800 – 2200 cm^{-1}.

Figure 1**:** Micro-Raman spectrometer at Material Characterization Facility of UCF (left) and meteorite powder on a silicon substrate (right) for measurements.

2.3 Synchrotron-based FTIR microspectroscopy

Fourier transform infrared (FTIR) microspectroscopy is an analytical technique for *in situ* identification of organic and inorganic functional groups within samples. Each absorption band in a spectrum corresponds to specific vibrational mode of a molecule, which is used for compositional identification. Especially mid-infrared region of the electromagnetic spectrum, 4000-800 cm^{-1}, provides helpful information through infrared absorption bands of organics and minerals, most of which appear in the 1700 – 800 cm^{-1} region called "fingerprint region" [e.g., 59, 61, 62-66].

Table 1: Synchrotron flux advantage (reprinted from [68]).

Source	Pixel size (μm^2)	Flux photon / pixel	Integration time (μs)
300 K Thermal background	40 X 40	10^{11}	300
Globar	6.25 X 6.25	10^{12}	50
Synchrotron	0.54 X 0.54	10^{13}	3

Advancements in infrared spectroscopy include replacement of thermal globar light source with synchrotron radiation, and replacement of single-element detector with a focal plane array (FPA) detector [67]. The former increased the signal-to-noise ratio as well as the spatial resolution significantly since synchrotron radiation is up to 1000 times brighter than regular thermal radiation sources, whereas the latter enabled and improved acquisition of simultaneous data from samples [67]. Advantage of synchrotron radiation is also pointed out in Table 1 [67]. Figure 2 presents signals of both light sources. As seen from the figure, synchrotron radiation has significantly higher signal to noise ratio. For further comparison, a ~30 μm size Orgueil meteorite grain was measured consecutively with both light sources. Figure 2 presents infrared spectra of the meteorite grain. Absorbance bands are more pronounced and better resolved in the

case of the synchrotron radiation. For instance, bands near 1000 cm^{-1} due to hydrated minerals, and features near 2900 cm^{-1} due to aliphatic organics are some of the observed features in the spectrum collected with the synchrotron radiation; however these absorbance bands, especially the latter, are difficult to observe in the spectrum collected with the globar source. Similarly, absorbance band near 3650 cm^{-1} due to structural OH in phyllosilicates is clearly observed in the spectrum collected with the synchrotron radiation; however this band is lost in the noise in the spectrum collected with globar light source. Furthermore, Figure 2 presents the same meteorite grain's visible micrograph and infrared image at 2850 cm^{-1}. Synchrotron light source yields much higher spatial resolution, which reveals concentrations of molecular functional groups within the meteorite grain, however these the infrared image collected with the globar light source fails to reveal these functional groups.

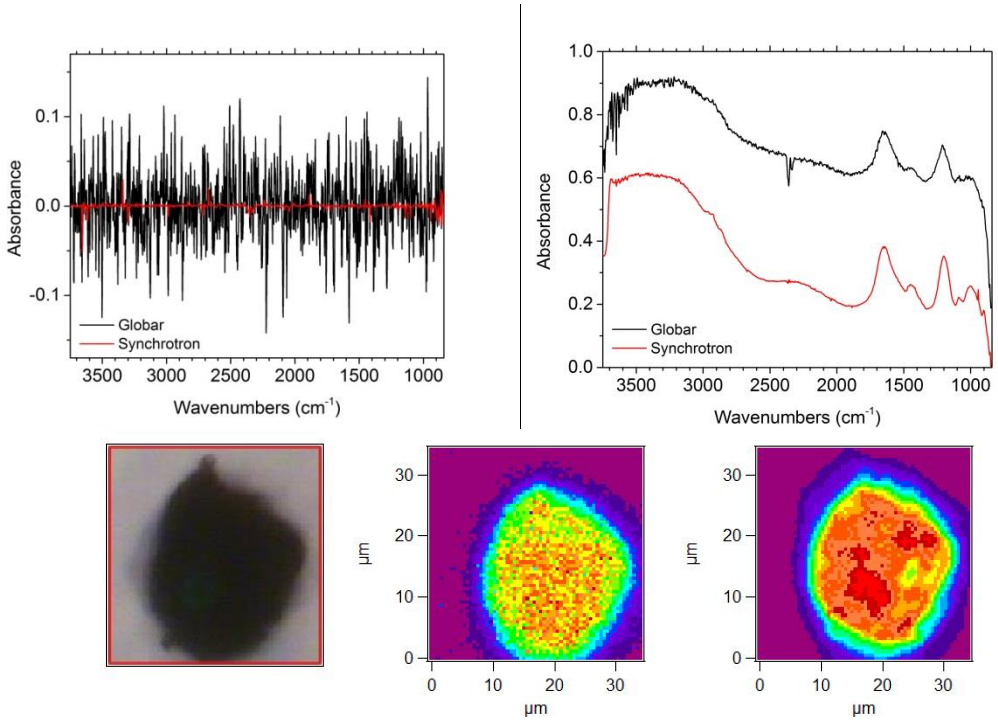

Figure 2: Spectrum of an Orgueil grain with both globar and synchrotron light sources for comparison. Top: Signal of both light sources (left), and mid-infrared spectrum of Orgueil meteorite grain collected with both light sources. Bottom: Visible micrograph (left), and infrared image of the Orgueil meteorite grain at 2850 cm^{-1} with globar light source (middle) and synchrotron radiation (right).

Therefore, synchrotron-based Fourier transform infrared microspectroscopy (micro-FTIR), which gives information on the organic and inorganic content in single chondrite grains with micron spatial resolution, is employed for this work. Infrared spectroscopic measurements were performed at Synchrotron Radiation Center (SRC), University of Wisconsin in Madison. The experiment is installed on the IRENI (Infrared Environmental Imaging) beam line [67-70]. Multiple fans of radiation extracted from a bending magnet are collimated, and rearranged with mirrors into a 3 × 4 matrix of beams, which homogeneously illuminate a 52 μm × 52 μm sample area (see Figure 3 for beam path illustration) in the commercial focal plane array (FPA). The endstation of the beamline is a Bruker Vertex 70 FTIR spectrometer connected to a Bruker Hyperion 3000 IR microscope equipped with an FPA detector of 3850 – 800 cm^{-1} spectral range

(2.5 – 12.5 μm). The microscope operates in transmission mode with a 74× magnification Schwarzchild-Cassegrain objective with numerical aperture (NA) of 0.65. The geometric effective area at the sample plane of 0.54 μm × 0.54 μm pixel imaged onto 40 μm × 40 μm pixels at the detector allows spatial oversampling, providing spatially resolved images that are diffraction-limited at all wavelengths. The single shot FPA image covers the field of view with 96 pixels × 96 pixels. A detailed review of the instruments is presented in [67]. Spectra were recorded with 4 cm-1 resolution using 128 co-added scans. A clean, sample-free region of the diamond window was used for reference spectra.

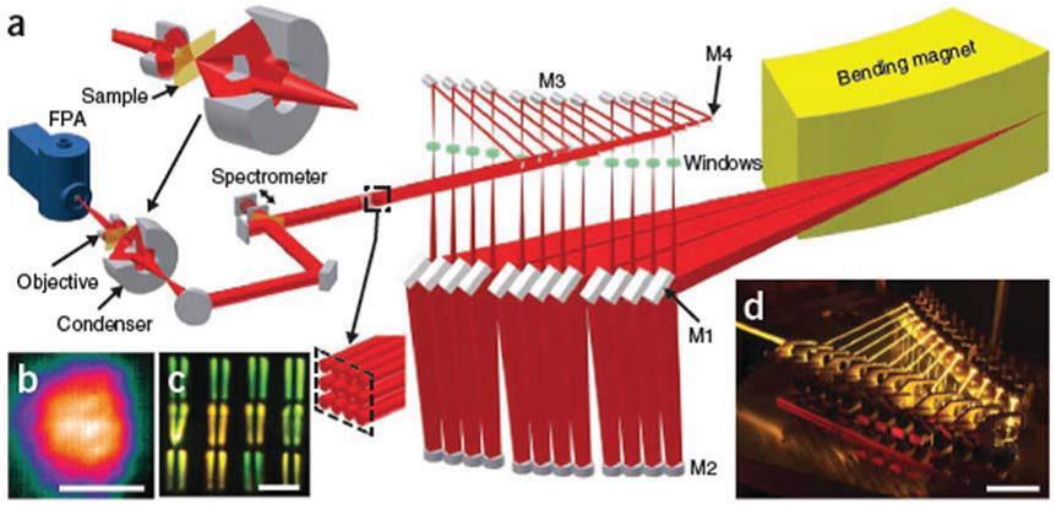

Figure 3: Schematic of IRENI. a) Optical arrangements of IRENI showing mirrors which direct the beam path from the bending magnet, to the spectrometer through the condensing onto the sample, through the objective and onto the detector. b) Defocused illumination of the IR beams onto the FPA detector. c) Conventional image of the visible portion of the focused synchrotron beams. d) Visualization of the beam path through the M3 and M4 mirrors by a photo generated by scattering the visible portion of the beams. Reprinted by permission from Macmillan Publishers Ltd: Nature Communications [68], copyright (2011).

Grain heterogeneity and correlations between different spectral features are revealed by investigating spectral and spatial relationships between organics and minerals studied *in situ* without chemical extraction. The sample to be analyzed is placed on a diamond window which is mounted onto a motorized, programmable mapping stage (see Fig. 4). After having defined the mapping parameters, an infrared spectrum at each pixel within the defined area is simultaneously collected within just minutes. Throughout the experiments, infrared spectra were recorded with 4 cm^{-1} resolution using 128 co-added scans. These raw spectra were later divided by reference spectra collected at a sample-free and clean region of the diamond substrate to obtain transmittance.

Figure 4: Experimental setup and instruments at the Synchrotron Radiation Center. Left: Optics, spectrometer, and the microscope. Right: Microscope with a joystick controlled sample stage.

Using IGOR Pro and IRidys software packages [69], a spatially averaged IR spectrum of a grain is obtained by masking out the sample-free regions of the image and averaging the spectra for all pixels in the unmasked region. Using these software packages, we also obtained line profiles across a meteorite grain by extracting individual spectra from adjacent pixels. The integrated absorbance of individual characteristic spectral features was taken as a measure of the relative concentrations of specific minerals and organics at a particular location within the grain.

These integrated intensity maps were used to obtain the spatial distribution of the various mineral and organic types within the grain. Correlation coefficients were obtained using the descriptive statistics function of the OriginPro software package. Certain ratios and their statistical distribution were analyzed to infer primitiveness of samples.

2.4 Three dimensional imaging with synchrotron FTIR spectro-microtomography

IRENI's capability of acquiring two dimensional high spatial resolution infrared images is described above. Recently, the instrumentation has been upgraded and three-dimensional FTIR spectro-microtomography made possible for the first time [71]. We measured three-dimensional synchrotron-based infrared spectro-microtomography of Murchison with the upgraded instrumentation. The experimental procedure is similar to what is discussed above for the acquisition of two dimensional infrared images, except that this time the meteorite sample of interest was rotated in time as its numerous projected two dimensional images are collected, after which four dimensional reconstructions are generated: three dimension for the spatial representation of a sample, and one for the full mid-infrared spectral dimension [e.g., 71]. Using this technique, the chemical composition of samples, spatial distributions of different molecular functional groups are revealed in three dimensional space [71].

FTIR spectro-microtomography experiments were conducted at IRENI beamline at the Synchrotron Radiation Center, University of Wisconsin in Madison. Single 50 µm X 50 µm sized grain of a pristine Murchison sample was mounted on a MiTeGen sample holders (e.g., [71]). This holder consists of a stainless steel rod and a tip. The tip is a 10 micron thick polyimide loop, which may introduce interference to the spectrum of the meteorite sample [71].

Nevertheless, spectral differences such as absence of CH stretching modes in spectrum of polyimide allow us to acquire data in the mid-infrared region from the meteorite sample itself [71].

The meteorite grain was mounted to the loop of the sample holder, and the sample holder was subsequently mounted to the sample rotation stage. Using 15X (N.A. = 0.5) condenser and 36X (N.A. = 0.5) objective [e.g., 71], the microscope was focused onto the meteorite grain. The rotation of the stage was computationally controlled for precise rotation of the sample under the microscope [e.g., 71]. The meteorite sample was rotated in increments of 1.6 degree, and spectral image of each orientation was collected, totaling to 225 two-dimensional transmission measurements over the 360 degree of rotation, each image with field of view size of 128 X 128 pixels spanning the field of view and giving 1.1 μm X 1.1 μm spatial resolution and 8 cm-1 spectral resolution. Thus, each three-dimensional reconstruction consists of millions of voxels, each with 1.1 μm X 1.1 μm X 1.1 μm size and a specific full mid-infrared range spectrum [71].

Reconstruction of these datasets is done by using software packages [71]. Integration wavelength range of each chemical component was determined from the grain averaged infrared spectrum from one of the 224 datasets. Namely, specific infrared absorbance bands are due to specific species present in the sample, and therefore peak positions of these bands are used for determining the frequency ranges for integration. Therefore, different frequency regions can be reconstructed for representation of amount of a particular component present within the sample. Moreover, any two or more frequency ranges can be reconstructed together, which would represent spatial distribution of combination of those species present in the sample [e.g., 71], revealing relative distributions of components. Different colors are assigned to reconstruction of different components such that these components are distinct within the reconstructed image.

CHAPTER THREE: ORGANIC AND MINERAL CORRELATIONS IN NORTHWEST AFRICA 852

3.1 Introduction

Northwest Africa 852 (NWA 852) was found in 2001 in Morocco. It is classified as a CR2 chondrite. It has large, millimeter size chondrules in addition to carbonates, aromatic and aliphatic organics. Additionally, NWA 852 has hydrous as well as anhydrous silicates, the latter being relatively in lesser amount. Significant amount of presolar grains have been identified in NWA 852, and considerable amount must have been lost due to aqueous alteration [1].

NWA 852 is a CR2 carbonaceous chondrite with low weathering grade (W1), 1.3 Fa (mol%), and 4.3 Fs (mol%) [117]. It reportedly presents low chondrule/matrix ratio and Fe-rich olivines [117]. Furthermore, NWA 852 presents high presolar grain abundances. Reported by [1] are 24 presolar silicates, 7 presolar oxides, and 8 SiC grains in NWA 852. However, to date no study exists on organic and mineral inventory of NWA 852.

3.2 IR spectral signatures

Figure 5 presents the spatially averaged mid-infrared spectrum for an NWA 852 grain that nearly fills a 34 μm × 34 μm field of view and which comprises the sum of individual spectra from ~3964 pixels (Fig. 6, right). Lettered arrows in Figure 5 indicate the location of distinct and identifiable absorbance bands.

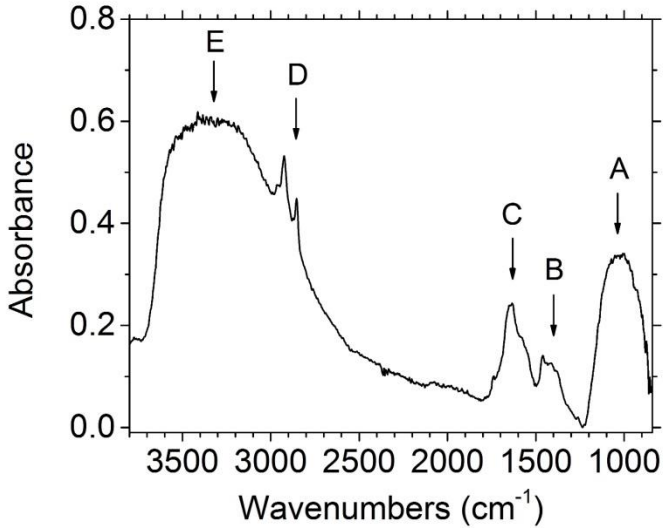

Figure 5: Average absorbance spectrum of NWA 852 (CR2) grain.

The symmetric band A near 1018 cm^{-1} is due to the Si-O stretch of hydrated silicates [60, 72]. The broad band E near 3400 cm^{-1} is a stretching mode of interlayer and/or adsorbed water [64]. Together these two bands indicate the presence in this sample of phyllosilicates, possibly clay minerals. This is consistent with the identification of clay in CR2 chondrites [e.g.,73]. On the other hand, the signature band of structural OH near 3650 cm^{-1}, as would be observed in some phyllosilicates, and which we have observed for grains of Orgueil and Tagish Lake is absent in this spectrum (see text).

An asymmetric broad band B shown in Figure 5 occurs within 1300 – 1500 cm^{-1}, which identified as the carbonate region [e.g., 60, 64, 72, 74]. This band is simply due to the C=O stretch of CO_3^{2-} in carbonate minerals.

The broad band C in Figure 5 occurs within 1500 – 1800 cm^{-1}, and due to a combination of organics and water. Shoulders appearing between 1520 - 1600 cm^{-1} and at 1632 cm^{-1} are due to the C=C bond in aromatics [e.g., 60, 75]. [3, 76] reported a C=C stretch at 1590 cm^{-1}, which is

indistinct in our spectrum. The band at 1650 cm^{-1} is due to bending vibrations of water [59, 64]. Shoulders at 1660 cm^{-1} and at 1700 cm^{-1} are stretching modes of C=O in carbonyl/carboxyl functional groups [3, 76]. The latter band has been attributed to the C=O stretch in saturated aliphatic ketone by [60]. The weak shoulder that we observe at 1715 cm^{-1} is due to saturated aliphatic ketones. Shoulders and together indicate the presence of aliphatic ketones. The more distinct shoulder at 1738 cm^{-1} can be due to C=O stretching mode in saturated aliphatic aldehydes and/or esters, except that aldehyde should also have a feature near 2730 cm^{-1} [e.g., 77], which is lacking. These identifications agree with the discussion of carbonyls by [78].

The sharp and distinct features comprising band D in Figure 5 are characteristic of aliphatic hydrocarbons. Features at 2854 cm^{-1} and at 2923 cm^{-1} are due to symmetric and asymmetric stretching modes of CH_2, while those at 2873 cm^{-1} and at 2952 cm^{-1} are due to corresponding modes of CH_3, respectively [59, 60, 79].

Although there is no clear identification for the weak broad band observed in Figure 5 between 1800 and 2130 cm^{-1}, this may be due to overtones of strong silicate band (A). Narrow spikes near 2360 cm^{-1} are artifacts due to atmospheric CO_2. Table 2 collects the observed bands, their positions, and their interpretations.

Table 2: Positions and assignments of the observed bands.

Label	Position (cm^{-1})	Mode	Possible assignments
A	1018	Si–O stretch [a]	Phyllosilicates
B	1440	C=O stretch	Carbonates
C	1650	H-O-H bend [b, d]	Water
D	3000-2800	C-H stretch [a, c, d]	Aliphatic hydrocarbons
E	3400	H-O-H stretch [b]	Interlayer/adsorbed water

[a] [60], [b] [64], [c] [79], [d] [59]

3.3 Spectral cross section of the grain

Figure 6 presents visible micrograph of the NWA 852 grain, and the infrared image at 2921 cm^{-1}, where the 16 level color scale in rainbow sequence indicates absorbance, red being the highest. The vertical lines define spectroscopic line profiles.

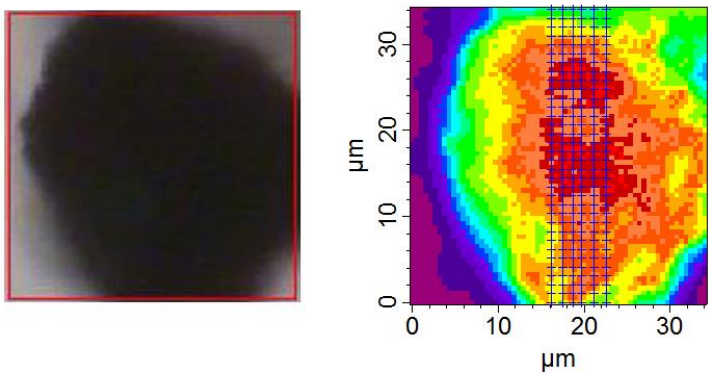

Figure 6: Visible micrograph (left), and infrared image of the NWA 852 grain at 2921 cm^{-1} (right).

The spectroscopic line profile across the grain is obtained for the slices indicated by the vertical line on the infrared image in Figure 6. Each line drawn consists of 63 pixels, each with an associated full mid-infrared range spectrum. Alternate pixels were selected for data analysis with 1 µm separation. As representative, the spectra of the rightmost slice shown in the infrared image are presented in Figure 7 with the ordering of the curves bottom to top following a bottom to top scan across the grain.

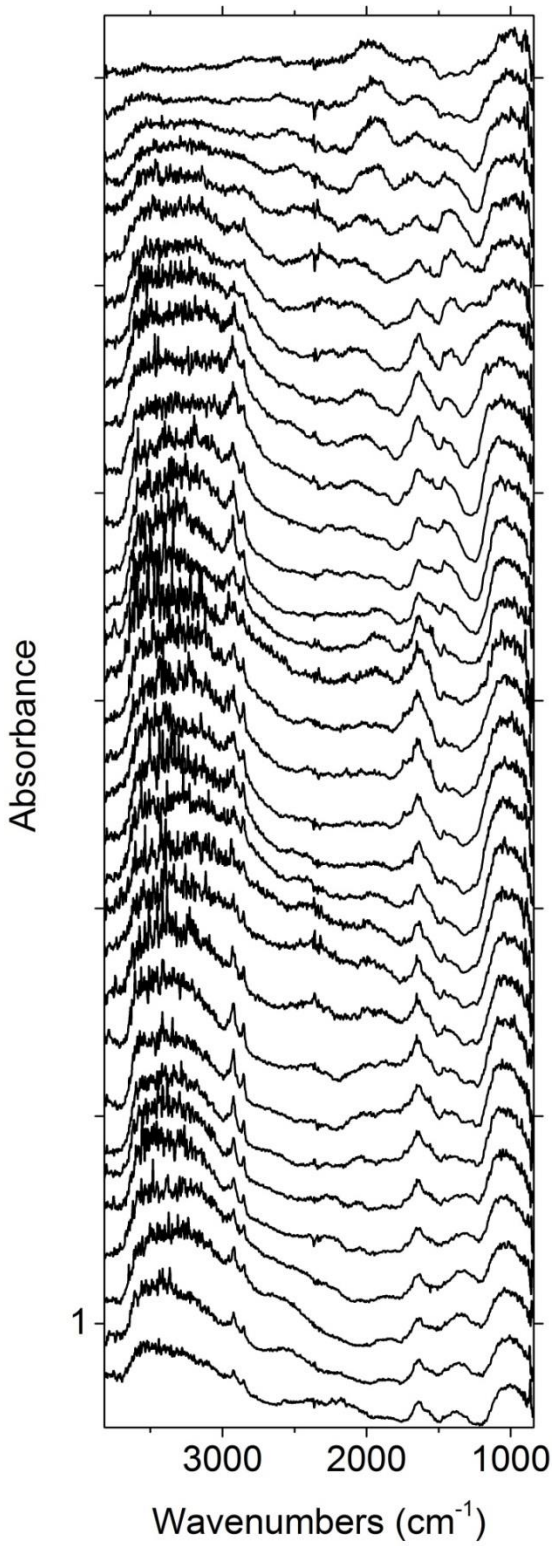

Figure 7: Spectral line scan of the rightmost cut indicated in Figure 9 (right). Each successive spectrum is offset vertically by 0.4 absorbance units for clarity.

Figure 8 presents a comparison of integrated intensities of bands A, B, C, D, and E. Total of 202 spectra obtained from the spectral cuts, shown in Figure 6. Integrated absorbance and widths of the various bands change with position across the grain. Absorbance is the product of absorption cross section, concentration, and thickness. If the changes were due simply to the non-uniform thickness of the grain, then all of the absorbances would change together. We see from Figure 7 and Figure 8 that they have different spatial dependences, indicating that the relative concentrations are spatially non-uniform. The most noticeable effect is that band B appears to be negatively correlated with band C. Furthermore, band D seems correlated with band E, dropping near six regions that correspond to the upper edge of the meteorite grain, and otherwise staying flat across the grain.

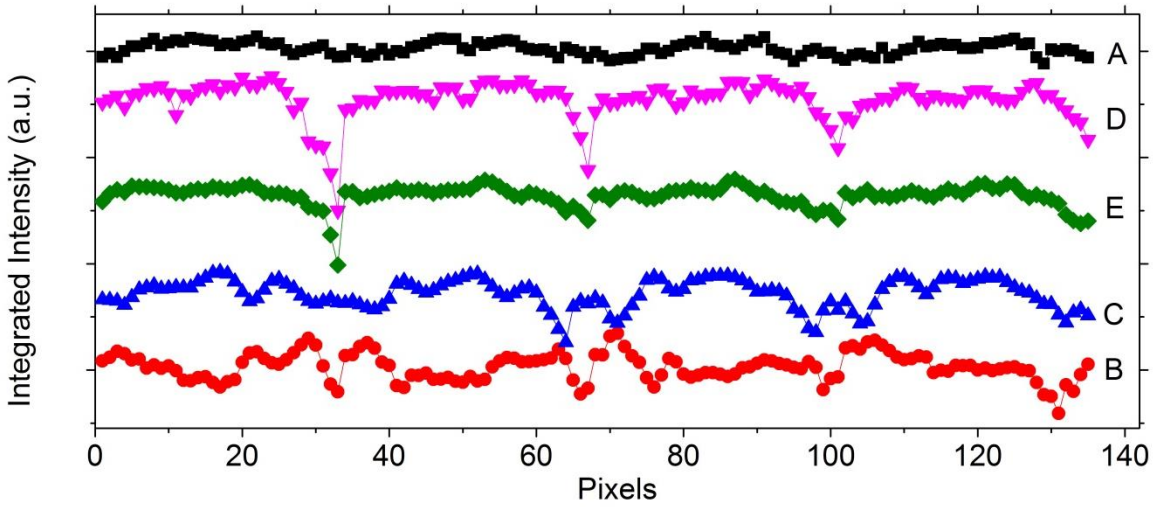

Figure 8: Comparison of integrated band strengths for the line scan across the grain. Letters in the legend represent the absorbance bands in Figure 5.

3.4 Pearson correlation coefficients

Although Figure 7 and 8 give insights of relationships of among functional groups within the grain, it is difficult to make any conclusion based on these graphs. More conclusive interpretations require quantitative statistical analysis methods such as Pearson's correlation coefficients. This method determines relationships among variables in a dataset [e.g., 80]. Mathematical calculation of such coefficients is as follows;

Let X represents the integrated area of one of the bands and let Y be the same for one of the other bands. The variance S_x^2 of X is calculated from

$$S_x{}^2 = \frac{\sum(X-\bar{X})(X-\bar{X})}{n-1}. \quad (1)$$

Eq. 1 is positive definite. The covariance (S_{xy}) is then calculated from

$$S_{xy} = \frac{\sum(X-\bar{X})(Y-\bar{Y})}{n-1}. \quad (2)$$

Eq. 2 may be positive or negative. For example, if at a given pixel the value of X exceeds its value averaged over all pixels, while the value of Y is less than its average, then at that pixel the argument of the sum is negative. We obtain S_{xy} by summing over all pixels, and if this sum is negative, then on average the X values exceed their average when the Y values are below theirs, and vice versa. Finally, by normalizing with Eq. 1, we obtain the correlation coefficient

$$r = \frac{S_{xy}}{S_x S_y}. \quad (3)$$

The values of *r* lie between -1 and +1. Negative values indicate anti-correlation and positive values indicate positive correlation. The strength of coefficients, as described by [47], given in

Table 3. Namely, the closer a coefficient is to ±1, the stronger is the correlation or anticorrelation. Although these limits are arbitrary and may vary in the context of meteorites.

Table 3: Correlation coefficients and their strength.

Coefficient	Strength of relation
|0.1 – 0.3|	Weak
|0.3 – 0.5|	Moderate
|0.5 – 1.0 |	Strong

For each spectrum in Figure 7, characteristic absorbance bands were linear-baseline corrected between the end points, and their intensities were integrated via equation (4) individually to obtain band area of each absorbance band in each spectrum.

$$A_{band} = \int_{band} I_\nu d_\nu \tag{4}$$

where I_ν is intensity, and A_{band} is integrated intensity (or area) of a band. These integrated intensities comprise the dataset for correlation analysis. Integration regions were 850–1200 for band A, 1200–1500 cm^{-1} for band B, 1500–1750 cm^{-1} for band C, 2800–3000 cm^{-1} for band D, and finally 3000–3700 cm^{-1} for band E.

Pearson correlation method makes several assumptions, some of which are i) variables must be interval measurements, ii) variables must be normally distributed, iii) variables must have equal variances. Visual inspection of the dataset confirms that all of these assumptions are satisfied. Commercial software OriginPro was used to calculate the correlation coefficients as well as their respective significance levels, which are collected in Table 4. A small value for significance indicates high confidence. Coefficients with "*"are significant at the 95% confidence level. In other words, possibility of a correlation being due to chance is 5% or lower.

Table 4: Pearson correlation coefficients for NWA 852. Letters represent the absorbance bands in Figure 5.

		A	B	C	D	E
A	*Corr.*	1	- 0.35*	0.48*	0.48*	0.52*
B	*Corr.*		1	- 0.28*	- 0.24*	- 0.05
C	*Corr.*			1	0.50*	0.63*
D	*Corr.*				1	0.66*
E	*Corr.*					1

A: Silicates, B: Carbonates, C: Organics+water, D: Aliphatic hydrocarbons, E: OH

We observed that band D (due to aliphatic hydrocarbons) is strongly correlated (r = 0.66) with band E (due to OH). Band A (silicates) is also strongly correlated with the OH band E (r = 0.52) and also with the aliphatic hydrocarbon band D (r = 0.48), however negatively correlated with the carbonate band B (r=-0.35). A negative correlation (r = - 0.28) was found between carbonates (band B) and organic+water combination (band C). Band C shows a strong positive correlation with D (r = 0.50) and E (r = 0.63). Since B and C are negatively correlated, and C is positively correlated with D and E, one may intuitively expect B to be negatively correlated with D and E. This is indeed the case, as shown in Table 4 that B is negatively correlated with D and E, though with relatively low confidence.

3.5 Infrared spatial distribution maps of organic and mineral compounds

Infrared images give the spatial distribution of absorbance at a particular wavenumber. Such maps may be used to infer the relative amounts of organic molecules or inorganic minerals present at particular locations within a grain. The high spatial resolution, broad spectral

coverage, and simultaneous data acquisition over the entire field of view allows us to acquire detailed spatial maps of composition for many grains in reasonable times. These maps are obtained by integrating the infrared image (Figure 6) over the frequency range of the spectral band of interest. This integration is done after a linear baseline is subtracted from the absorption band in the same range. Figure 9 presents these integrated absorbance maps of the bands indicated in Figure 5. The integration range for each map was same as integration of individual bands for correlation analyses.

Figure 9a indicates that silicates are distributed across the grain. The highest absorbance comes from the central region, presumably where the grain is thicker, around the coordinates (20 μm, 20 μm). Figure 9e presents the spatial distribution for OH, which also has prominent absorption in the region near (20 μm, 20 μm). The spectral overlap for these two plots is less in other spatial regions. Thus, the region near (20 μm, 20 μm) may have abundant hydrous silicates (e.g., phyllosilicates) while the other regions of strong absorption in Figure 9a may correspond to anhydrous silicates (e.g., olivine). Note that the olivine shoulders at 873, 925, and 956 cm^{-1} are within the band-A integration range.

Figure 9b is the carbonate map, which indicates high absorbance along the outer edges of the grain and none within the center. In particular, the carbonates overlap little with silicates (Figure 9a) or OH (Figure 9e).

Figure 9c presents the map of absorbance due to both organics and water, where the organics are mostly carbonyls with aromatic contributions. The islands of strong absorbance do not overlap with the carbonate concentrations (Figure 9b). As in [64], organics and water appear to be interleaved with carbonate regions.

The map for the C–H stretching in aliphatic hydrocarbons (Figure 9d) overlaps with OH (Figure 9e) more than it overlaps the silicates map (Figure 9a). This is consistent with the association of organics with phyllosilicates [e.g., 28, 64].

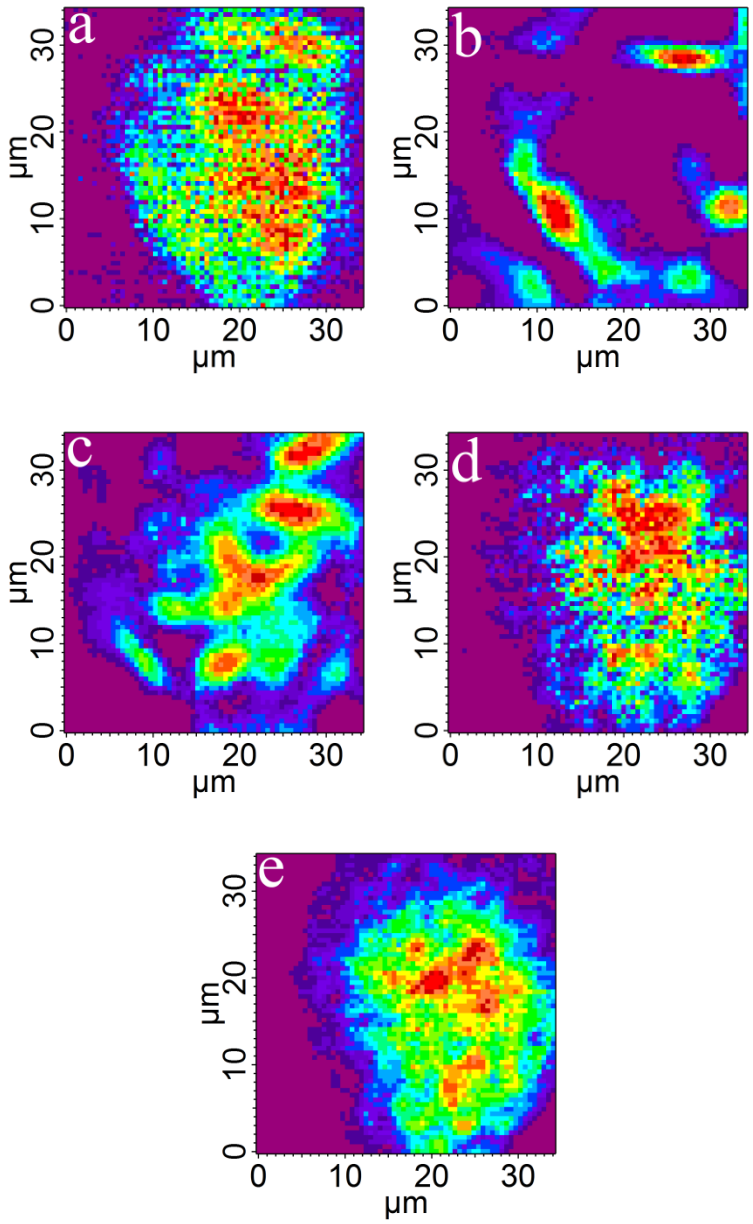

Figure 9: Integration maps of NWA 852 grain for characteristic absorbance features. a) Silicates, b) Carbonates, c) Carbonyls and water, d) Aliphatic hydrocarbons, e) O–H, The color scale in rainbow sequence indicates absorbance in 16 levels, red being the highest.

3.6 CH_2 / CH_3 ratios and comparison to astronomical objects

Aliphatic hydrocarbons give rise to infrared features between 2800 and 3000 cm^{-1} (Figure 8), whose peak positions and chemical assignments are collected in Table 2. Aliphatic chain length and degree of branching can be inferred from the CH_2 / CH_3 absorbance ratios [64, 81, 82]. A high ratio indicates long aliphatic chains and/or a low degree of branching [60]. Hence, a high ratio suggests primitiveness and low parent body alteration. We baseline corrected the band D region (2800-3000 cm^{-1}) by subtracting a straight line that is tangent to either end-points of the region in the grain-averaged spectrum (Fig. 5). After linear baseline correction, the CH_2 / CH_3 absorbance ratio for NWA 852 was determined to have the average value 2.53, which is compared in Table 5 to values reported for other meteorites, interplanetary dust particles (IDPs), diffuse interstellar medium (DISM) objects, and cometary dust particles. The value for NWA 852 is similar to that of IDPs and Wild 2 cometary dust particle. It exceeds that of DISM and several carbonaceous chondrites of petrologic type 1 and 2, indicating that such chondrites have experienced a higher degree of aqueous alteration than has NWA 852. In other words, the grain-averaged ratio suggests that NWA 852 is comparable to more primitive and less altered objects.

Table 5: Astronomical objects and their CH_2 / CH_3 ratios.

Objects	I_{CH2} / I_{CH3}
NWA 852 (CR2)	2.53 [a]
Wild 2 particles	2.50 [b]
IDPs (anhydrous)	2.46 [c, z]
IDPs (hydrous)	2.31 [c, z]
DISM	1.17 [d, z], 1.07 [e, z]
Paris (CM)	1.80 [g]
Bells (CM2)	1.40 [f]
Murchison (CM2)	1.00 [f]
Orgueil (CI1)	1.40 [f]

[a] This study, [b] [62], [c] [83], [d] [84], [e] [85], [f] [64], [g] [72], [z] Average.

On the other hand, the ratio shows strong variability across the grain, ranging in value from 1.7 to 3.7 for the rightmost line scan in Figure 6. The variation in ratio values suggests that the grain contains a mixture of very primitive and strongly altered material. The distribution of ratios for nearly 250 pixels from the central part of the grain is presented in Figure 10. The mean value is 2.34. The difference between this determination and that given in Table 4 for the grain-averaged spectrum (Figure 5) indicates a ~10% uncertainty for the average ratio value.

In principle, the ratios may depend on the strength of the absorption. For instance, it could happen that as the total concentration of CH increases, one component might increase faster than another, i.e. that the ratio depends physically on the concentration of organic material. To test this, ratios were binned, averaged, and plotted together for three ranges of integrated area for the CH band "D" (Figure 11). The CH_2 / CH_3 ratios decrease from 2.74 to 2.10 with increasing band strength, suggesting that while overall CH band area is increasing, and the CH_3 band grows faster than CH_2 band. This suggests that CH_3 is favored over CH_2 by high organic concentrations. On the other hand, the standard deviation of binned ratio values, also plotted in

Figure 11, exceeds the differences in average ratio values, suggesting that their decrease with intensity may be statistically insignificant.

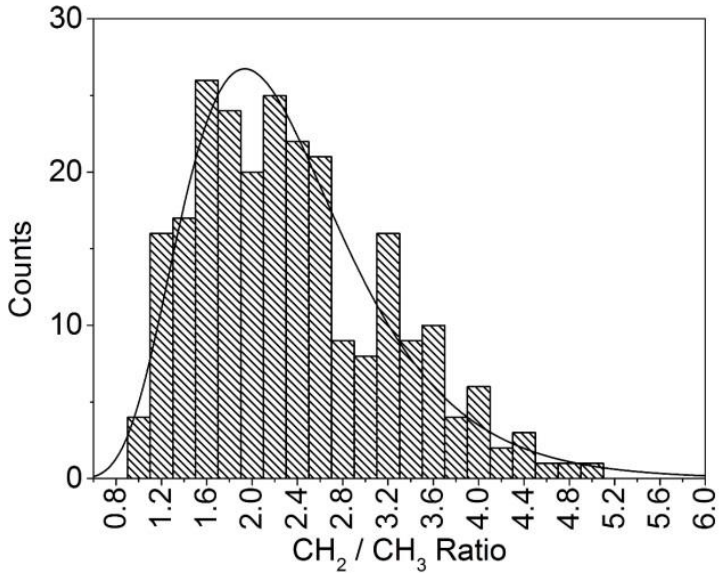

Figure 10: Histogram of the CH_2 / CH_3 ratios.

One expects the uncertainty in the ratio values to be larger for the weaker bands. Indeed, Figure 11 shows that the standard deviation is higher for the weaker bands, but only slightly so. Thus, "extreme" values of the ratios are not artifacts due to inclusion of weak bands. Hence, the possibility is real that NWA 852 contains a fraction of non-primitive or heavily altered material.

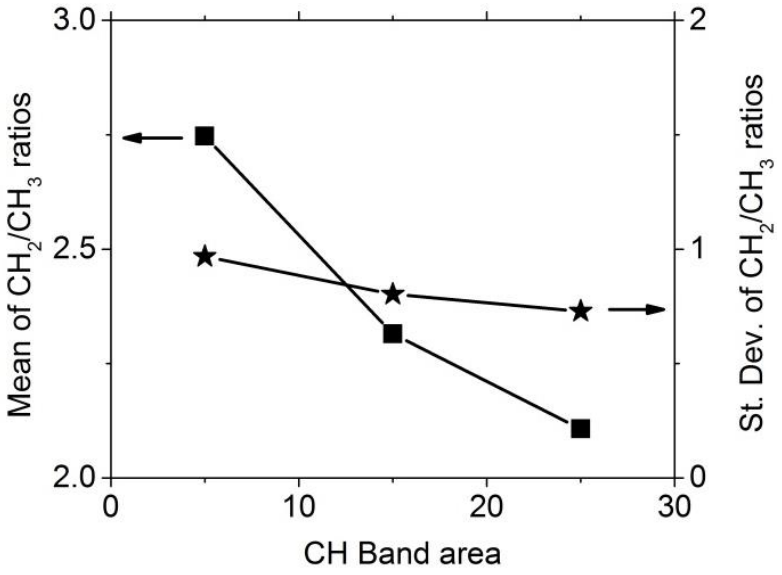

Figure 11: Mean and standard deviation of the CH_2 / CH_3 ratios.

3.7 Discussion

In this chapter, we showed a correlation between aliphatic type organics and silicates in NWA 852. Infrared maps show that the silicate concentration overlapping with aliphatic organics also overlaps with the OH concentration. This indicates that hydrated silicates are closely associated with organics in NWA 852. Therefore, our results indicate that such silicates may have played an important role for production of organics in NWA 852.

Presolar grains previously have been found in meteorites and IDPs. [87] reported abundant presolar grains in CR3 chondrites, Meteorite Hills (MET 00426) and Queen Alexandra Range (QUE 99177). Presolar grains in IPDs have been reported by [118]. Parent body processing such as aqueous alteration and thermal metamorphism tend to alter/destroy presolar grains, therefore resulting in less presolar grain abundances [e.g., 1, 120, 119]. Namely, presolar grain abundance goes from higher to lower in type 3 to type 1 carbonaceous chondrites, respectively. NWA 852 is unique among CR chondrites with abundant presolar ^{17}O and $\delta^{15}N$

enriched grains [e.g., 1], which indicates parent body alteration at a lesser extent. Thermal metamorphism may particularly modify aliphatic type organics such that the CH_2 / CH_3 would be lower. For instance, irradiation by energetic particles may break – CH2 – CH3 bonds, and heating may aromatize aliphatic molecules. Both processes shorten chain lengths and result in lower CH_2 / CH_3 ratios [72]. Raman features for insoluble organic matter show that CR chondrites are more primitive than CI and CM chondrites based on their D and G band profiles (e.g., [86]). We observed that NWA 852 lacks an infrared band due to aromatics near 3050 cm^{-1} which has been observed in altered meteorites with low CH_2 / CH_3 ratios, e.g., Murchison [89] and Paris [72]. The broad CH_2 / CH_3 ratio distribution (Fig. 10) suggests that NWA 852 is far from uniformly primitive, and there exists considerable amounts of altered material concentrated within the individual grain studied. This is consistent with previous reports discussed here.

IDPs and Wild 2 cometary dust particles have similar mid-infrared spectral profile near the C-H stretching region of aliphatic hydrocarbons [62, 90]. We see similar spectral profile in terms of peak shapes and CH_2/CH_3 ratios in NWA 852. For instance, NWA 852 and Wild 2 samples have the same CH_2/CH_3 band strength ratio (~2.5), which is clearly larger than that of other primitive carbonaceous chondrites such as Orgueil and Murchison (~1.1) and of diffuse ISM objects (~1.2) (Table 5). This indicates longer (or less branched) aliphatic hydrocarbon chains for Wild 2 particles, IDPs, and NWA 852 than those in the diffuse ISM material and several other carbonaceous chondrites, suggesting that the organic matter in these two different group of astronomical samples may have formed in different locations (or under different conditions) [90].

Based on the evidences presented here, we believe that NWA 852 is (on average) on the low aqueous-alteration side of petrologic type 2 with little thermal metamorphism. It would be

useful to extend our technique to other meteorites to characterize the effects of parent body thermal metamorphism on the organic molecules and mineral species. In principle, our technique could deconvolve the imprints of thermal and aqueous alteration on the parent body from nebular signatures based on spatial distributions of spectral signatures: carbonates are secondary products that result from aqueous alteration; thermally metamorphosed material has little or no hydration; a nebular signature is the high ratio of CH_2 / CH_3. The question is whether regions of high ratio (primitive) are spatially distinct from regions of high carbonates (altered) and regions of low hydration (metamorphosed). In case of NWA 852, visual inspection of Figure 9 suggests that carbonate-rich regions have lower CH_2 / CH_3 ratios compared to values for regions that are relatively carbonate-poor, suggesting a negative correlation between carbonates and aliphatic type organics.

Aqueous alteration may have redistributed the soluble organic material, which would tend to erase the mineralogical context of the organic molecules present. However, the insoluble fraction of organic matter (IOM) ranges from 70 to 99% of the total in carbonaceous chondrites [76, 87]. Although there has been no report of the percent IOM in NWA 852, the soluble fraction is in any case a minority. Even then, dissolved materials stay close to their source in CR chondrites [73]. In highly altered grains, characteristic ~100 μm migration distances are two orders more than length scale of spatial variations we observe in NWA 852, which agrees with its relatively low alteration. In other words, alteration in NWA 852 has not "washed out" the spatial heterogeneity of its organics.

Few reports exist on infrared spatial mapping of meteorites. For instance, [59] reported absorbance maps of Murchison and Orgueil using synchrotron based FTIR microspectroscopy with relatively low spatial resolution. Additionally, Spatial mapping at single wavelengths in

Bells meteorite by near-field infrared microspectroscopy was reported by [64], however less information is provided than by characterization over the full mid-IR range, and spatial mapping by step scanning is time consuming. We presented infrared microspectroscopy of one grain of a CR2 chondrite NWA 852, demonstrating high spatial resolution and with high spectral information. We have also demonstrated chemically-specific heterogeneity on 1 micron length scales.

IOM extracts may give different conclusions than *in situ* characterization such as ours. IOM is obtained by demineralizing the bulk sample in acidic solvents such as HF and HCl [e.g., 3, 76]. After demineralization, the remaining material is the IOM residue. Whether chemical alteration of organic matter through acidic demineralization occurs [88, 89], or not [90], is controversial. [89] showed that the Murchison IOM and in situ organic matter of bulk Murchison sample are significantly different. Chemical alteration effects include a decrease in the aliphatic CH_2 / CH_3 ratios (giving shorter chains or more branching) and increase in aromatic CH content.

3.8 Conclusions

We investigated relationships among organics and minerals by mid-infrared synchrotron-based imaging micro-FTIR spectroscopy of the CR2 chondrite NWA 852. These data constitute the first reported infrared spectra for this meteorite. A spectroscopic line profile for the particular NWA 852 grain studied shows that the relative intensity of the characteristic absorbance bands varies across the grain on 1 micron length scales. Statistical analysis shows that the silicate-band is positively correlated with OH and CH bands, which are correlated with each other. However, the spatial overlap of silicate and OH is imperfect, due probably to a heterogeneous mixture of

anhydrous and hydrated silicates. Strong negative correlation has been observed between carbonate bands and the carbonyl-water combination band, and the two have clear spatial separation within the grain.

The average CH_2 / CH_3 ratio for NWA 852 indicates a predominance of CH_2 over CH_3 that is comparable to that in IDPs and Wild 2 cometary dust particles. The ratio exceeds that for DISM and several carbonaceous chondrites, indicating longer carbon chain lengths and/or smaller degree of branching. This may also indicate similar origin, formation, and/or processing of organic matter in NWA 852, IDPs, and Wild 2 particles, but rather different than diffuse ISM organic matter. Spatially resolved ratios indicate a considerable distribution, with a sizeable fraction of strongly altered material despite the petrologic classification of 2.

CHAPTER FOUR: ORGANIC AND INORGANIC CORRELATIONS IN TAGISH LAKE

4.1 Introduction

Tagish Lake meteorite ("Tagish Lake" hereafter) fell in January 18 2000 in British Columbia, Canada. Some fragments fell and landed on Taku Arm of the Tagish Lake. First fragments were recovered on 25 January 2000 from the surface of a frozen lake. Further expeditions collected more fragments within the region, most of which were on the frozen lake surface and some below the surface [51]. Interaction of specimens with melted water might have altered them at varying extends.

Tagish Lake is thought to be the most pristine carbonaceous chondrite among all recovered meteorites [120]. It is a petrologic type 2 ungrouped carbonaceous chondrite with affinities to CI, CM, and possibly CR chondrites [120, 121]. It is a breccia with matrix that consists of olivine, phyllosilicates, carbonates, and sulfides, however bulk composition consists of phyllosilicates, carbonates, olivine, magnetite, calcium- aluminum-rich inclusions (CAIs), sulfides, and presolar grains [51]. It is C-rich aqueously altered meteorite. In Tagish Lake, nearly 3.7 wt.% C derives from carbonates and the rest from organics, while this is different than CI and CM chondritic carbon distribution, in which ~0.35 wt.% C derives from carbonates [51]. Soluble organic C in Tagish Lake is only about 1 %, and the rest is insoluble organic matter (IOM) [50]. P- and D-type asteroids, and extinct comets have been suggested as candidates of parent body of Tagish Lake based on compositional properties and characteristics such as abundant carbon, aqueous alteration, abundant presolar grains, abundant carbonates with varying compositions, low abundance of chondrules and CAIs [51, and references therein]. Spectroscopic

data also points to a D-type asteroids [52]. Density of bulk Tagish Lake is measured as 1.66 ± 0.08 g/cc [53].

Two different Tagish Lake lithologies have been reported, carbonate-rich, and carbonate-poor, where the former has a lower abundance of magnetite and a higher abundance of calcite, and almost no CAI than the latter [53, 54].

Here we present results of infrared spectra, correlation coefficients, and spatial distribution maps of two Tagish Lake grains. Spectral signatures shown here suggest that the Tagish Lake sample studied here belongs to the carbonate-rich lithology. Grain-averaged infrared spectra of Tagish Lake show prominent absorbance bands that are signatures of silicates, carbonates, aliphatic and aromatic organic matter, and water. Total of 200 spectra obtained from the meteorite grains were studied for correlations of organic and inorganic materials that are present within the grains. Infrared images of both Tagish Lake grains were integrated between a set of frequencies for the identification of relative concentration regions, and two-dimensional spatial maps were obtained.

4.2 IR spectral signatures

Figure 12 presents the spatially grain-averaged mid-infrared spectra of two Tagish Lake meteorite grains. Grains were enumerated as #3 and #24 to distinguish them in the field of view. The size of the former grain is almost 34 μm × 34 μm, while the latter nearly fills 68 μm × 34 μm field of view. Lettered arrows indicate the position of distinct and identifiable absorbance bands.

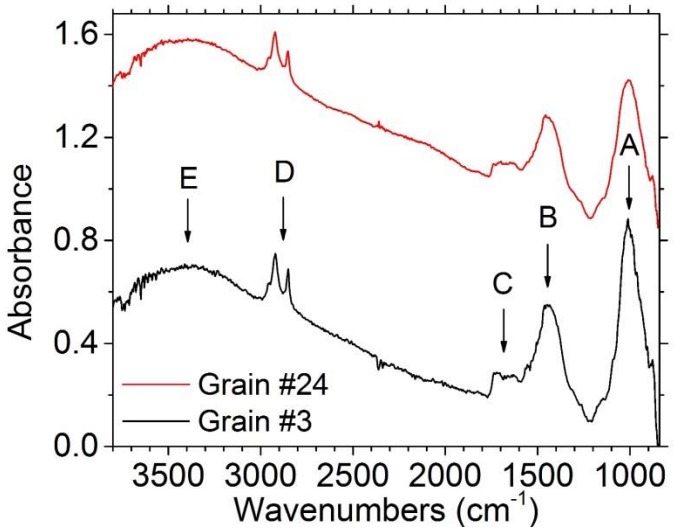

Figure 12: Average absorbance spectra of Tagish Lake (C2ung) grains. Spectra were offset for clarity.

In general, infrared absorbance spectra of Tagish Lake presented here have similar spectral profile to that of NWA 852. Absorbance band identifications in Tagish Lake are as follows. Band A centered near 1000 cm^{-1} is due to Si-O stretch in silicates. Note that grain #3 presents somewhat sharper silicate band relative to grain #24. Carbonate region (band B) presents a strong and broad absorbance band centered near 1450 cm^{-1}. This band is due to C=O stretching of CO_3^{2-} in carbonates. Band C is due to combination of organics and water, and centered near 1680 cm^{-1}. Note that the shape of this band is significantly different than the one seen in NWA 852. Band D is comprised by sharp and distinct features between 3000 – 2800 cm^{-1}, and these features are due to symmetric and asymmetric stretching modes of CH_2 as well as CH_3 in aliphatic hydrocarbons. Finally, the broad band E centered near 3400 cm^{-1} is due to stretching mode of interlayer and/or adsorbed water. Although not as prominent, the broad O-H band is accompanied by a small feature at 3660 cm^{-1} due to structural O-H in phyllosilicates.

Finally, small structures near 2360 cm^{-1} are artifacts due to atmospheric CO_2. These identifications are in well agreement with reported works [60, 76].

4.3 Spectral cross section of grain

Figure 13 presents visible micrographs of the grain #3 and grain #24, as well as their corresponding infrared images at 2921 cm^{-1}. The 16 level color scale in rainbow sequence indicates absorbance, red being the highest in infrared images. The blue color lines in the two infrared images define spectroscopic line profiles considered for this study.

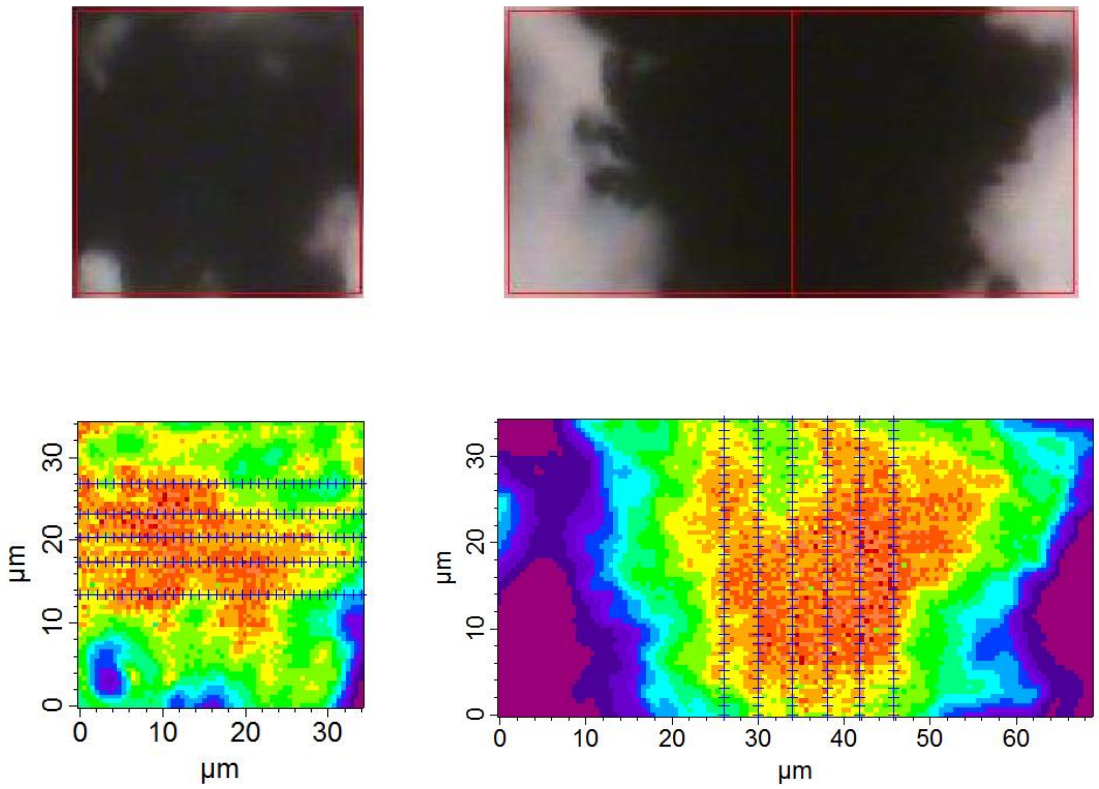

Figure 13: Visible micrographs (top), and infrared images (bottom) of the Tagish Lake grain #3 (left) and grain #24 (right) at 2921 cm^{-1}.

The spectroscopic line profiles were obtained for the slices across the grains indicated by the blue lines in the infrared images. (Figure 13, bottom). Each line drawn consists of pixels, each with an associated full range mid-infrared range spectrum. Alternate pixels were selected for data analysis with 1 μm separation. As representative, spectra extracted from the infrared image of grain #3 (forth slice from top in Figure 13) are presented in Figure 14 with the ordering of the curves bottom to top following a left to right scan across the grain.

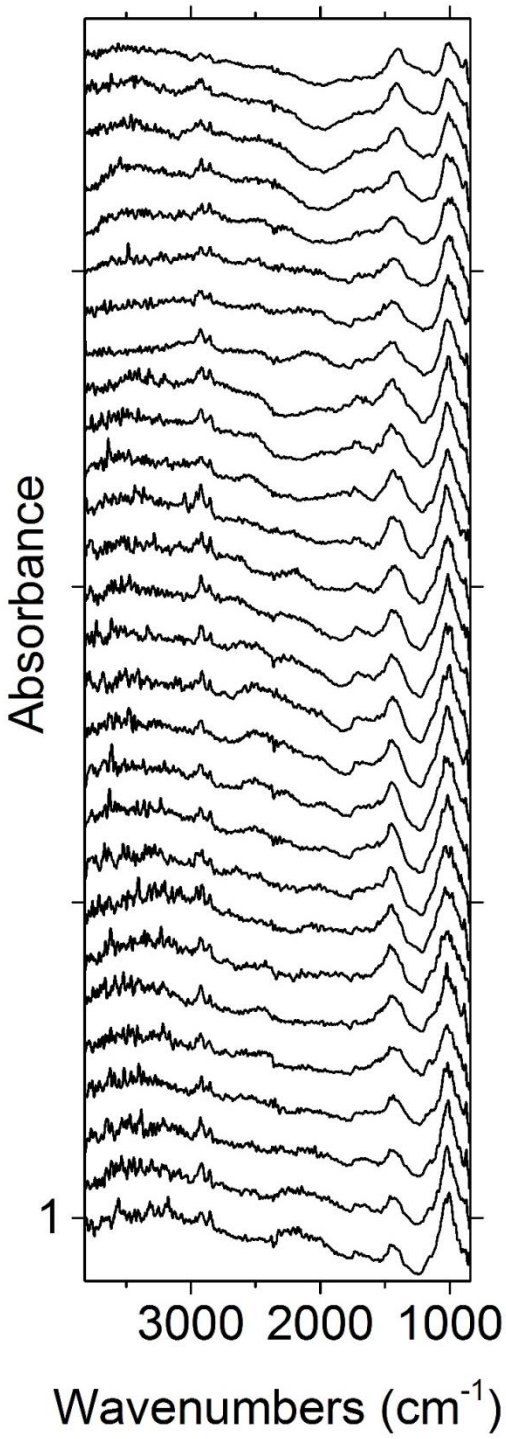

Figure 14: Spectral line profile of the fourth slice from top in the infrared image of the Tagish Lake grain #3 shown in Figure 13 (left). Each successive spectrum is offset vertically by 0.7 absorbance units for clarity.

Integrated intensity of each absorbance band in each spectrum was calculated individually. Figure 15 presents a comparison of these integrated intensities of bands A, B, C, D, and E. The most noticeable relation is the negative correlation between band B due to carbonates and band C due to certain organics and water in Tagish Lake, similar to the relation seen in NWA 852. Namely, integrated intensity of band B increases with decreasing intensity of band C, or vice versa. It is evident from Figure 14 and Figure 15 that each component has different spatial dependences, indicating that the relative concentrations are spatially non-uniform in Tagish Lake.

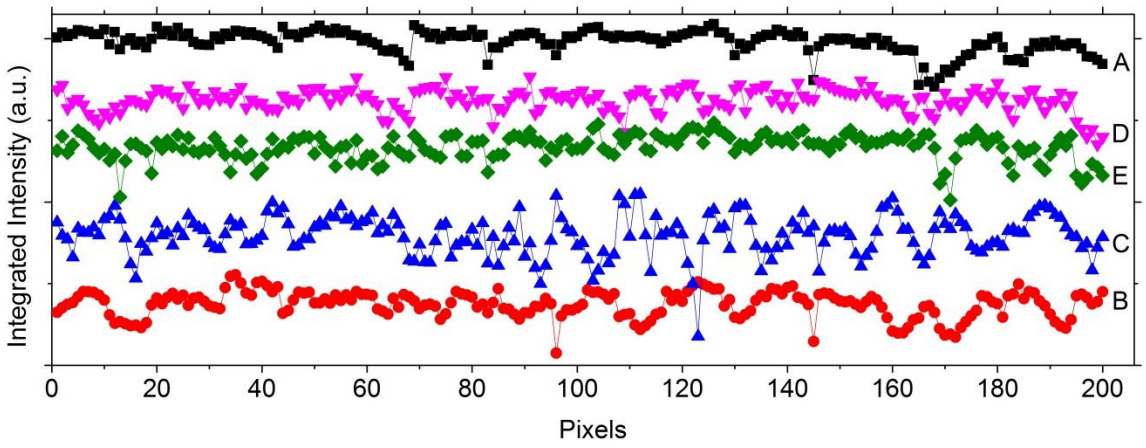

Figure 15: Comparison of integrated band strengths for the line profiles across the Tagish Lake grains. Letters in the legend represent the absorbance bands in Figure 12.

4.4 Pearson correlation coefficients

Across the meteorite grains, behavior of each component varies and these variations are presented in Figure 15. Statistical correlation analysis was performed in order to obtain relationships of organics and minerals quantitatively in the Tagish Lake dataset which consists of

integrated intensities of bands A, B, C, D, and E obtained from 200 infrared spectra. For this dataset, Pearson correlation coefficients were calculated following the procedure presented in Chapter 3. These correlation coefficients as well as their respective significance levels are collected in Table 6. Coefficients with "*"are significant at the 95% confidence level.

Table 6: Pearson correlation coefficients for Tagish Lake. Letters represent the absorbance bands in Figure 12.

		A	B	C	D	E
A	*Corr.*	1	0.40*	-0.04	0.35*	0.41*
B	*Corr.*		1	-0.26*	0.03	0.03
C	*Corr.*			1	-0.07	-0.05
D	*Corr.*				1	0.39*
E	*Corr.*					1

A: Silicates, B: Carbonates, C: Organics+water, D: Aliphatic hydrocarbons, E: OH

Correlation coefficients for Tagish Lake meteorite are presented in Table 6. A positive correlation (r=0.40) between band A (due to silicates) and band B (due to carbonates) is found. Note that this is opposite of what is found for NWA 852. Band D (due to aliphatic hydrocarbons) is correlated (r = 0.39) with band E (due to OH). Band A (silicates) is also correlated with the OH band E (r = 0.41) and also with the aliphatic hydrocarbon band D (r = 0.35). A negative correlation is found between absorbance bands B and C (r = - 0.26). This confirms what was noted in the qualitative discussion regarding Figure 18. Although with low confidence, band C shows a negative correlation with D (r = -0.07) and E (r = -0.05). Since B and C are negatively correlated, and C is positively correlated with D and E, it is intuitively expected that B is

negatively correlated with D and E. This is indeed the case in Tagish Lake, as shown in Table 6 that B is positively correlated with D and E.

4.5 Infrared spatial distribution maps of organic and mineral compounds

The infrared maps for Tagish Lake grains were obtained by integrating the infrared images shown in Figure 13 over ranges of frequencies wherever the spectral band of interest happens to be. These integrations were done after a linear baseline tangent to either endpoints of a band was subtracted from absorbance bands. Figure 16a-i presents these integrated absorbance maps of the Tagish Lake grains for the bands indicated by letters in Figure 12. The integration range for each map is as follows: Silicates: 850 – 1200 cm^{-1}, carbonates: 1200 – 1500 cm^{-1}, water + organics combination: 1500 – 1800 cm^{-1}, aliphatic hydrocarbons: 2800 – 3000 cm^{-1}, and finally O–H: 3000 – 3700 cm^{-1}.

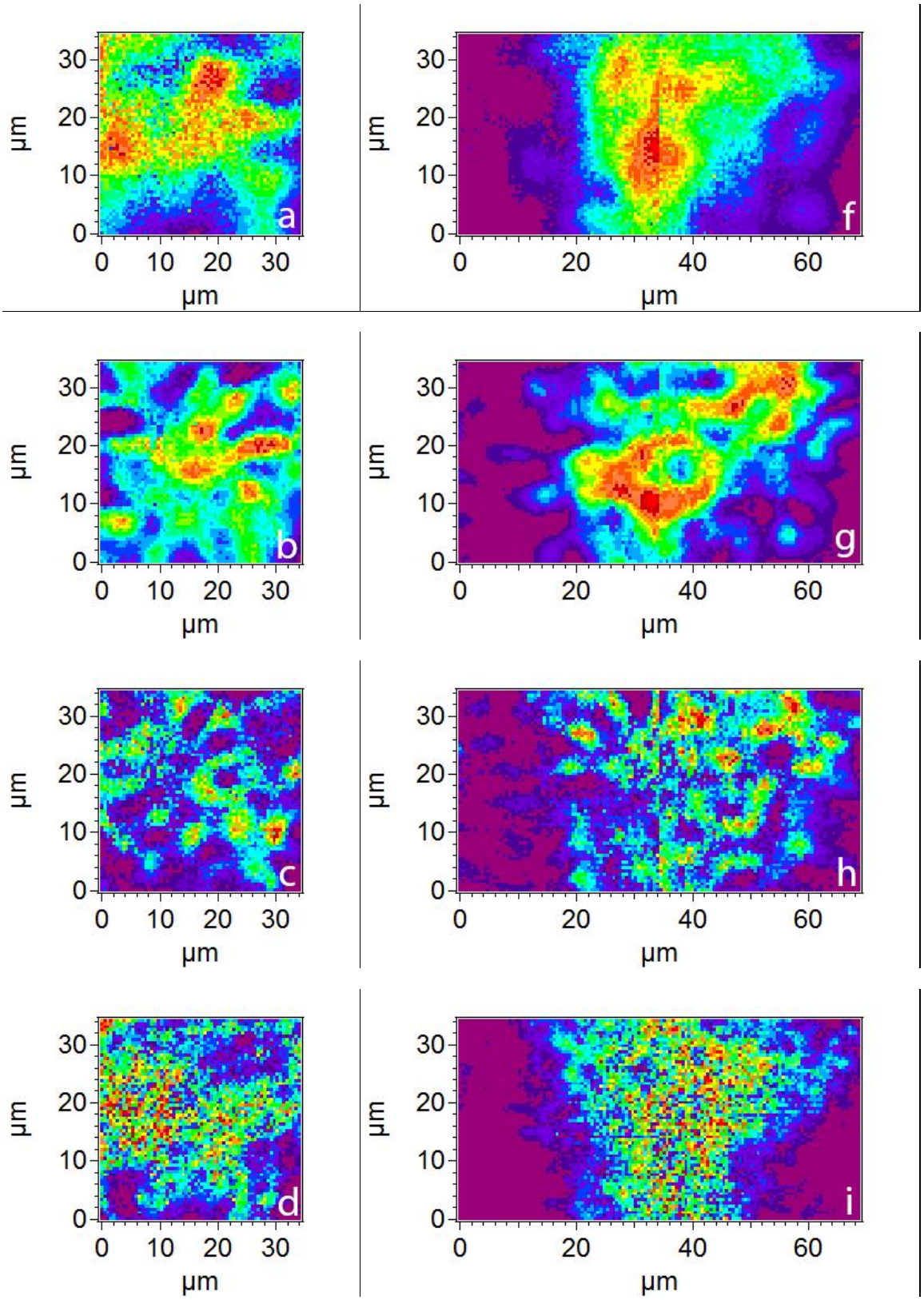
a
b
c
d
f
g
h
i
μm
0
10
20
30
40
60

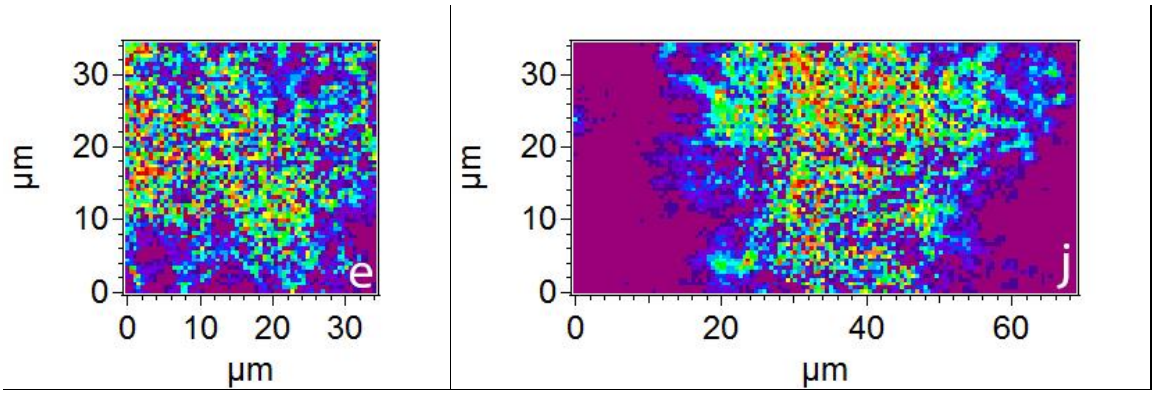

Figure 16: Integration maps of Tagish Lake grain #3 (left) and grain #24 (right) for characteristic absorbance features. a,f) Silicates; b,g) Carbonates; c,h) water + organics combination; d,i) Aliphatic hydrocarbons; e,j) O–H.

Silicates (band A) seem to be located within the centers of both grains. Carbonates (band B) partially overlap with silicates, and has a proportion which shows no overlapping but in close proximity. Carbonates also seem to be distributed adjacent to carbonyl and water combination (band C) with minor overlapping. Aliphatic C-H (band D) and O-H (band E) concentration seem to be distributed in a very similar way. They are distributed across the grain and almost uniformly. Both components therefore show overlapping with silicates for the most part.

4.6 CH_2 / CH_3 ratios

Sharp features due to C-H stretching modes in aliphatic hydrocarbons (band D) were observed in both Tagish Lake grains. We baseline corrected this region (3000 - 2800 cm^{-1}) by subtracting a straight line that is tangent to either end-points of the region in the grain-averaged spectrum of each grain (Figure 12). After linear baseline correction, the CH_2 / CH_3 absorbance ratio of both Tagish Lake grains were determined to have the average value of 2.57, which is compared in Table 5 (Chapter 3) to values reported for other meteorites, interplanetary dust

particles (IDPs), diffuse interstellar medium (DISM) objects, and cometary dust particles. The CH_2 / CH_3 ratio for Tagish Lake is similar to those of NWA 852, IDPs, and Wild 2 cometary dust particle. It exceeds CH_2 / CH_3 ratios of DISM and several carbonaceous chondrites of petrologic type 1 and 2. The grain-averaged ratio suggests that Tagish Lake is comparable to more primitive and less altered objects.

4.7 Discussion

4.7.1 Spectral signatures

Tagish Lake has two lithologies, carbonate-rich and carbonate-poor [53]. [60] studied carbonate-rich lithology of Tagish Lake, and reported presence of aliphatics, ketone or carboxylic group, and polyaromatic compound mainly composed of C=C. [75] reported, on the other hand, that carbonate-poor lithology contains aliphatics, esters, and aromatics. Based on these identifications as well as signatures we observed in both grains (e.g., abundant phyllosilicates, aliphatic organic matter, and water + organic combination), the Tagish Lake grains studied here belong to the carbonate-rich lithology of the meteorite.

A weak band near 1700 cm^{-1} is observed in spectra of both Tagish Lake grains. This band is due to C=O stretching in carbonyl compounds such as aldehyde and ketone. In general, presence of aldehyde is confirmed by an additional absorbance band near 2700 cm^{-1}, which is absent in the spectra presented here. This indicates absence of aldehyde, however note that ketone abundance must also be minor since the band near 1700 cm^{-1} is weak.

4.7.2 Spatial relations

Tagish Lake is known to have multiple lithologies, two of which are carbonate-rich and carbonate-poor. These two lithologies were distinct and easily recognized in Tagish Lake samples, suggesting that carbonates in Tagish Lake may be unique and different than in other meteorites. In previous studies of Tagish Lake, carbonates were found to rim phyllosilicates in some cases, and in others they were found to be intergrown with phyllosilicates [e.g., 53]. In terms of spatial relationships, the former (non-overlapping phyllosilicates and carbonates) would yield a negative correlation between the two, while the latter (overlapping phyllosilicates and carbonates) would yield a positive correlation. In our data, we found a positive correlation between phyllosilicates and carbonates. This correlation is somewhat small (0.40), which can be due to presence of non-overlapping regions of phyllosilicates and carbonates. It is evident from spatial distribution maps (Figure 16) that carbonates mostly overlap with silicates in both Tagish Lake grains, however there are concentration regions where carbonates do not overlap with silicates. Carbonates spatially appear to be concentrated adjacent to carbonyl concentration with minor overlapping. Aliphatic organic material seems to be distributed across the Tagish Lake grains. Similar is also true for O-H concentration (Figure 16a,j).

Spatial maps of organic matter in Tagish Lake studied here suggest highly homogeneous distribution of organics in this meteorite. This is consistent with the absence of bands near 2980 and 2990 cm^{-1} that are due to volatile organics [e.g., 89, 60].

Band C is due to combination of water and carbonyls with unknown proportions. No correlation between band C and band E was observed in Tagish Lake. Unlike Tagish Lake, NWA 852 and Orgueil shows strong positive correlations between band C and band E (see

chapters 3 and 6). Furthermore, band C and E are mostly due to water in Orgueil. This suggests that band C in NWA 852 is probably dominated by water with carbonyl contribution at lesser extent, and in Tagish Lake by carbonyl with water abundance at a lesser extent. This is also evident from the infrared spectra of meteorites, for instance band C is quite different in NWA 852 relative to the band in Tagish Lake.

4.7.3 CH ratios

[60] compared infrared spectral features of aliphatic organic material in Tagish Lake with those of organic material chemically extracted from Orgueil and Murchison, and found that Tagish Lake presents different spectral profile than Orgueil and Muchison, but similar to those of IDPs. Diffuse ISM spectra were found to be similar to the spectra of Murchison and Orgueil [85, 112]. Several groups obtained CH_2 / CH_3 ratios for IOM chemically extracted from meteorites through demineralization procedures. It was shown that acid treatment of meteorites alter the organics [89]. Therefore, we compare our results with those obtained from measurement of samples *insitu* and were not exposed to chemical processing. The CH_2 / CH_3 ratio for both Tagish Lake grains in this study was found to be 2.57. Although this is lower than what was found (4.3) in [60], it is still quite higher than the ratio ~1.17 for DISM [84], 1.40 for Orgueil [64], and 1.00 for Murchison [64]. On the other hand, ratio for Tagish Lake is very close to the ratio 2.53 for NWA 852 [65], ~2.40 for IDPs [83].

4.8 Conclusions

We presented relationships among organics and minerals in Tagish Lake, an ungroupped C2 chondrite, with mid-infrared synchrotron-based imaging micro-FTIR spectroscopy. Spectroscopic line profiles for two Tagish Lake grains studied here show that the relative intensity of the characteristic absorbance bands varies across the grain on 1 micron length scales. Statistical correlation analysis shows that the silicate band is positively correlated with OH and CH bands, which are also correlated with each other. Negative correlation is observed between carbonate band and the water + organic combination band. Concentrations of these two components have clear spatial separation within the grains studied here.

Carbonate bands in Tagish Lake are positively correlated with silicate bands. This is opposite of what is seen in NWA 852 (Chapter 3) and Orgueil (Chapter 5), and perhaps due to unique nature of carbonates and/or formation conditions in Tagish Lake.

The average CH_2 / CH_3 ratio for Tagish Lake indicates a predominance of CH_2 over CH_3 that is comparable to that in IDPs and Wild 2 cometary dust particles. The ratio exceeds that for DISM and several carbonaceous chondrites, indicating longer carbon chain lengths and/or smaller degree of branching. This may also indicate similar origin, formation, and/or processing of organic matter in Tagish Lake, NWA 852, IDPs, and Wild 2 particles, but rather different than diffuse ISM organic matter.

CHAPTER FIVE: ORGANIC AND INORGANIC CORRELATIONS IN ORGUEIL

5.1 Introduction

Orgueil meteorite fell on 14 May 1864 in France. It is classified as a CI1 chondrite. Its petrology and mineralogy shows signatures of extensive aqueous alteration. Aqueous alteration in CI chondrites occurred at temperatures no higher than 50 – 100 ºC [49].It is believed that the lack of chondrules in Orgueil is due to such extensive alteration. CI chondrites show similar but not exclusively same infrared spectra to CM chondrites [91]. Orgueil spectra show presence of abundant phyllosilicates (mostly serpentine, saponite, and montmorillonite), carbonates, aliphatic and aromatic organic matter, and abundant water. It is known to be the most volatile-rich meteorite to date, and contain more than 3 wt% carbon [6, 48]. Using gas chromatography mass spectroscopy, [92] found that Orgueil contains only aromatic acids and not aliphatic acids.

Here we present infrared spectral signatures, correlation coefficients and spatial distribution maps of organic as well as inorganic material present in an Orgueil grain. Grain-averaged infrared spectrum of Orgueil shows prominent absorbance bands that are due to silicates, carbonates, aliphatic organic matter, and water (Figure 17).

5.2 IR spectral signatures

Single 34 µm x 68 µm size Orgueil grain was studied. Figure 17 presents the spatially grain-averaged mid-infrared spectrum of the grain. Lettered arrows indicate positions of distinct and identifiable absorbance bands due to specific functional groups present in this particular grain.

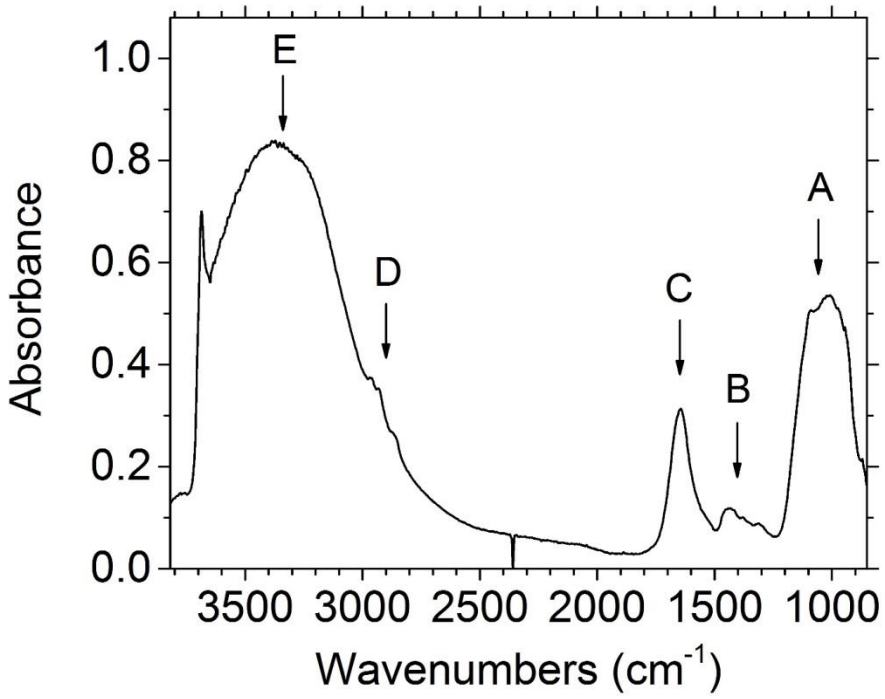

Figure 17: Average absorbance spectrum of Orgueil (CI1) chondrite grain.

Band A is due to the Si-O stretch of silicates. Sharp and distinct band at 3690 cm^{-1} is due to OH in phyllosilicates, possibly serpentine and saponite. Presence of this band indicates high abundance of phyllosilicates in this particular Orgueil grain. Band A, therefore, is due to phyllosilicates. Band C and E are due to bending and stretching vibrations of interlayer and/or adsorbed water in Orgueil, respectively. Band B is due to carbonates with minor contribution from bending mode of C-H. Symmetric and asymmetric stretching modes of aliphatic C-H are represented by weak but distinct structures between 2800 – 3000 cm^{-1}, labeled as band D. Small structure near 2360 cm^{-1} is an artifact due to atmospheric CO_2.

5.3 Spectral cross section of the meteorite grain

Figure 18 presents visible micrograph of the grain as well as the infrared image at 2921 cm^{-1}. The 16 level color scale in rainbow sequence indicates absorbance, red being the highest in infrared images. The blue color vertical lines define spectroscopic line profiles.

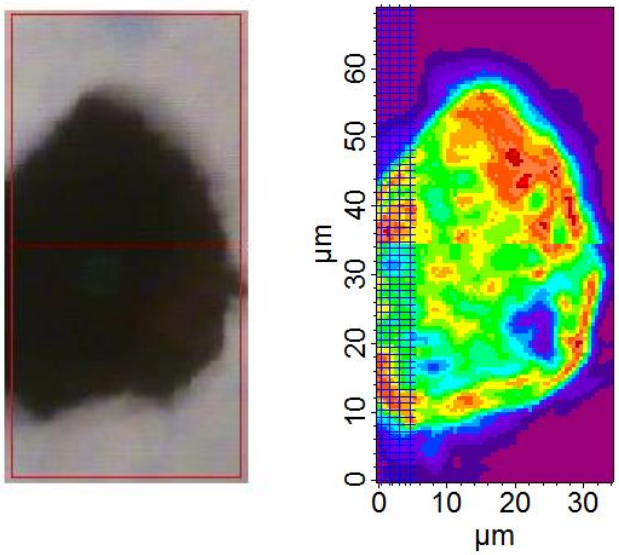

Figure 18: Visible micrograph (left), and infrared image of the Orgueil grain at 2921 cm^{-1} (right).

The spectroscopic line profile across the grain is obtained for the slices indicated by vertical lines on the infrared image in Figure 18 (right). As seen from this figure, there are parts of the vertical lines that correspond to sample-free regions in the field of view, however pixels that correspond to these grain-free regions were eliminated, and remaining pixels were selected for data analysis with 1 µm separation. As representative, the spectra of the second slice from left shown in the infrared image are presented in Figure 19 with the ordering of the curves bottom to top following a bottom to top scan across the grain.

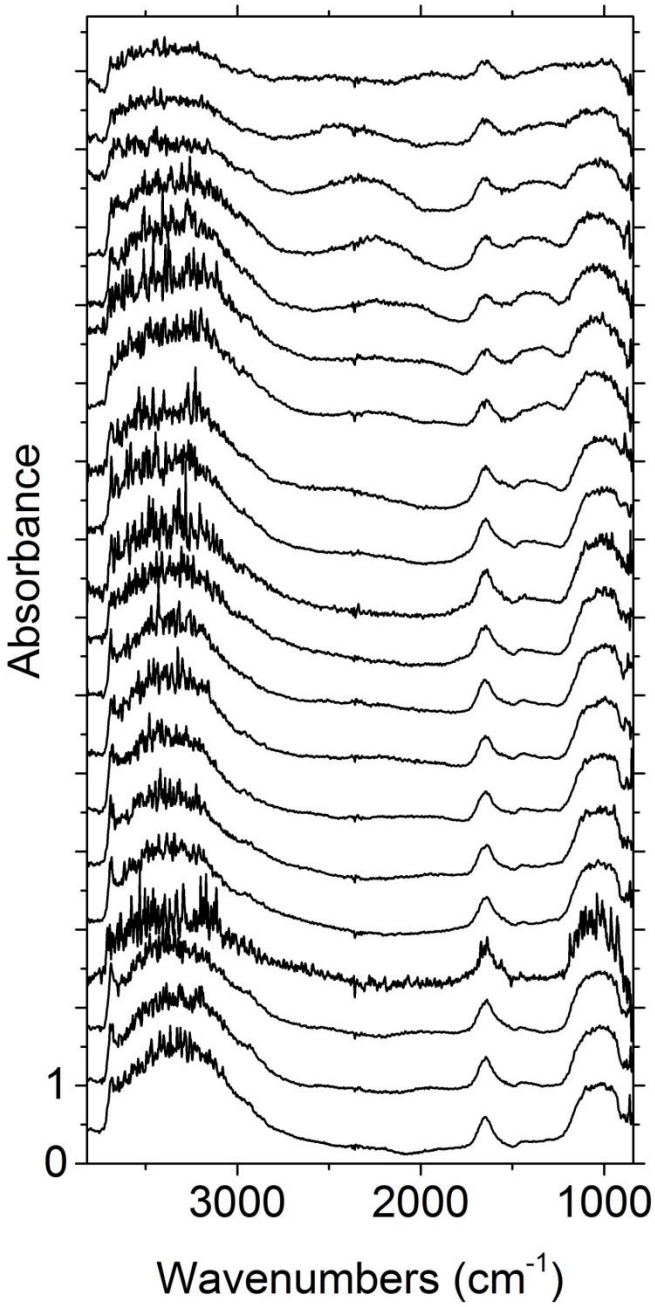

Figure 19: Spectral line scan of the second cut from left in the infrared image of the Orgueil grain shown in Figure 18 (right). Each successive spectrum is offset vertically by 0.7 absorbance units for clarity.

Figure 20 presents a comparison of integrated intensities of bands A, B, C, D, and E. As in NWA 852 and Tagish Lake, the most noticeable effect in Orgueil is the negative correlation between band B due to carbonates and band C due to water in Orgueil. Band A seems to be correlated with band E. Their integrated intensity also drops near four regions that correspond to the upper edge of the meteorite grain. Band D, due to aliphatic organics, seems to stay flat across the grain. Further interpretation of bands from Figure 20 is somewhat challenging, however, as in NWA 852 and Tagish Lake, it is evident from Figure 19 and Figure 20 that each component has different spatial dependences, indicating that the relative concentrations are spatially non-uniform in Orgueil.

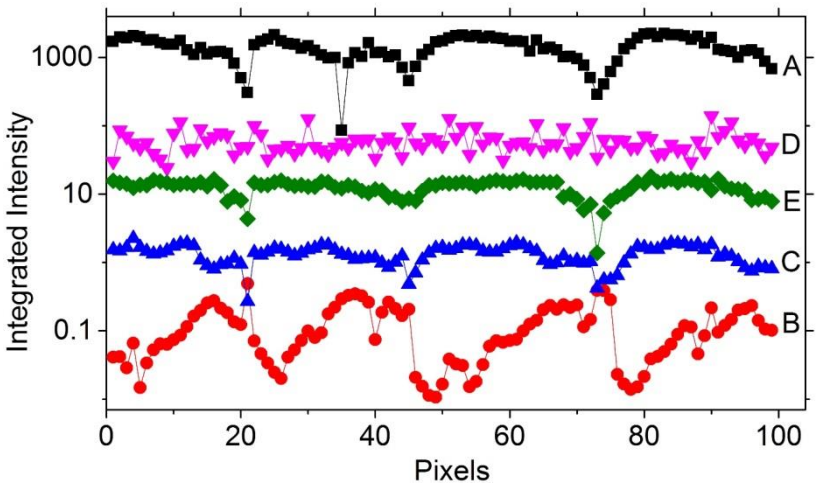

Figure 20: Comparison of integrated band strengths for the line scans across the Orgueil grain. Letters represent the absorbance bands in Figure 17.

5.4 Pearson correlation coefficients

Our dataset for the Orgueil grain consists of integrated intensities of bands A, B, C, D, and E obtained from 99 spectra. For this dataset, Pearson correlation coefficients were calculated

following the same procedure shown above in Chapter 3. Obtained correlation coefficients as well as their respective significance levels are collected in Table 7. A small value for significance indicates high confidence. Coefficients with "*"are significant at the 95% confidence level.

Table 7: Pearson correlation coefficients for Orgueil. Letters represent the absorbance bands in Figure 20.

		A	B	C	D	E
A	*Corr.*	1	-0.67*	0.75*	0.08	0.75*
B	*Corr.*		1	-0.60*	0.04	-0.53*
C	*Corr.*			1	0.02	0.73*
D	*Corr.*				1	-0.04
E	*Corr.*					1

A: Silicates, B: Carbonates, C: Water, D: Aliphatic hydrocarbons, E: OH

Correlation coefficients for Orgueil are presented in Table 7. A strong negative correlation (r = -0.67) was observed between silicate band (band A) carbonates (band B). This is similar to the case in NWA 852, however opposite of what is observed in Tagish Lake. Silicate band is also positively correlated (r = 0.75) with OH (band E). Similar to NWA 852 and Tagish Lake, a negative correlation (r = - 0.60) is found between carbonates (band B) and water (band C). The latter is also strongly negatively correlated (r = -0.73) with OH (band E). Note that band D is due to aliphatic organics, and it is not correlated with any of the bands. This could be due to lack of absorption from aliphatic organic matter near 3000 – 2800 cm^{-1}, evident from the infrared spectrum of the Orgueil in Figure 17. Another reason could be the origin of these aliphatic type organics. Since carbonate and water bands are negatively correlated, and water band is positively

correlated with OH band, it is expected that carbonate band is negatively correlated with the OH band. This is indeed the case in Orgueil, as shown in Table 7 that carbonate band is negatively correlated with OH band. It is important to remark that, unlike NWA 852 and Tagish Lake, band C in spectra of Orgueil is merely due to water, and it is not surprising that C is positively correlated with E. Similarly, it makes sense that silicates (band A), water (band C), and OH (band E) are all positively correlated with each other.

5.5 Spatial distribution maps of organic and mineral compounds

Infrared maps were used here to infer the relative amounts of organic molecules or inorganic minerals present at particular locations within the Orgueil grain. The infrared maps were obtained by integrating the infrared image shown in Figure 18 over the ranges of frequencies of the spectral bands of interest. Similarly, these integrations were done after a linear baseline was subtracted from between the endpoints of each band. Figure 21 presents these integrated absorbance maps of the Orgueil grain for the bands indicated be letters in Figure 17. The integration range for each map is as follows. Silicates: 850 – 1200 cm^{-1}, carbonates: 1200 – 1500 cm^{-1}, water: 1500 – 1800 cm^{-1}, aliphatic hydrocarbons: 2800 – 3000 cm^{-1}, and finally O-H: 3000 – 3700 cm^{-1}.

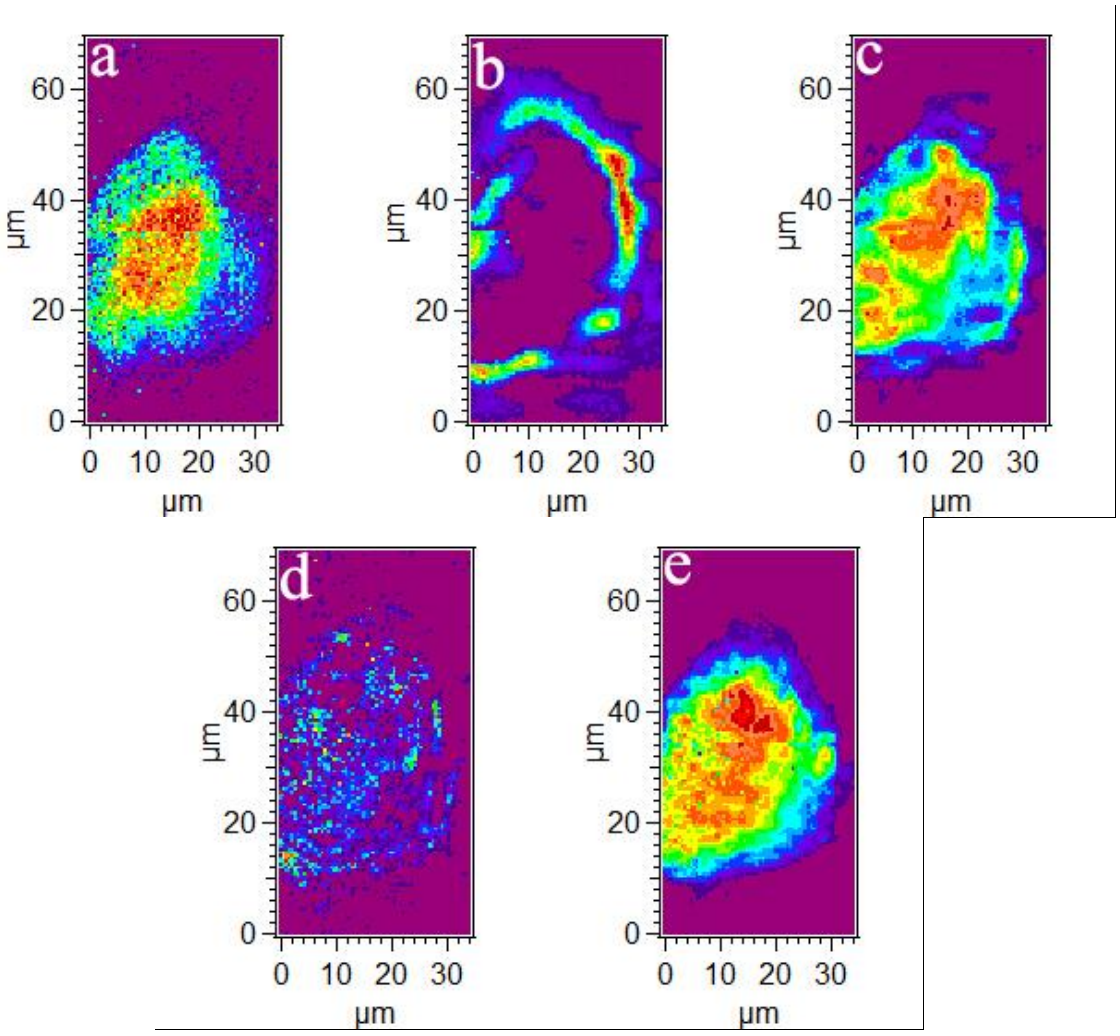

Figure 21: Integration maps of Orgueil for characteristic absorbance features. a) Silicates, b) Carbonates, c) Water, d) Aliphatic hydrocarbons, e) O–H.

Spatial distribution maps presented in Figure 21 show that silicates (Fig. 21a) are concentrated within the center of the meteorite grain. Water (Fig. 21c) and OH (Fig. 21e) concentrations also seem to be distributed near the center of the grain, with slightly more concentration towards the upper-half of the grain. Nevertheless, these three components have significant overlapping. On the other hand, carbonates (Fig. 21b) are distributed only around the outer edges of the grain, and have no overlapping with any of the components. Spatial

distribution of aliphatic CH (Fig. 21d) is somewhat homogeneous across the grain, and its significantly low concentration is consistent with the infrared spectrum shown in Figure 17.

5.6 CH_2 / CH_3 ratios

In order to obtain CH_2 / CH_3 ratio of Orgueil, we baseline corrected the band D region (2800-3000 cm^{-1}) by subtracting a straight line that is tangent to either end-points of the region in the grain-averaged spectrum of Orgueil (Figure 17), after which the CH_2 / CH_3 absorbance ratio was determined to have the value of 1.33. This value is compared in Table 5 to values reported for other meteorites, interplanetary dust particles (IDPs), diffuse interstellar medium (DISM) objects, and cometary dust particles. Orgueil presents one of the lowest CH_2 / CH_3 ratios among the objects listed in Table 5. As opposed to NWA 852 and Tagish Lake, Orgueil's CH_2 / CH_3 value is similar to DISM objects and several type 1 and 2 carbonaceous chondrites, however clearly lower than those of IDPs, and Wild 2 cometary dust particle.

5.7 Discussion

Infrared spectrum of Orgueil is different than those of NWA 852 and Tagish Lake in several ways. For instance, Orgueil has a sharp and distinct band near 3690 cm^{-1}. This band is absent in NWA 852, and almost completely absent in Tagish Lake. This difference is simply due to composition of phyllosilicates that are present in the chemical composition of the meteorites. As seen from the infrared spectra of these meteorite samples, they all present different spectral profile for the silicate band. Additionally, this compositional variety between the three meteorites is probably due to parent body aqueous alteration processes and their extents. In fact, Orgueil is

petrologic type 1 whereas NWA 852 and Tagish Lake are type 2 carbonaceous chondrites. Moreover, absorbance band near 1650 cm^{-1} in spectra of Orgueil is due to only water, however this band includes additional features in spectra of NWA 852 and Tagish Lake due to presence of organic compounds.

Carbonates (band B) in Ogueil shows strong negative correlation with water (band C) and OH (band E). Although carbonates are secondary products of aqueous alteration, this negative correlation is perhaps due to extent, type, temperature, and duration of aqueous alteration in the parent body of Orgueil, which spatially affected the distribution of carbonates. The fact that aliphatic CH stretching (band D) has no relation of any kind with any of the other components in Orgueil is may be due to low concentration of aliphatic organics, however the statistical analyses is independent of the range of variables, therefore this is not plausible. Another reason could be the origin of aliphatic hydrocarbons in Orguil, as well as processing they may have undergone (i.e., interstellar origin vs. nebular origin).

The CH_2 / CH_3 ratio of Orgueil studied here is 1.33. This value is in agreement with previous reports of Orgueil's CH_2 / CH_3 ratio, value of 1.5 by [112] and 1.4 by [64]. This ratio is very similar to ratios of other astronomical objects such as Murchison and DISM objects, (Table 5). Additionally, [72] found CH_2 / CH_3 ratio of Paris meteorite (CM chondrite) as 1.8, and showed that composition of Paris may have interstellar organic material. Perhaps, Orgueil preserved an interstellar aliphatic organic matter that gives rise to a CH ratio of 1.33. We also note that CH_2 / CH_3 ratio of Orgueil is also significantly lower than those of NWA 852 (2.53), Tagish Lake (2.57), IDPs (2.31, 2.46), and Wild 2 cometary particles (2.5), whose aliphatic organic matter may be of nebular origin, and not interstellar. Nevertheless, CH_2 / CH_3 ratio of

1.33 suggests more complicated branching and/or shorter aliphatic chains in Orgueil compared to others discussed above.

5.8 Conclusions

In this chapter, I presented infrared spectral signatures as well as correlations of organics with minerals in an Orgueil grain. Infrared spectrum of the grain suggests abundant phyllosilicates and water, carbonates, and aliphatic hydrocarbons (although very little). Unlike other meteorite samples studied here, the band near 1650 cm^{-1} is merely due to water with no contribution from organics. Spatial distribution maps of Orgueil suggest that silicates are strongly positively correlated with water and OH bands, but strongly negatively correlated with carbonates. Additionally, aliphatic hydrocarbons in Orgueil has no correlation with any of the components, most likely to be due to origin and/or processing history of aliphatic organic matter in this particular grain. The CH_2 / CH_3 ratio of Orgueil is in well agreement with previous reports. This ratio is similar to those of DISM object, Murchison, and Paris, however significantly lower than NWA 852, Tagish Lake, IDPs, and Wild 2 cometary particles. This suggests perhaps Orgueil contains aliphatic organic matter of interstellar origin. This also suggests different type of parent body processing in these objects. In any case, aliphatic hydrocarbons in Orgueil are shorter in length and/or more branched than those of objects discussed above.

CHAPTER SIX: INFRARED IMAGING SPECTROSCOPY WITH MICRON RESOLUTION OF SUTTER'S MILL METEORITE GRAINS

6.1 Introduction

The Sutter's Mill (SM) meteorite is a regolith breccia composed of a variety of CM1 and CM2 clasts in a CM type matrix [55, 95]. The meteorite is officially classified as "C" chondrite. The material is of interest because it represents surface material from a primitive asteroid, the target of upcoming space missions OSIRIS-REx and Hayabusa 2. The meteorite fell in El Dorado County in California on 22 April 2012, and the first three meteorites were found before rains hit the area (now numbered SM1, 2 and 3). In total, 77 meteorites were recovered from this fall. Meteorite SM12 was collected from the field during a volunteer search coordinated by NASA Ames Research Center.

An initial study by members of the Sutter's Mill meteorite consortium found that individually recovered meteorites showed a range for the signatures of aqueous alteration and thermal metamorphism [55]. Based on Raman spectra of macromolecular carbon and using the method of [94], Marc Fries and coworkers found that parts of SM2 experienced temperatures no higher than 153 ± 27 ºC, whereas SM12 reached up to 268 ± 42 ºC. As part of this study, Monica Grady and coworkers found that SM contains the lowest known $\delta^{15}N$ (ratio of stable isotopes $^{15}N/^{14}N$) among CM2 chondrites, which may mean that SM has N-bearing organic molecules whose compositions are different than those in other CM2 chondrites.

These temperature history and compositional differences immediately raise questions about how they occurred and what they may tell us about the formation and evolution of the CM chondrite parent body. For example, individual clasts may sample different temperature and

aqueous alteration histories on the surface of the parent body. Another possibility is that the Sutter's Mill meteorite is an aggregate of fragments that originated from different parent body asteroids, or perhaps even of comets [55].

In this paper, we investigate the thermal and aqueous alteration history of the materials further using synchrotron-based Fourier transform infrared (FTIR) microspectroscopy in the range of 3850 – 900 cm^{-1} and micro-Raman spectroscopy in the range of 2200 – 800 cm^{-1}. Spectral signatures and spatial distribution of organics as well as minerals are investigated *in-situ* in multiple grains from SM2 and SM12, mapping the different functional groups with micron spatial resolution. This work compliments the infrared study by [95] and [96], which investigated differences among SM meteorites on a larger spatial scale.

6.2 Samples and Experimental Details

We received samples of SM2 (pre-rain fragment) and SM12 (post-rain fragment) in the form of chips through the Sutter's Mill meteorite consortium. SM2 was found by Peter Jenniskens in fragmented form on the surface of a parking lot, likely crushed by a car [55]. It was collected in aluminum foil and stored in a freezer at NASA Ames prior to rain hitting the area, but it may have been contaminated to some extend by the asphalt of the parking lot surface and any other organic material that came in contact with the meteorite, such as a car tire and compounds in the air. Nevertheless, [93] reported finding oldhamite in a small chip of SM2, a mineral very sensitive to water. Our sample of SM2 came from an internal part of the rock, which had no direct contact with the asphalt surface. Studies of amino acids [97], which are

present in the meteorite at only very low level, showed that SM2 and SM12 may contain amino acids of terrestrial origin, but the extent of the contamination is ambiguous.

The fully crusted SM12 was recovered after the heavy rain [55]. It was found stuck on a narrow side path in (dried up) muddy soil, from which the porous meteorite may have picked up contaminants. It was briefly touched, then collected in aluminum foil and stored in a freezer at NASA Ames Research Center. The SM12 chip studied here came from the center of a stone, at least 0.5 cm from the nearest fusion crust.

We ground each sample in a mortar and pestle down to tens of micrometer size grains. These grains are expected to represent the different lithologies in the chips studied here. Subsequently, these grains were placed on a diamond window, which was placed under the infrared microscope for transmission measurements, or on a silicon substrate for micro-Raman measurements. Detailed procedures for these experiments are described in Chapter 2 of this dissertation.

6.3 Results

6.3.1 Micro-Raman spectroscopy

The structural order of the carbonaceous material in each grain was inferred from the Raman peak positions, intensities, and widths of D (disordered) and G (graphite) bands, which are located near 1370 and 1600 cm^{-1}, respectively [86]. The D band is due to disordered sp^3 carbons, whereas the G band is due to graphite-like sp^2 carbon bonds [98]. The spectra of 5 grains from each SM fragment in the region of 2200 – 800 cm^{-1} are presented in Figure 22. Spectra are offset vertically from each other for clarity. Vertical lines indicate the positions of the

D and G bands. A linear baseline was subtracted from each spectrum, which was then fit to a pair of Lorentzians to determine peak characteristics such as peak centers, widths, and relative intensities of the D and G bands.

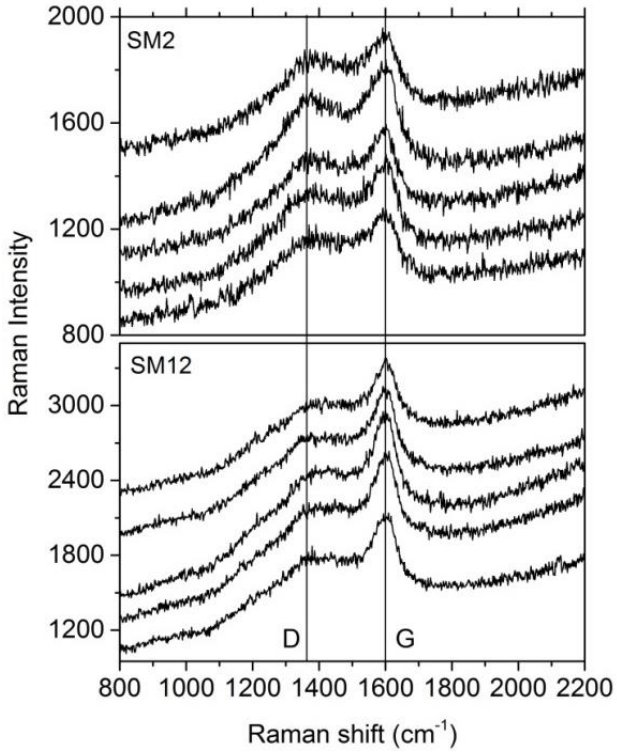

Figure 22: Micro Raman spectra of multiple SM2 and SM12 grains from the Sutter's Mill meteorite.

Figure 23 presents the Full Width at Half Maximum (FWHM) of the G band versus its center frequency. Our results for SM2 and SM12 grains are in good agreement with data from Fries and coworkers presented in [55]. The trends marked by arrows characterize the degree of thermal metamorphism and disorder of the carbon [55, 86]. According to Figure 23, the G-bands of SM2 grains are all wider and redder than those of the SM12 grains studied here. Increasing

disorder of C is known to red shift the G-band [86]. Thus, we confirm from different parts of the meteorites SM2 and SM12 than studied by [99] that the macromolecular carbon in SM2 is relatively more disordered and SM12 is thermally more metamorphosed. SM2 and SM12 show evidence of heating to an intermediate degree while CR1, CR2, and CM2 chondrites show relatively less thermal alteration, unlike CV3 chondrites (Fig. 23).

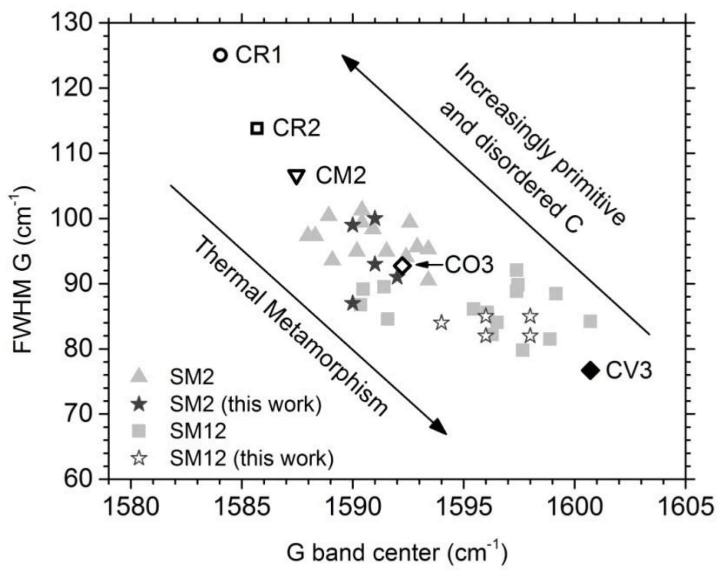

Figure 23: FWHM of G-band versus the G-band center for SM2 and SM12 grains from this study plotted with data by Marc Fries (from [55]).

[94] proposed a thermometry, which combines Raman spectroscopy with thermometric relationship by [86], and obtained the following relationship between effective metamorphism temperature (T_{EFF}) and Raman G-band FWHM (Γ_G),

$$T_{EFF}\ (^{o}C) = 1594.4 - 20.4\ \Gamma_G + 5.8 \times 10^{-2}\ \Gamma_G^2 \ldots\ldots\ldots\ldots\ldots\ldots\ldots\ldots \ (5)$$

Raman G-band FWHM of our SM2 grains varies from 87 to 100 cm^{-1}, and from 82 to 85 cm^{-1} for SM12 grains. Using these parameters and equation (5), we obtained T_{EFF} = 134º - 259ºC for SM2 grains, and T_{EFF} = 279º - 312ºC for SM12 grains. These values are in good agreement with the values of 153º ± 27ºC for SM2 and 268º ± 42ºC for SM12 reported earlier [55].

6.3.2 Micro-FTIR spectroscopy

The spatially-resolved infrared spectra of SM2 and SM12 grains show variations due to the compositional heterogeneity. Figure 24 presents representative infrared spectra of different SM2 and SM12 grains, each ~15 - 30 μm in diameter. Labels enumerate the individual grains that appear in our field of view. Our assignments of the observed IR absorption bands, following [100], are summarized in Table 8. The strongest feature in all spectra (except SM12 grain #1) is a broad band centered around 1080 – 900 cm^{-1} due to Si-O stretching vibrations within silicate minerals. Most spectra also exhibit a broad band centered around 1500 – 1400 cm^{-1} due to asymmetric stretching vibrations of the CO_3^{2-} ion within carbonate minerals, a band at 1640 cm^{-1} due to the H-O-H bending modes of water, and a broad band around 3700 – 3000 cm^{-1} due to O-H stretching modes. Some spectra reveal weak but sharp structures in the range 3000 – 2800 cm^{-1} due to the C-H stretching vibrational modes within aliphatic hydrocarbons. Most of the bands tend to be broad in these spectra because each such band represents the average over the grain of different minerals from the same group (e.g., different carbonates).

Table 8. Positions and interpretation of the observed infrared bands.

Position (cm^{-1})	Mode	Assignment
870 – 910	Si-O	Olivine
950 – 1000	Si-O	Olivine + Pyroxene + Phyllosilicates
1070 – 1080	Si-O	Pyroxene
1150 – 1180	SO_4	Sulfates
1240	Unknown	Unassigned
1410 – 1480	CO_3	Carbonates
1625	C=C	Aromatic
1640 – 1650	H-O-H	Water
2350	CO_2	Atmospheric
2800 – 3000	C-H	Aliphatic
3000 – 3700	O-H	Water
3650	O-H	Phyllosilicates

In Figure 24, there are three main peaks observed within the Si-O stretching region of SM2. These appear at 1080 – 1070 cm^{-1}, 1000 – 970 cm^{-1}, and 900 cm^{-1}, which are assigned to pyroxene, pyroxene + olivine, and olivine, respectively. Unlike SM2, infrared spectra of SM12 grains present a single band at ~1000 cm^{-1}, and a small structure appears near 3650 cm^{-1} due to O-H. These are typical features of phyllosilicates. The presence of a phyllosilicate O-H feature at 3650 cm^{-1} in spectra of SM2 grains is more ambiguous, suggesting lesser phyllosilicate abundances.

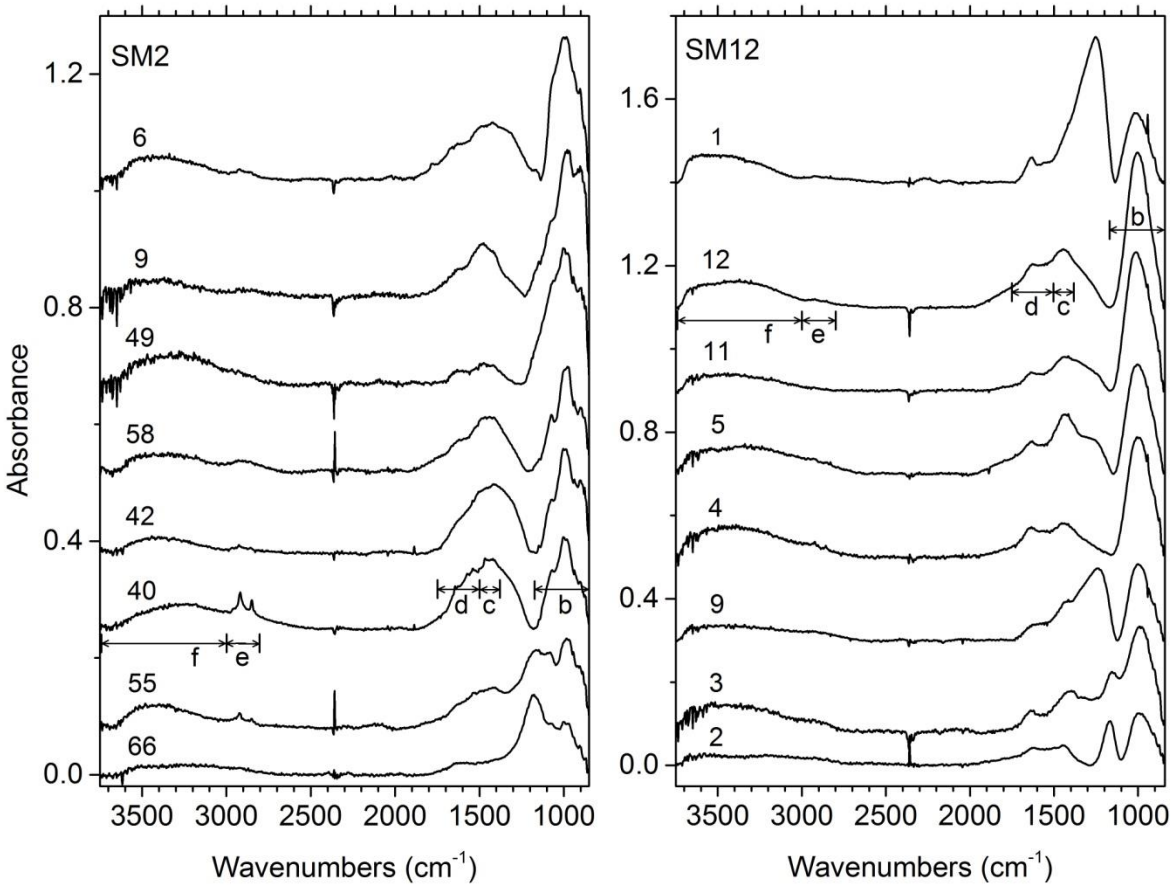

Figure 24: IR absorbance spectra of individual SM2 and SM12 grains. Labels enumerate the grains in the field of view. Each spectrum is offset for clarity.

Shape and position of the carbonate band varies with carbonate species. For instance, the band center in dolomite appears at higher frequencies than in calcite. Absorbance bands in the spectra of SM2 and SM12 grains near 1450 cm^{-1} suggest an abundance of carbonates. Compared to the spectra of SM12 grains, SM2 grains have broader absorbance bands with more spectral variations near the carbonate region, which indicates a greater variety of carbonate species in SM2 grains than in SM12.

All Sutter's Mill meteorite grain spectra show absorbance bands between 3700-3000 cm^{-1} and at 1640 cm^{-1} due to H-O-H stretching and bending vibrational modes of water, respectively. A weak feature at 3650 cm^{-1} is observed in spectra of SM12 grains due to structural O-H in phyllosilicates, as already noted. We remark that the contribution of telluric water absorbed by minerals in SM12 meteorite should be very low, because the absorbed water evaporates very quickly from the small grains. The band at 1640 cm^{-1} likely also includes significant contributions from carbonyl (C=O) and aromatics (C=C) which appear near 1700 cm^{-1} and 1600 cm^{-1}, respectively. The carbonyl band near 1700 cm^{-1} [64] amounts to only a small bump or shoulder in some spectra, so that its comparatively insignificant contribution will be ignored in the subsequent discussion. Spectra of a few SM2 grains show aliphatic C-H stretching peaks between 3000 and 2800 cm^{-1} due to organics, but these peaks are very weak in spectra of SM12 grains.

Some spectra in both SM2 and SM12 show a band centered at 1180 – 1150 cm^{-1}. The origin of this band is currently unknown, but it is within the range of sulfates [100]. Some SM12 spectra show a large band at 1240 cm^{-1}, which is also currently unidentified.

6.3.3 Spatial distributions

Absorbance maps of specific infrared absorption bands reveal the spatial distributions and relationships between different minerals and organic molecules within individual meteorite grains [e.g., 65,66]. We present such maps for one grain each of SM2 and SM12, whose grain-averaged spectra were presented in Figure 24. We integrated the spectrum for each individual pixel over ranges given in Table 9 and indicated in Figure 24 (for the two grains studied) by

horizontal lettered bars. Infrared absorbance maps of specific functional groups for SM2 grain #40 and SM12 grain #12 are presented in Figures 25 and 26, respectively.

Table 9: Integration ranges for spatial distribution maps.

Group	Integration range (cm^{-1})
OH	3750 – 3000
Aliphatic CH	3000 – 2800
H_2O + aromatics	1750 – 1500
Carbonates	1500 – 1380
Silicates	1170 – 850

For instance, for carbonates we integrated from 1500 to 1380 cm^{-1}. In these spectra of individual pixels, the carbonate bands can be narrower than the full 120 cm^{-1} width of the integration window. However, this window insures that we catch the carbonate band, wherever its center frequency happens to be. This allows the automatic analysis of thousands of spectra, without having to separately inspect each one, with good confidence that the result represents carbonate intensity.

Figure 25a presents the visible microscope image of SM2 grain #40. The other parts of Figure 25 are infrared images giving spatial distributions for different compounds in this grain. The negative correlation between carbonates (Fig. 25c) and H_2O + aromatic C=C (Fig. 25d) is very strong. The negative correlation between carbonates and CH (Fig. 25e) is also strong. There is no significant correlation between H_2O+aromatic C=C stretch (Fig. 25d) and OH (Fig. 25f), which should be due to both water and phyllosilicates. This confirms the significant contribution from aromatic C=C, besides the H_2O, in the 1750 – 1500 cm^{-1} integration range. There exists a somewhat positive correlation between aliphatic C-H (Fig. 25e) and silicates (Fig. 25b). There is no significant correlation between aliphatic C-H and OH (Fig. 25f).

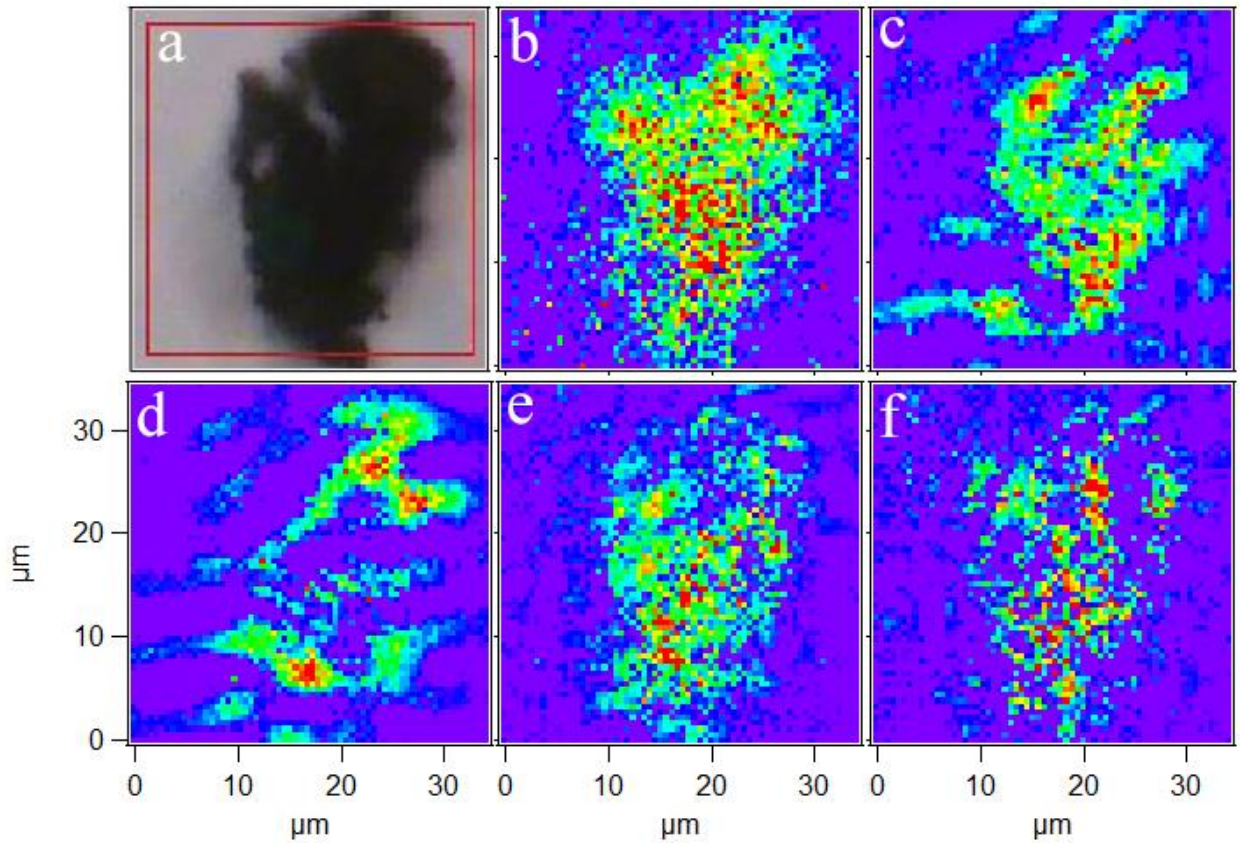

Figure 25: Spatial distributions of characteristic absorbance in SM2 grain #40: a) Visible micrograph; b) Silicates, c) Carbonates, d) H_2O + aromatic C=C stretch, e) Aliphatic C-H stretch, f) OH.

Figure 26a presents a visible microscope image of SM12 grain #12 together with infrared images giving spatial distributions of different compounds in SM12 grain #12. Here, too, the carbonates (Fig. 26c) and H_2O+aromatic C=C (Fig. 26d) have a very strong negative correlation, and the negative correlation between carbonates and aliphatic CH (Fig. 26e) is also strong. In contrast with SM2, here H_2O + aromatic C=C (Fig. 26d) are negatively correlated with OH (Fig.

26f). Unlike SM2 grains, SM12 grains present a weak infrared band near 3650 cm^{-1} due to phyllosilicates, but its contribution to the integrated absorbance is minor.

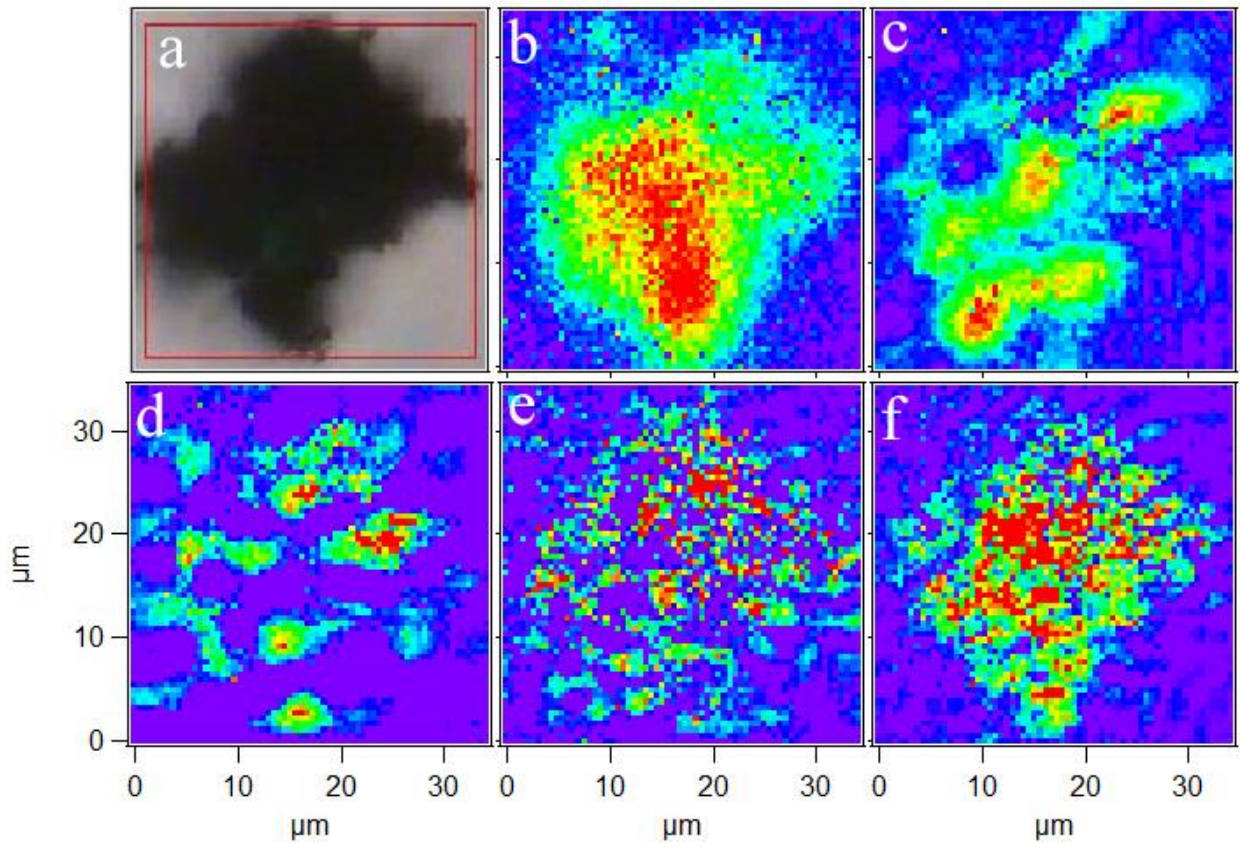

Figure 26: Spatial distributions of characteristic absorbance in SM12 grain #12: a) Visible micrograph; b) Silicates, c) Carbonates, d) H_2O + aromatic C=C stretch, e) Aliphatic C-H stretch, f) OH.

6.3.4 CH_2 / CH_3 ratios

The C-H stretching vibrational modes of aliphatic hydrocarbons are responsible for the weak but comparatively sharp infrared absorbance bands between 3000 – 2800 cm^{-1}. There are 4 peaks in this region, two for CH_2, (at 2854 and 2917 cm^{-1}) and two for CH_3 (at 2870 and 2952

cm^{-1}). After subtracting a linear baseline in the 3000 – 2800 cm^{-1} region, we obtained the CH_2/CH_3 ratios from the peak heights for SM2 (grain #40) and SM12 (grain #12) to be 4.00 ± 0.06 and 2.44 ± 0.07, respectively.

6.4 Discussion

6.4.1 Thermal metamorphism and aqueous alteration

SM2 shows IR signatures of pyroxene, olivine, and carbonates. In contrast, SM12 shows mainly carbonates and phyllosilicates with hardly any evidence for pyroxene and olivine. These observations are in agreement with [97, 98]. Typical CM2 chondrites lack significant carbonate, pyroxene, or olivine IR signatures. Instead, they are dominated by phyllosilicates [45, 93, 101]. Only the unusual CM2 chondrite Bells, and the ungrouped C-chondrite Tagish Lake have significant infrared carbonate and phyllosilicate features [60, 79, 102]. On the basis of carbonates, SM2 and SM12 are more like Bells and Tagish Lake than they are like typical CM2s. However, on the basis of phyllosilicates, SM2 is not like Bells or Tagish Lake.

The Raman spectra reveal that organic matter in SM2 is more primitive and less thermally metamorphosed than in SM12 (Fig. 23). The mean G-band FWHM for SM2 grains falls close to the value for CO3 chondrites, while the mean G-band FWHM for SM12 grains falls between the values for CO3 and CV3. As pointed out before, these results imply that the Sutter's Mill meteorite was heated more than typical CMs [55].

Some CM chondrites have been heated more than others, e.g. the so-called "heated-CM chondrites", whose aqueous alteration was followed by heating above 500 ºC [113]. These exhibit evidence of secondary olivine produced by dehydration of phyllosilicates (e.g., [103]).

SM2 is less thermally metamorphosed than SM12, according to the analysis of our Raman spectra. Yet SM2 is dominated by the anhydrous silicates olivine and pyroxene while SM12 is dominated by phyllosilicates. Hence, the anhydrous silicates in SM2 are unlikely due to simple heating of material that was originally like SM12. This suggests different mineralogical history and precursor material for SM2 and SM12. In fact, [93] suggested physical mixing of C and E type asteroids based on the abundance of oldhamite, phosphides, and enstatite in Sutter's Mill. Our observations provide additional evidence and support the possibility that SM2 and SM12 are not both CM chondrites.

Olivine in SM2 grains might be the dehydration product of phyllosilicates. However, secondary olivine cannot be formed at the temperature lower than ~500 C [103]. On the other hand, even such heating events as experienced by the heated-CMs, does not change Raman G-band characteristics significantly from non-heated CMs, in comparison to the thermally metamorphosed COs and CVs. For example, the G-band FWHM of Yamato 86720 (a CM heated over 750 C) is 96.0 ± 0.2 cm^{-1}, which falls within the range of values of for non-heated CMs [86]. Therefore, the T_{EFF} of 134 – 259 C obtained from G-band FWHM of SM2 grains might be underestimated. This possibility is due to the assumption for the T_{EFF} calculation that isothermal heating of a parent body occurred for ~10^7 years, which may not be the case in the Sutter's Mill meteorite parent body or bodies.

Raman spectra show that heating in SM was more severe than for CMs but less severe than for heated-CMs. Heating events in the latter are considered to be short-duration events [104], as might be due to impacts. Heating of regular CMs is considered to be long-term at much lower temperatures [114]. It is reasonable to suppose that the duration and temperature of heating for SM was intermediate between usual CMs and heated CMs.

Sutter's Mill entered Earth's atmosphere at high speed (28.6 km/s) and broke at a high altitude [55]. Based on the uneven fusion crust on most of the SM meteorites, they continued to fragment on the way down. Thermoluminescense (TL) measurements by Derek Sears and coworkers (consortium study, [55]) showed that SM2 was heated to 300 ± 20 C to a depth of 5-6 mm below the fusion crust, without the ~0.2 Ma needed for TL to recover. This heating could have been due to the entry, or because of solar heating near perihelion in the past <0.2 Ma [55]. In either case, it is unlikely that such heating could cause the degree of thermal metamorphoses inferred from the Raman spectra, since this would require more prolonged (> 1 Ma) heating at these relatively low temperatures.

Some Sutter's Mill meteorites were exposed to heavy rain for several days. Generally, rain quickly oxidizes the iron content. Rain may hydrate anhydrous minerals, but this takes significantly longer and requires higher temperatures than was possible for those SM samples. Thus, SM12 hydrated silicate bands near ~1000 cm^{-1} (Fig. 24) cannot be attributed to hydration of anhydrous silicates by rain.

The OH stretching band for SM2 grains is systematically different than for SM12 grains. Specifically, the band center for SM2 grains appears near 3380 cm^{-1} while that for SM12 grains appears near 3450 cm^{-1}. This is in agreement with [105] that the OH band in olivine- and pyroxene-rich meteorites appears at lower frequencies.

Differences in linewidths are also potentially interesting, since differences in inhomogenous broadening may indicate differences in parent body processing history. Vibrational lines are broader in amorphous solids than in crystals of the same chemical composition. For grain-integrated spectra (Fig. 24) widths of characteristic bands tend to be

broad, but there are clear differences between different grains. Bands in spectra from individual pixels tend to be sharper. To compare our band widths with those from independent measurements, we note that [106] presented infrared transmittance spectra with spot size of 7 μm x 7 μm for SM20 and SM30 meteorites. We converted their spectra to absorbance so that quantitative full width at half maxima could be obtained independent of absorption strength. Next, we obtained from our data a number of infrared spectra for different 7 μm x 7 μm areas of one SM12 grain for comparison. The results for five spectra in [106] and for five of ours show full width at half maxima for the carbonate band of 91 ± 18 and 99 ± 11, respectively. These widths are the same within the statistical uncertainty.

6.4.2 Spatial relationships

Our investigation of spatial relationships between different compounds is preliminary and qualitative, since just two grains were analyzed. Future work will perform quantitative numerical correlation analysis on the ~20 grains for which we have already collected a large amount of data for both meteorites. Nevertheless, the preliminary results presented here allow a few notable observations and demonstrate the potential of the technique. A sense of the correlations is most easily obtained by viewing rapidly alternating pairs of images, while watching the blinking of concentration hot spots. The most prominent observation is the strong negative correlation between carbonates and H_2O+aromatic C=C for both grains. Similarly, the spatial correlation of carbonates and aliphatic C-H is negative.

Association of aliphatic organic matter with phyllosilicates is shown in Bells [64], in NWA 852 [65], in CI1, CM2 chondrites as well as Tagish Lake [28, 107]. We observed in SM2

grain #40 that the spatial distribution of aliphatic C-H only partially overlaps with that of silicates, while the overlap between aliphatic CH and OH is even less. Thus, aliphatic organic matter is not strongly correlated with phyllosilicates in SM2 grain #40, in contrast to Bells, NWA 852, and Tagish Lake.

In SM12 grain #12 the overlap between silicates and aliphatic CH is even less than in SM2 grain#40. If significant, it suggests that the aqueous alteration history for SM12 differs from that of SM2, supporting the hypothesis that the parent body of the Sutter's Mill meteorite is combination of multiple parent bodies.

Spatial distributions of silicates and OH in SM2 grain #40 only partially overlap, which is probably due to the abundance of anhydrous silicates indicated by the infrared spectrum (Fig. 24). In contrast, for SM12 grain #12 the correlation between silicates and OH seems somewhat stronger, consistent with the abundant phyllosilicates indicated by the infrared spectrum (Fig. 24).

6.4.3 C-H stretching intensity ratios

Peak intensity ratio of asymmetric CH_2 to CH_3 bands can be used to roughly infer aliphatic chain lengths and/or branching levels [81], which are affected by processing. For instance, energetic particles may break bonds, and heating may aromatize aliphatic molecules, both of which shorten chain lengths and give lower CH_2/CH_3 ratios [72]. Fewer aromatics and higher CH_2/CH_3 ratios suggest dense clouds and/or protosolar nebular processes [108]. The higher ratio for SM2 than for SM12 suggests that the aliphatic organics in these materials may have different origins and/or have undergone different parent body processing. Our results

suggest that SM12 was subjected to higher metamorphism temperatures (T_{EFF} = 279 - 312 C) than SM2 (T_{EFF} = 134 - 259 C), which is consistent with the lower CH_2/CH_3 ratio for SM12.

The aliphatic type organic matter in Sutter's Mill is largely different from that in CM and CI chondrites. The CH_2/CH_3 ratios of various astronomical objects were previously reported (Table 10). The measured ratio is close to 1.0 for CM chondrites, but around 2.5 for cometary dust and interplanetary dust particles. The high ratios for SM2 and SM12 are closer to those of interplanetary dust and cometary matter, as well as to some other carbonaceous chondrites. The ratio for Tagish Lake (3.0) is in between that of SM2 and SM12. We note that the CH_2/CH_3 ratio of Tagish Lake IOM was recently re-evaluated after IOM extraction via solvents to be in the range 1.2 – 1.9 [115]. However, CH_2-rich material in the bulk Tagish Lake may be lost during the IOM purification processes, causing ratios determined using this procedure to be systematically underestimated in comparison to those determined by analysis of organics *in situ*.

The high CH_2/CH_3 ratios in SM2 and SM12 are consistent with reports that organic matter in Sutter's Mill is unique among typical CM and other primitive chondrites. First, laboratory hydrothermal treatment of Sutter's Mill caused release of complex polyether- and ester-containing alkyl molecules which were never before detected in meteorites [109]. Second, a bimodality in the C release suggests a combination of volatile-rich and volatile-poor organic components [55]. Third, C and N isotopic ratios vary widely between different SM fragments [55].

The similarity to cometary organics is of particular interest, because the pre-atmospheric orbit of Sutter's Mill, like that of CM chondrite Maribo, was very similar to that of a Jupiter-family comet 2P/Encke, having a Tisserand parameter on the border of the comet and asteroid

fields [55]. It has been argued that these meteorites may originate, in fact, from Jupiter family comets [110].

A possible source of uncertainty regarding CH_2/CH_3 ratios is contamination, to which the spectral region of the C-H stretch is susceptible [57]. This may be a particular issue for SM2, which was recovered from an asphalt surface. The C-H stretch absorption is in fact stronger for *some* of the SM2 grains than for any of the SM12 grains that we studied here. However, we remind that all grains studied in this paper were extracted from the interior of the meteorite, while it was the exterior that contacted the asphalt surface. Also, the amino acid analysis [97] suggests a higher contamination for SM12 than for SM2.

A second source of uncertainty in the ratios is that overtones of the strong absorption bands at lower frequencies overlap the aliphatic C-H stretching bands in the 2980 – 2870 cm^{-1} region [95]. However, the low frequency bands, which include contributions from many different chemical moieties and mineral species (Table 8) are very broad, and overtones should reproduce the general shape of those fundamentals. There is no evidence of such in Figure 24 for SM2 grain #40 or SM12 grain #12. In particular, the CH stretch modes are much sharper than any possible overtone band, so that the latter would mainly affect the baseline, which has been subtracted off. Moreover, if the aliphatic C-H bands had significant contribution from, say, carbonate overtones, their spatial distributions (Fig. 25c,e and Fig. 26c,e) would be more similar than observed.

Table 10. The CH_2/CH_3 ratios of SM meteorites and various astronomical objects.

Objects	CH_2/CH_3 band strength ratio	Source
SM2 (grain #40)	4.00 ± 0.06	[116]
SM12 (grain #12)	2.44 ± 0.07	[116]
Comet Wild-2 coma dust	2.5 ± 0.1	[62]
Anhydrous IDPs	2.46 ± 0.01	[83]
Hydrated IDPs	2.31 ± 0.01	[83]
NWA 852 (CR2)	2.53 ± 0.05	[65]
Tagish Lake (C)	2.57 ± 0.04	this work
DISM	1.17 ± 0.2‡	[84]
Paris (CM)	1.8 ± 0.2	[72]
Orgueil (CI)	1.4 ± 0.1	[64]
Bells (CM, anom.)	1.4 ± 0.2	[64]
Murchison (CM)	1.0 ± 0.1	[64]

‡ Average.

6.5 Conclusions

Synchrotron-based micro-scale FTIR spectroscopy of Sutter's Mill meteorites SM2 and SM12 shows that the spatial distributions of carbonates and both aromatic and aliphatic hydrocarbons are negatively correlated. The spatial distribution of aliphatic organic matter and OH relative to the distributions of silicates in SM2 differs somewhat from that in SM12, supporting a hypothesis that the parent body of Sutter's Mill is a combination of multiple bodies. From the micro-Raman spectra, we confirm that SM12 experienced higher thermal metamorphism than did SM2, although SM2 contains a greater proportion of olivine. The CH_2/CH_3 ratio in Sutter's Mill is higher than found in bulk CM and CI chondrites, but it is similar to that of interplanetary dust particles and comets. These differences may indicate a different origin and/or parent body processing of the aliphatic organic matter in SM2 and SM12 than in other CM and CI chondrites and diffuse ISM objects.

CHAPTER SEVEN: THREE DIMENSIONAL IMAGING OF MURCHISON WITH SYNCHROTRON FTIR SPECTROMICROTOMOGRAPHY

7.1 Introduction

Hitherto, we have investigated spatial relationships of organics and minerals that constitute carbonaceous chondrites. This investigation took advantage of a highly analytical instrumentation installed at the IRENI beamline at Synchrotron Radiation Center, University of Wisconsin in Madison that allows acquisition of two-dimensional high resolution infrared maps. Such maps present distribution of concentrations due to specific molecular functional groups in meteorite samples, therefore allowing us to study their spatial and spectroscopic relations.

Upgrades to the instrumentation at the IRENI beamline has made spectral imaging with synchrotron FTIR spectro-microtomography possible [71]. This technique offers investigation of spatial distributions of chemical components in samples of interest in three-dimension and with full color [71]. To our knowledge, no study exists on three-dimensional spectro-microtomography of any astronomical sample in the infrared range.

Study of carbonaceous chondrites in three-dimension is particularly interesting due to their organic and mineral abundances as well as relationships of these components. Three-dimensional distributions of such components would reveal mineralogical and chemical heterogeneity as well as petrology of meteorites in the mid-infrared region in three-dimension, which would help better understand processes that the meteorite parent body might have undergone.

Recently we studied a carbonaceous chondrite, Murchison (CM2), with this highly novel technique. Here we present our results of the measurements. We remark that analysis of this kind of data is quite new and results presented here are preliminary.

7.2 Results

Figure 27 presents the visible micrograph as well as the infrared image of the Murchison grain studied here. Due to its rough surface, some parts of the grain always out of focus under the microscope, as seen in the visible micrograph, however this does not effect the acquisition of the spectral data.

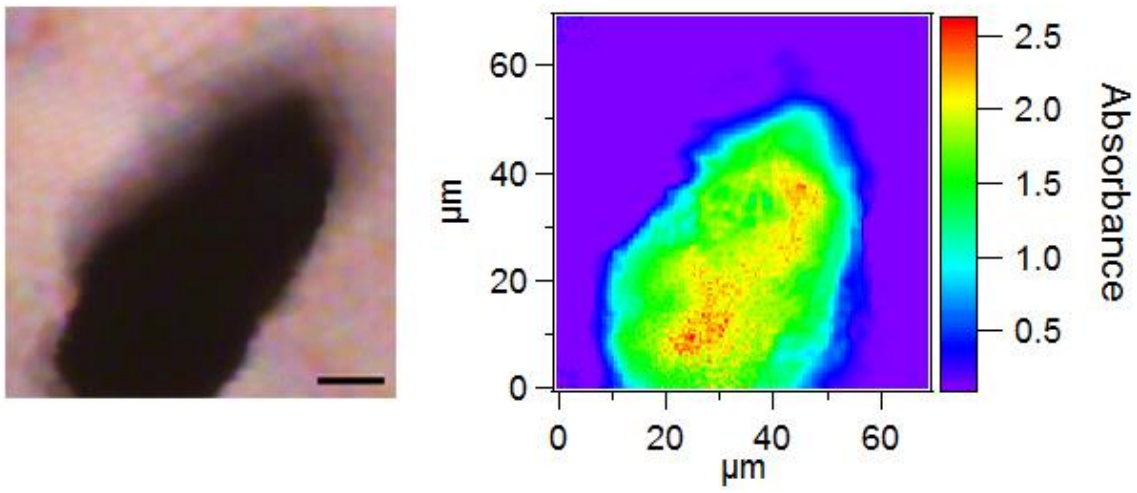

Figure 27: Visible photomicrograph (left) and the infrared image of the Murchison grain. Bar is ~10 µm

In order to identify molecular functional groups present in the studied sample, infrared spectrum of the Murchison grain was obtained after masking the sample-free regions. Figure 28 presents grain-averaged mid-infrared spectrum of Murchison, in which distinct absorbance peaks

are visible. These peaks are due to silicates, sulfates, aliphatic hydrocarbons, carbonates, water, and carbonyls. Positions and assignments of observed absorbance peaks are collected in Table 1. Spectral region between 2800 – 2000 cm^{-1} is omitted in the spectrum since this region presents no infrared feature except artifacts such as features of atmospheric CO_2.

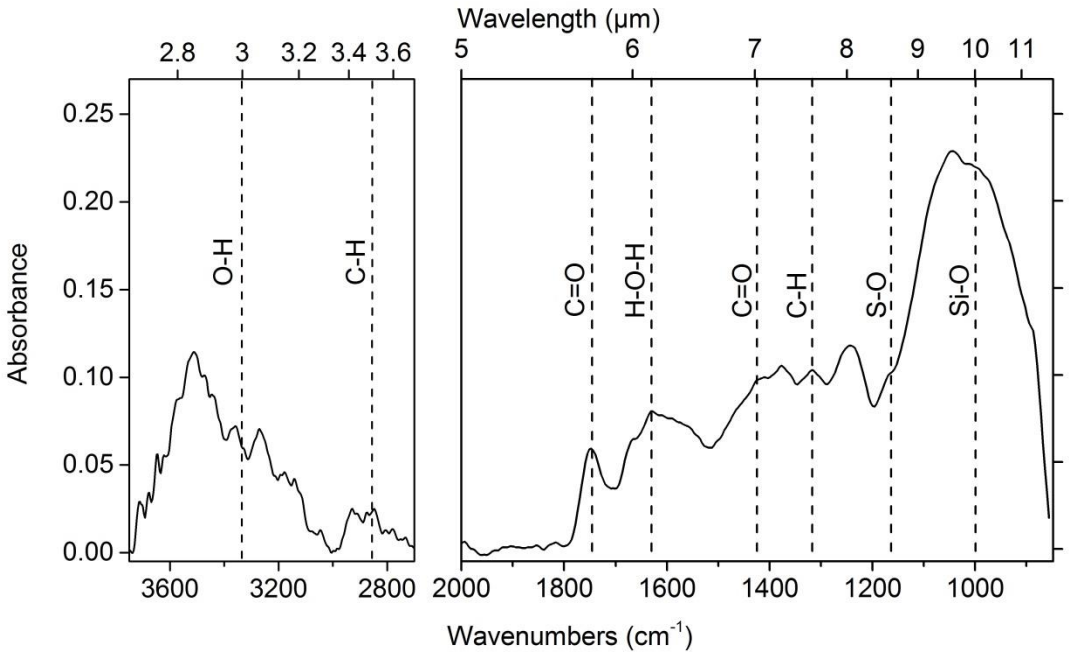

Figure 28: Infrared spectrum of the Murchison grain studied in this work. Vertical dashed lines represent positions of specific vibrational modes.

These positions of specific infrared features were used for the reconstruction of the respective components after a linear baseline that is tangent to either end-points of a peak was subtracted. Table 11 lists these integration regions for different compounds present in Murchison.

Table 11. Integration regions, assignments, and reconstruction labels/colors of functional groups observed in Murchison.

Integration Region (cm^{-1})	Assignment	Labels/colors in Fig. 3
1140 – 850	Silicate	a / green
1200 – 1140	Sulfate	b / yellow
1390 – 1200	Aliphatics	c / pink
1520 – 1390	Carbonate	d / blue (dark)
1690 – 1520	Water	e / red
1790 – 1690	Carbonyl	f / blue (cambridge)
3000 – 2800	Aliphatics	g / blue (light)
3650 – 3100	Water	h / grey

Figure 28 presents reconstruction images of these components in the Murchison grain studied. These three-dimensional reconstruction movies can be viewed online at "http://myesiltas.net/tomography-videos.html". Silicates seem to be concentrated mostly in the upper parts of the grain, however there are smaller blobs of these material near the lower portion of the grain as well. Contents due to H-O-H bending and OH stretching vibrational modes seem to be distributed throughout the grain. This particular grain of Murchison has only small amount of aliphatic hydrocarbons, and its spatial distribution is somewhat different than others (mostly in the upper and lower portions with a gap in between).

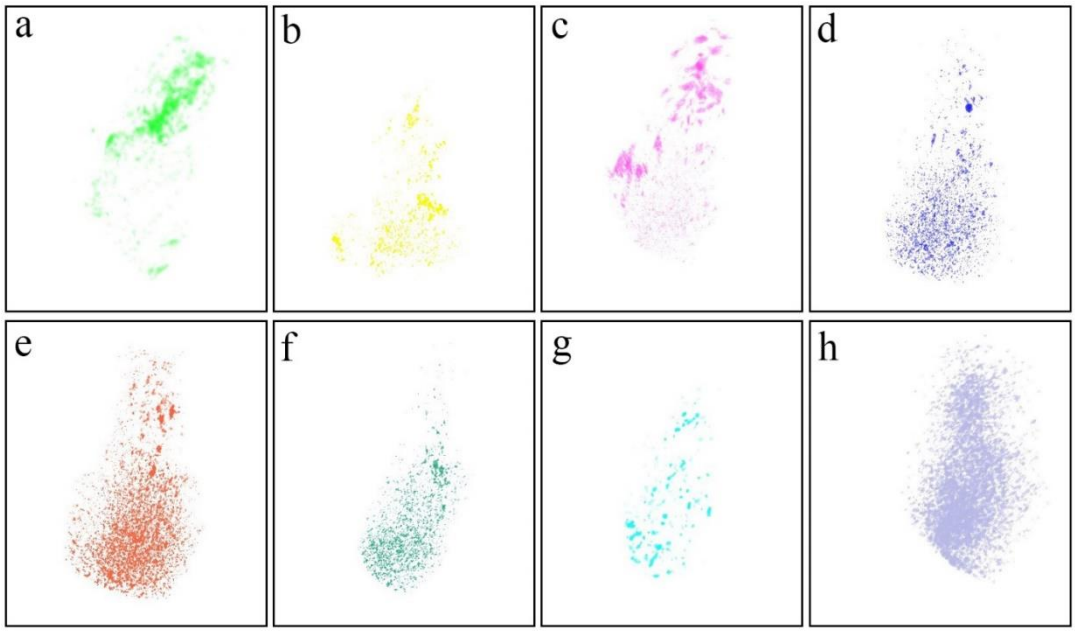

Figure 29: Images of three-dimensional reconstructions of organics and minerals. a: Si-O stretch in silicates, b: S-O stretch in sulfates, c: C-H bend in aliphatics, d: C=O stretch in carbonates, e: O-H bend in water, f: C=O stretch in carbonyls, g: C-H stretch in aliphatics, h: O-H stretch in water.

Additionally, any two or more of these components can be combined for pair-wise comparison of their spatial distributions in three-dimensional space. For instance, Figure 30 shows tomographic reconstruction of multiple components. Silicate + OH combination shows that they are spatially overlap up to some extent. Namely, the upper portion of the grain has more overlap than the lower portion since silicates lack in the lower portion (Fig. 30a). Combination of silicates and aliphatic hydrocarbons (stretching mode) appears to have little overlapping and they are both distributed around the "right" side of the grain (Fig. 30b).. Finally, Figure 30c presents spatial distribution of all components together, making up the whole meteorite grain.

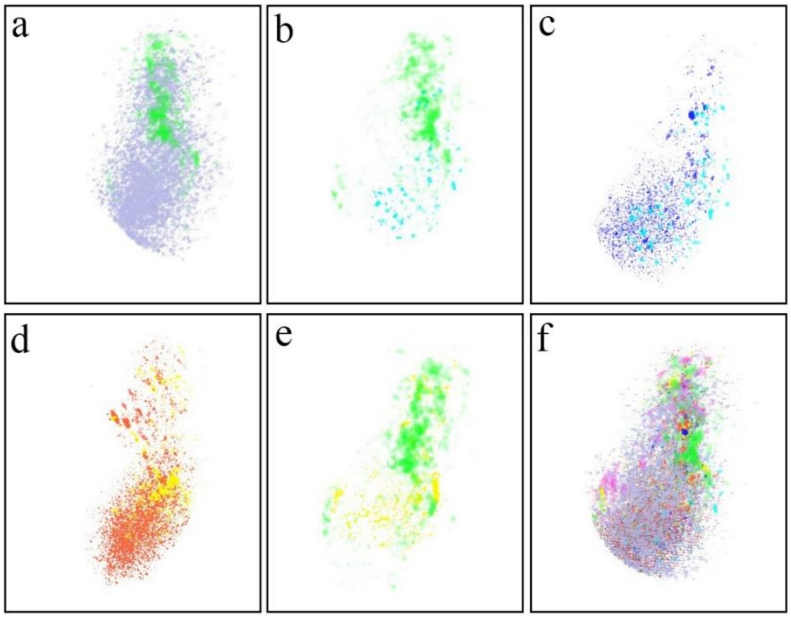

Figure 30: Images of combined three-dimensional reconstructions of organics and minerals.

The fourth dimension in our dataset is the infrared spectra. In addition to visual investigation in three-dimensional space, different regions of the grain can be studied spectrally since reconstruction of the whole Murchison grain investigated here consists of more than two million voxels, each with associated full mid-infrared spectrum. Molecular compounds are distributed quite heterogeneously in Murchison, therefore the strength of absorbance bands varies with varying locations. In this work, we studied infrared spectra obtained from different regions of the Murchison grain in order to see spectral variations and perform quantitative analyses. Namely, we extracted infrared spectra from rows along the x-axis for a fixed z-axis location (z=64), and varying y-axis locations. Corresponding pixels are y=15, 30, 45, 60, 75, 90, 105, and 120. For each row, spectra from all pixels along the raw were extracted, those of sample-free regions were removed, and the remaining ones were averaged. Figure 31 presents

extracted infrared spectra in the fingerprint region. Vertical lines indicate infrared features of specific functional groups studied in this work and shown in Figure 28.

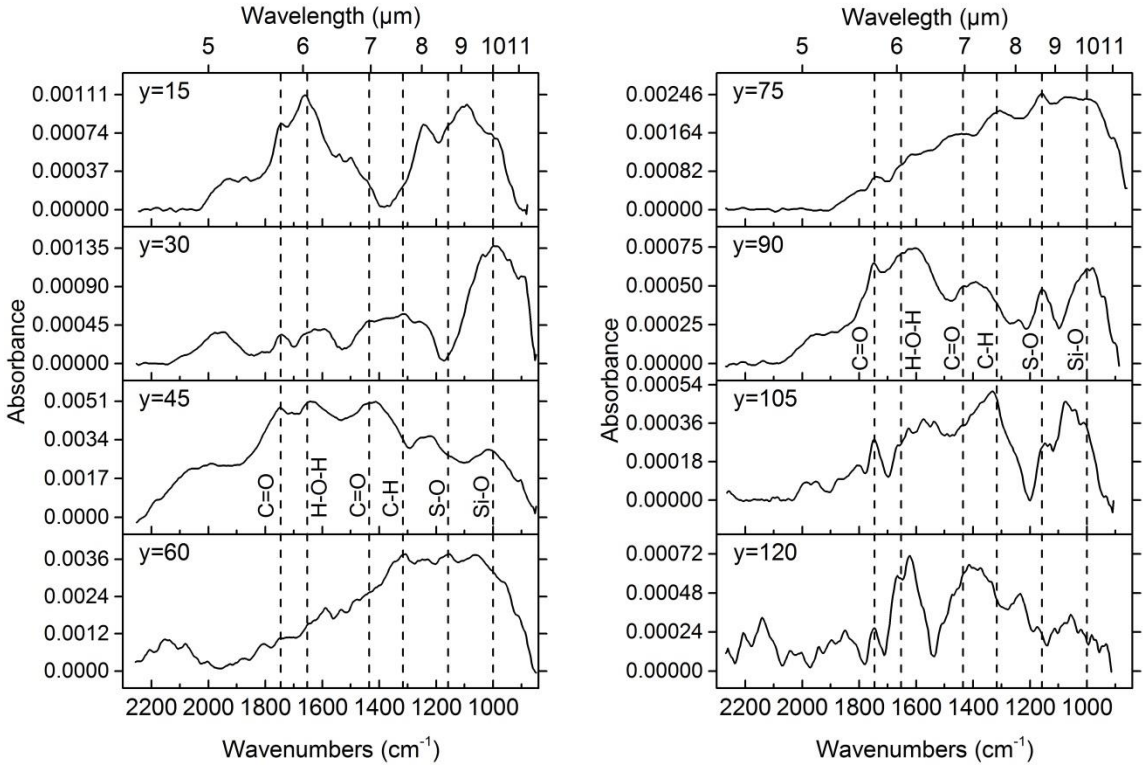

Figure 31: Infrared spectra of rows on x-axis, extracted from different y-axes for z=64. Vertical dashed lines show position of different functional groups.

Since FTIR spectro-microtomography provides rich spectral information (i.e. millions of spectra), variety of quantitative analyses can be performed, such as principal component analyses and correlation analyses for further spectral characterization of the sample. Here in this study, we performed a quantitative analyses, correlation analyses of chemical components identified in Murchison, in order to study possible interdependences of different molecular functional groups. Using a Gaussian fitting procedure, we integrated intensity of each absorbance band in the fingerprint region for rows y=15, y=30, y=45, y=60, y=75, y=90, and y=105, after which correlations of these integrated intensities were investigated. Our quantitative analyses show that

silicates and sulfates appear to be positively correlated with carbonates. Figure 32 presents these relations as well as corresponding correlation coefficient (r) values obtained with 95% confidence level.

We remark that these three components are products of aqueous alteration, therefore their positive correlations are reasonable and expected. Namely, the silicate content of Murchison is mostly hydrated silicates. Similarly, sulfates and carbonates form in the presence of water. We acknowledge that our correlation analysis shown here is based on very limited data points, and therefore only preliminary, however more work is currently in progress for investigation of many more data points, which will yield much more meaningful correlations.

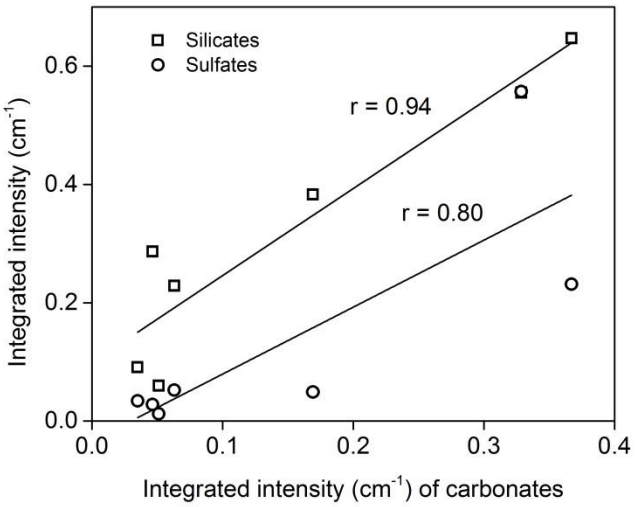

Figure 32: Variations of band areas of silicates and sulfates relative to that of carbonates. Straight lines indicate linear fits with corresponding r values obtained with 95% confidence level.

7.3 Conclusions

We presented the first-ever three-dimensional spectro-microtomography measurement on an extraterrestrial sample in the infrared with high spatial resolution. This highly novel non-destructive technique has the advantage of locating specific organics and minerals within samples of interest in three-dimensional space and reveals their relationships. Study of meteoritic organics and minerals can reveal information about their origin as well as processes they may have undergone. Additionally, infrared spectra obtained from voxels offer spectral characterization of meteoritic constituents within their local mineralogy. These spectral data can be used for quantitative analyses such as principle component analyses and correlation analyses.

Work presented here extracts qualitative and quantitative information from a single Murchison grain. Spatial distribution of silicates relative to that of structural and interlayer water reveals where hydrous and anhydrous silicates are located within the Murchison grain. Sulfates are distributed in a way that water surrounds them. Spectral and statistical study of Murchison indicates that carbonates are positively correlated with silicates ($r = 0.94$) and sulfates ($r = 0.80$).

Three-dimensional FTIR spectro-microtomography is a remarkable advancement and has significant potential for the investigation and characterization of extraterrestrial samples including samples returned from missions such as Osiris-REx and Hayabusa-2, which are going to bring samples back to Earth from the surface of primitive asteroids. From curation to in-depth investigation of returned samples, three-dimensional FTIR spectro-microtomography can provide vast amount of information without damaging and altering the studied samples.

CHAPTER EIGHT: CONCLUDING REMARKS

Meteorites have long been studied through variety of techniques, yet relationships of organics and minerals in meteorites have not been fully understood. Work in this dissertation provided relations of organics with minerals in carbonaceous chondrites both qualitatively and quantitatively.

Formation of organic molecules through catalytic reactions on mineral surfaces has been suggested. Phyllosilicates have been shown to be appropriate catalyst minerals for such production. A genetic relation between minerals and organics is highly likely, and can be studied into detail within the mineralogical context of meteorites.

We have utilized two nondestructive, highly analytical techniques for our experiments, micro-Raman spectroscopy and FTIR microspectroscopy. Two-dimensional infrared spatial distribution maps with significantly high resolution have been obtained for meteorites and presented in this dissertation. Such maps are used to infer spatial relationships of different chemical constituents in meteorites studied here. Additionally, we performed three-dimensional spectro-microtomography measurements on a carbonaceous chondrite. To our knowledge, this is the first study ever in any kind of meteorite.

As presented in this work, infrared spectra of NWA 852, Tagish Lake, and Orgueil show signatures variety of organics and minerals. In the case of NWA 852 and Tagish Lake, silicates and aliphatic type organics are positively correlated, however this relation is not observed in Orgueil, perhaps due to presence of different aliphatic type organics within the measured grains of these meteorites. Possible reason for this difference is origin, and processing of organics in the

parent body (i.e., interstellar vs. nebular origin). In all meteorites, silicates are positively correlated with OH content. This is most likely due to presence of phyllosilicates in these carbonaceous chondrites. Note that the correlation coefficient varies for the three meteorites due to contribution from anhydrous silicates at varying abundances. Furthermore, Tagish Lake has different silicate-carbonate relation.

Carbonate content of Tagish Lake is distinct among meteorites, which is one of the reasons why Tagish Lake is considered to be a member of the "unusual CM" chondrites. In fact, first lithologies that were discovered in Tagish Lake were "carbonate-rich" and "carbonate-poor" lighologies. We have showed that unlike in NWA 852 and Orgueil, silicates are positively correlated with carbonates in Tagish Lake. Also shown in this dissertation is that carbonates are always negatively correlated with water+organic combination in all meteorites.

In Chapter 6, we presented results of our experiments on the Sutter's Mill meteorite. By investigating two fragments, SM2 and SM12, we provided further evidences which indicate that parent body of Sutter's Mill meteorite is combination of multiple bodies. These evidences include distinct infrared spectra, mineralogy, and relative spatial distributions of organic and inorganic molecules. For instance, SM2 is dominated by anhydrous silicates, while SM12 presents abundant hydrous silicates. CH_2/CH_3 ratio of SM2 and SM12 are 4.00 and 2.44, respectively, indicating different origin and/or processing of organics.

To our knowledge, there is no study exists on three-dimensional FTIR spectro-microtomography of meteorites. We have studied Murchison with this highly novel technique, and in Chapter 7, we presented results of our three-dimensional experiments on a Murchison grain. Relative distributions of organics and minerals show highly heterogeneous state of the

meteorite grain. These reconstructions in three-dimensional space allow us to study spatial distributions of specific molecular functional groups within the local mineralogy of the meteorite sample. Infrared spectrum of voxels as a forth dimension additionally not only provides spectral investigation on the mineralogy of Murchison but also allows us to quantitatively study mineral-organic relations.

APPENDIX: PUBLICATIONS

Journal:

1. Deep Panjwani, Mehmet Yesiltas, Simranjit Singh, Enrique Del Barco, Robert E. Peale, Carol Hirschmugl, and Julia Sedlmair, "Stencil lithography of gold-black IR absorption coatings", Infrared Physics & Technology, 66:1-5 (2014).
2. Mehmet Yesiltas, Yoko Kebukawa, Robert E. Peale, Eric Mattson, Carol J. Hirschmugl, and Peter Jenniskens, "Infrared imaging spectroscopy with micron resolution of Sutter's Mill meteorite grains", Meteoritics & Planetary Science, 49, 2027-2037, (2014).
3. Deep Panjwani, Mehmet Yesiltas, Janardan Nath, Doug E. Maukonen, Imen Rezadad, Evan M. Smith, Robert E. Peale, Carol J. Hirschmugl, Julia Sedlemair, Ralf Wehlitz, Miriam Unger, and Glenn Boreman, "Patterning of oxide-hardened gold black by photolithography and metal lift-off", Infrared Physics & Technology, 62:94-99, (2013).
4. Mehmet Yesiltas, Robert E. Peale, and Carol J. Hirschmugl, "Organic and inorganic correlations for Northwest Africa 852 by synchrotron-based Fourier transform infrared microspectroscopy", Meteoritics & Planetary Science, under review.
5. Tatiana Brusentsova, Mehmet Yesiltas, Robert E. Peale, Doug Maukonen, Pedro Figueiredo, George E. Harlow, Denton S. Ebel, A. Nissinboim, K. Sherman, and Casey M. Lisse, "Far-infrared spectroscopy of Terrestrial Phyllosilicate Astrophysical Dust Analogues", in preparation.

Conference:

1. Mehmet Yesiltas, Yoko Kebukawa, Eric Mattson, Carol J. Hirschmugl, and Robert E. Peale, "Micro-Infrared and micro-Raman spectroscopy of Sutter's Mill meteorite grains", LPSC, abstract: 1396, (2014).
2. Mehmet Yesiltas, Carol J. Hirschmugl, and Robert E. Peale, "In Situ Investigation of Meteoritic Organic-Mineral Relationships by High Spatial Resolution Infrared Spectroscopy", 76th Annual Meeting of Meteoritical Society, abstract: 5068, (2013).
3. Mehmet Yesiltas, Miriam Unger, Julia Sedlmair, Carol J. Hirschmugl, Tatiana N. Brusentsova, and R. E. Peale, "Microspectroscopy of Meteorites: Search for Organic-Mineral Correlations", LPSC, abstract: 2717, (2013).
4. Mehmet Yesiltas, Tatiana Brusentsova, Robert E. Peale, Doug Maukonen, Pedro Figueiredo, George E. Harlow, Denton S. Ebel, A. Nissinboim, K. Sherman, and Casey M. Lisse, "Laboratory far-infrared spectroscopy of phyllosilicates", 219th AAS, abstract: 238.05, (2012).

LIST OF REFERENCES

[1] J. Leitner, C. Vollmer, P. Hoppe, and J. Zipfel, "Characterization of presolar material in the CR chondrite Northwest Africa 852", Astrophysical Journal **745**, (2012).

[2] L. A. Garvie and P. R. Buseck, "Prebiotic carbon in clays from Orgueil and Ivuna (CI), and Tagish Lake (C2 ungrouped) meteorites", Meteoritics & Planetary Science, **42**, 2111-2117, (2007).

[3] F. R. Orthous-Daunay, E. Quirico, P. Beck, O. Brissaud, E. Dartois, T. Pino, and B. Schmitt, "Mid-infrared study of the molecular structure variability of insoluble organic matter from primitive chondrites", Icarus, **223,**534-543, (2013).

[4] M. A. Sephton, "Organic compounds in carbonaceous meteorites", Natural Product Reports, **19**, 292-311, (2002).

[5] M. M. Grady, A. B. Verchovsky, I. A. Franchi, I. P. Wright, and C.T. Pillinger, "Light dement geochemistry of the Tagish Lake CI2 chondrite: Comparison with CI1 and CM2 meteorites", Meteoritics & Planetary Science, **37**,713-735, (2002).

[6] Z. Martins, "Organic chemistry of carbonaceous meteorites", Elements, **7**,35-40 (2011).

[7] M. A. Sephton, C. T. Pillinger, and I. Gilmour, delta(13)C of free and macromolecular aromatic structures in the Murchison meteorite", Geochimica Et Cosmochimica Acta, **62**, 1821-1828, (1998).

[8] M. A. Sephton, A. B. Verchovsky, P. A. Bland, I. Gilmour, M. M. Grady, and I. P. Wright, "Investigating the variations in carbon and nitrogen isotopes in carbonaceous chondrites", Geochimica Et Cosmochimica Acta, **67**, 2093-2108, (2003).

[9] C. Chyba and C. Sagan, Endogenous production, exogenous delivery and impact-shock synthesis of organic molecules - An inventory for the origins of life", Nature, **355**, 125-132, (1992).

[10] J. H. Cleaves, S. A. Michalkova, F. C. Hill, J. Leszczynski, N. Sahai, and R. Hazen, "Mineral-organic interfacial processes: potential roles in the origins of life", Chemical Society Reviews, **41**, 5502-5525, (2012).

[11] T. Owen and A. Bar-Nun, Comets, impacts, and atmospheres", Icarus, **116,** 215-226, (1995).

[12] H. Campins, K. Hargrove, N. Pinilla-Alonso, E. S. Howell, M. S. Kelley, J. Licandro, T. Mothe-Diniz, Y. Fernandez, and J. Ziffer, Water ice and organics on the surface of the asteroid 24 Themis", Nature, **464**,1320-1321, (2010).

[13] J. Licandro, H. Campins, M. Kelley, K. Hargrove, N. Pinilla-Alonso, D. Cruikshank, A. S. Rivkin, and J. Emery, (65) Cybele: detection of small silicate grains, water-ice, and organics", A&A, **525**, (2011).

[14] A. Morbidelli, J. Chambers, J. I. Lunine, J. M. Petit, F. Robert, G. B. Valsecchi, and K. E. Cyr, "Source regions and timescales for the delivery of water to the Earth", Meteoritics & Planetary Science, **35**, 1309-1320, (2000).

[15] A. S. Rivkin and J. P. Emery, Detection of ice and organics on an asteroidal surface", Nature, **464**, 1322-1323, (2010).

[16] C. Ponnamperuma, A. Shimoyama, and E. Friebele, "Clay and the origin of life", Origins of Life and Evolution of the Biosphere, **12**, 9-40, (1982).

[17] J. Lederberg and D. B. Cowie, "Moondust: The study of this covering layer by space vehicles may offer clues to the biochemical origin of life", Science, **127**, 1473-1475, (1958).

[18] P. Ehrenfreund and S. B. Charnley, "Organic molecules in the interstellar medium, comets, and meteorites: A voyage from dark clouds to the early Earth", Annual Review of Astronomy and Astrophysics, **38**, 427-483, (2000).

[19] R. Saladino, C. Crestini, G. Costanzo, R. Negri, and E. Di Mauro, "A possible prebiotic synthesis of purine, adenine, cytosine, and 4(3H)-pyrimidinone from formamide: Implications for the origin of life", Bioorganic & Medicinal Chemistry, **9**, 1249-1253, (2001).

[20] P. Ehrenfreund, W. Irvine, L. Becker, J. Blank, J. R. Brucato, L. Colangeli, S. Derenne, D. Despois, A. Dutrey, H. Fraaije, A. Lazcano, T. Owen, F. Robert, and Intl Space Sci, I. Issi Team, "Astrophysical and astrochemical insights into the origin of life", Reports on Progress in Physics, **65**, 1427-1487, (2002).

[21] S. M. Miller and and L.E. Orgel, "The origins of life on the earth", Engelwood Cliffs, NJ: Prentice-Hall, Inc., (1974).

[22] S. J. Clemett, S. Messenger, K. L. Thomas-Keprta, E. K. Gibson, and D. K. Ross, "In situ mapping of the organic matter in carbonaceous chondrites and mineral relationships", Meteoritics and Planetary Science Supplement, 7**5**, 5330, (2012).

[23] M. R. Wing and J. L. Bada, "Geochromatography on the parent body of the carbonaceous chondrite Ivuna", Geochimica et Cosmochimica Acta, **55**, 2937-2942, (1991).

[24] E. Escamilla-Roa and F. Moreno, "Adsorption of glycine by cometary dust: Astrobiological implications", Planetary and Space Science, **70**, 1-9, (2012).

[25] S. Pizzarello and E. Shock, "The Organic Composition of Carbonaceous Meteorites: The Evolutionary Story Ahead of Biochemistry", Cold Spring Harbor Perspectives in Biology, **2**, (2010).

[26] R. Hayatsu and E. Anders, "Organic compounds in meteorites and their origins, in Cosmo-and geochemistry", Springer. **Vol**, 1-37, (1981).

[27] M. Mortland, "Clay-organic complexes and interactions", Adv. Agron, **22**, 117, (1970).

[28] V. K. Pearson, M. A., Sephton, A. T. Kearsley, P. A. Bland, I. A. Franchi, and I. Gilmour, "Clay mineral-organic matter relationships in the early solar system", Meteoritics & Planetary Science, **37**, 1829-1833, (2002).

[29] R. Hayatsu, M. H. Studier, and E. Anders, "Origin of organic matter in early solar system—IV. Amino acids: Confirmation of catalytic synthesis by mass spectrometry", Geochimica et Cosmochimica Acta, **35**, 939-951, (1971).

[30] E. Anders, R. Hayatsu, and M. H. Studier, "Interstellar Molecules: Origin by Catalytic Reactions on Grain Surfaces?", Astrophysical Journal, **192**, L101, (1974).

[31] T. Alam, H. Tarannum, M. N. Ravi Kumar, and Kamaluddin, "Adsorption and oxidation of aromatic amines by metal hexacyanoferrates(II)", Talanta, **51**, 1097-1105, (2000).

[32] M. Paecht-Horowitz, "The possible role of clays in prebiotic peptide synthesis", Origins of Life, **5**, 173-87, (1974).

[33] E. T. Degens and J. Matheja, "Formation of organic polymers on inorganic templates" in *Prebiotic and Biochemical Evolution*, A.P.K.a.J. Oro, Editor.: North Holland, Amsterdam, 39-69, (1971).

[34] H. Hanafusa and S. Akabori, "Polymerization of aminoacetonitrile", Bulletin of the Chemical Society of Japan, **32**, 626-630 (1959).

[35] P. J. Gasda, G. J. Taylor, A. Misra, and S. K. Sharma, "MAPPING ORGANIC MATERIALS IN CARBONACEOUS CHONDRITES", Meteoritics & Planetary Science.**47**, A143-A143 (2012).

[36] B. G. Saikia, G. Parthasarathy, and N. Sarmah, "Fourier Transform Infrared Spectroscopic Characterization of Dergaon H5 Chondrite: Evidence of Aliphatic Organic Compound", Nature and Science, **7**, 45-51, (2009).

[37] J. Makjanic, R. D. Vis, J. W. Hovenier, and D. Heymann, "Carbon in the matrices of ordinary chondrites", Meteoritics and Planetary Science, **28**, 63-70, (1993).

[38] J. D. Bernal, "The physical basis of life", Routledge and Paul, (1951).

[39] G. Lagaly, R. M. Barrer, and K. Goulding, "Clay-Organic Interactions [and Discussion]", Philosophical Transactions of the Royal Society of London. Series A, Mathematical and Physical Sciences, **311**, 315-332, (1984).

[40] A. Weiss, "Organic derivatives of clay minerals, zeolites, and related minerals, in Organic geochemistry", Springer, 737-781, (1969).

[41] B. K. Theng, "The Chemistry of Clay-Organic Reactions", The Chemistry of Clay-Organic Reactions, (1974).

[42] N. Lahav and S. Chang, "The possible role of solid surface area in condensation reactions during chemical evolution: reevaluation", Journal of molecular evolution, **8**, 357-380, (1976).

[43] L. B. Williams, B. Canfield, K. M. Voglesonger, J. R. Holloway, "Organic molecules formed in a “primordial womb", Geology, **33**, 913-916, (2005).

[44] P. Vernazza, B. Carry, J. Emery, J. L. Hora, D. Cruikshank, R. P. Binzel, J. Jackson, J. Helbert, and A. Maturilli, "Mid-infrared spectral variability for compositionally similar asteroids: Implications for asteroid particle size distributions", Icarus, **207**, 800-809, (2010).

[45] P. Beck, E. Quirico, G. Montes-Hernandez, L. Bonal, J. Bollard, F. R. Orthous-Daunay, K. T. Howard, B. Schmitt, O. Brissaud, F. Deschamps, B. Wunder, and S. Guillot, "Hydrous mineralogy of CM and CI chondrites from infrared spectroscopy and their relationship with low albedo asteroids", Geochimica et Cosmochimica Acta, **74**, 4881-4892, (2010).

[46] A. Morlok, J. Bowey, M. Kohler, and M. M. Grady, "FTIR 2–16 micron spectroscopy of micron-sized olivines from primitive meteorites", Meteoritics & Planetary Science, **41**, 773-784, (2006).

[47] J. Cohen, "Statistical power analysis for the behavioral sciences", 2nd ed. Lawrence Erlbaum Associates Publishers, (1998).

[48] J. F. Kerridge, "Carbon, hydrogen and nitrogen in carbonaceous chondrites: Abundances and isotopic compositions in bulk samples", Geochimica et Cosmochimica Acta, **49**, 1707-1714, (1985).

[49] E. S. Bullock, M. Gounelle, D. S. Lauretta, M. M. Grady, and S. S. Russell, "Mineralogy and texture of Fe-Ni sulfides in CI1 chondrites: Clues to the extent of aqueous alteration on the CI1 parent body", Geochimica et Cosmochimica Acta, **69**, 2687-2700, (2005).

[50] S. Pizzarello, Y. Huang, L. Becker, R. J. Poreda, R. A. Nieman, G. Cooper, and M. Williams, "The organic content of the Tagish Lake meteorite", Science, **293**, 2236-2239, (2001).

[51] P. G. Brown, A. R. Hildebrand, M. E. Zolensky, M. M. Grady, R. N. Clayton, T. K. Mayeda, E. Tagliaferri, R. Spalding, N. D. MacRae, and *E. L. Hoffman*, "The fall, recovery, orbit, and composition of the Tagish Lake meteorite: A new type of carbonaceous chondrite", Science, **290**, 320-325, (2000).

[52] T. Hiroi, M. E. Zolensky, and C. M. Pieters, "The Tagish Lake meteorite: A possible sample from a D-type asteroid", Science, **293**, 2234-2236, (2001).

[53] M. E. Zolensky, K. Nakamura, M. Gounelle, T. Mikouchi, T. Kasama, O. Tachikawa, and E. Tonui, "Mineralogy of Tagish Lake: An ungrouped type 2 carbonaceous chondrite", Meteoritics & Planetary Science, **37**, 737-761 (2002).

[54] T. Nakamura, T. Noguchi, M. E. Zolensky, and M. Tanaka, "Mineralogy and noble-gas signatures of the carbonate-rich lithology of the Tagish Lake carbonaceous chondrite: evidence for an accretionary breccia", Earth and Planetary Science Letters, **207**, 83-101, (2003).

[55] P. Jenniskens, M. D. Fries, Q. Z. Yin, M.E. Zolensky, A. N. Krot, S. A. Sandford, D. Sears, R. Beauford, D. S. Ebel, J. M. Friedrich, K. Nagashima, J. Wimpenny, A. Yamakawa, K. Nishiizumi, Y. Hamajima, M. W. Caffee, K. C. Welten, M. Laubenstein, A. M. Davis, S. B. Simon, P. R. Heck, E. D. Young, I. E. Kohl, M. H. Thiemens, M. H. Nunn, T. Mikouchi, K. Hagiya, K. Ohsumi, Thomas A. Cahill, Jonathan A. Lawton, David Barnes, Andrew Steele, Pierre Rochette, K. L. Verosub, J. Gattacceca, G. Cooper, D. P. Glavin, A. S. Burton, J. P. Dworkin, J. E. Elsila, S. Pizzarello, R. Ogliore, P. Schmitt-Kopplin, M. Harir, N. Hertkorn, A. Verchovsky, M. Grady, K. Nagao, R. Okazaki, H. Takechi, T. Hiroi, K. Smith, E. A. Silber, P. G. Brown, J. Albers, D. Klotz, M. Hankey, R. Matson, J. A. Fries, R. J. Walker, I. Puchtel, C. A. Lee, M. E. Erdman, G.

R. Eppich, S. Roeske, Z. Gabelica, M. Lerche, M. Nuevo, B. Girten, and S. P. Wordenet, "*Radar-Enabled Recovery of the Sutter's Mill Meteorite, a Carbonaceous Chondrite Regolith Breccia.* Science, **338**, 1583-1587, (2012).

[56] O. Botta and J. L. Bada, "Extraterrestrial organic compounds in meteorites", Surveys in Geophysics, **23**, 411-467, (2002).

[57] Y. Kebukawa, S. Nakashima, T. Otsuka, K. Nakamura-Messenger, M. E. Zolensky, and E. Michael, "Rapid contamination during storage of carbonaceous chondrites prepared for micro FTIR measurements", Meteoritics & Planetary Science, **44**, 545-557, (2009).

[58] V. K. Pearson, M. A. Sephton, I. A. Franchi, J. M. Gibson, and I. Gilmour, "Carbon and nitrogen in carbonaceous chondrites: Elemental abundances and stable isotopic compositions", Meteoritics & Planetary Science, **41**, 1899-1918, (2006).

[59] P. I. Raynal, E. Quirico, J. Borg, D. Deboffle, P. Dumas, L. d'Hendecourt, J. P. Bibring, and Y. Langevin, "Synchrotron infrared microscopy of micron-sized extraterrestrial grains", Planetary and Space Science, **48**, 1329-1339, (2000).

[60] G. Matrajt, J. Borg, P. I. Raynal, Z. Djouadi, L. d'Hendecourt, G. Flynn, and D. Deboffle, "FTIR and Raman analyses of the Tagish Lake meteorite: Relationship with the aliphatic hydrocarbons observed in the Diffuse Interstellar Medium", Astronomy & Astrophysics, **416**, 983-990, (2004).

[61] S. A. Sandford and R. M. Walker, "Laboratory infrared transmission spectra of individual interplanetary dust particles from 2. 5 to 25 microns", Astrophysical Journal, **291**, (1985).

[62] L. P. Keller, S. Bajt, G. A. Baratta, J. Borg, J. P. Bradley, D. E. Brownlee, J. R. Brucato, M. J. Burchell, H. Busemann, L. Colangeli, L. D'Hendecourt, Z. Djouadi, G. Ferrini, G.

Flynn, I. A. Franchi, M. Fries, M. M. Grady, M. K. Gilles, A. Graham, F. Grossemy, A. Kearsley, G. Matrajt, K. Nakamura-Messanger, V. Mennella, L. R. Nittler, M. E. Palumbo, A. Rotundi, S. A. Sandford, C. J. Snead, F. J. Stadermann, A. Steele, P. Tsou, D. Wooden, and M. Zolensky, "Infrared spectroscopy of Comet 81P/Wild 2 samples returned by Stardust", Science, **314**, 1728–1731, (2006).

[63] A. Rotundi, G. A. Baratta, J. Borg, J. R. Brucato, H. Busemann, L. Colangeli, L. D'Hendecourt, Z. Djouadi, G. Ferrini, I. A. Franchi, M. Fries, F. Grossemy, L. P. Keller, V. Mennella, K. Nakamura, L. R. Nittler, M. E. Palumbo, S. A. Sandford, A. Steele, and B. Wopenka, "Combined micro-Raman, micro-infrared, and field emission scanning electron microscope analyses of comet 81P/Wild 2 particles collected by Stardust", Meteoritics & Planetary Science, **43**, 367-397, (2008).

[64] Y. Kebukawa, S. Nakashima, M. Ishikawa, K. Aizawa, T. Inoue, K. Nakamura-Messenger, and M. Zolensky, "Spatial distribution of organic matter in the Bells CM2 chondrite using near-field infrared microspectroscopy", Meteoritics & Planetary Science, **45**, 394-405, (2010).

[65] M. Yesiltas, C. J. Hirschmugl, and R. E. Peale, "In situ investigation of meteoritic organic-mineral relationships by high spatial resolution infrared spectroscopy", 76th Annual Meteoritical Society Meeting, (2013.)

[66] M. Yesiltas, C. J. Hirschmugl, and R. E. Peale, "Microspectroscopy of meteorites: Search for organic-mineral correlations", in LPI Contributions, (2013).

[67] C. J. Hirschmugl and K. M. Gough, "Fourier transform infrared spectrochemical imaging: Review of design and applications with a focal plane array and multiple beam synchrotron radiation source", Appl. Spectrosc., **66**, 475-491, (2012).

[68] M. J. Nasse, M. J. Walsh, E. C. Mattson, R. Reininger, A. Kajdacsy-Balla, V. Macias, R. Bhargava, and C. J. Hirschmugl, "High-resolution Fourier-transform infrared chemical imaging with multiple synchrotron beams", Nat Meth, **8**, 413-416, (2011).

[69] M. J. Nasse, E. C. Mattson, R. Reininger, T. Kubala, S. Janowski, Z. El-Bayyari, and C. J. Hirschmugl, "Multi-beam synchrotron infrared chemical imaging with high spatial resolution: Beamline realization and first reports on image restoration", Nuclear Instruments and Methods in Physics Research Section A: Accelerators, Spectrometers, Detectors and Associated Equipment, **649**, 172-176, (2011).

[70] M. J. Nasse, R. Reininger, T. Kubala, S. Janowski, and C. J. Hirschmugl, "Synchrotron infrared microspectroscopy imaging using a multi-element detector (IRMSI-MED) for diffraction-limited chemical imaging", Nuclear Instruments and Methods in Physics Research Section A: Accelerators, Spectrometers, Detectors and Associated Equipment, **582**, 107-110, (2007).

[71] M. C. Martin, C. Dabat-Blondeau, M. Unger, J. Sedlmair, D. Y. Parkinson, H. A. Bechtel, B. Illman, J. M. Castro, M. Keiluweit, D. Buschke, B. Ogle, M. J. Nasse, and C. J. Hirschmugl, "3D spectral imaging with synchrotron Fourier transform infrared spectro-microtomography", Nature Methods, **10**, 861-864, (2013).

[72] S. Merouane, Z. Djouadi, L. S. d'Hendecourt, B. Zanda, and J. Borg, "Hydrocarbon materials of likely interstellar origin from the Paris meteorite", The Astrophysical Journal, **756**, 154, (2012).

[73] A. Morlok and G. Libourel, "Aqueous alteration in CR chondrites: Meteorite parent body processes as analogue for long-term corrosion processes relevant for nuclear waste disposal", Geochimica et Cosmochimica Acta, **103**, 76-103, (2013).

[74] S. A. Sandford, M. Nuevo, G. J. Flynn, S. Wirick, "Mid-Infrared Study of Samples from Several Stones from the Sutter's Mill Meteorite", LPI Contributions, **1719**, 1663, (2013).

[75] K. Nakamura, S. Nakashima, S. Tomita, M. E. Zolensky, L. P. Keller, and K. Tomeoka, "Hollow organic globules in the Tagish Lake meteorite as possible products of primitive organic reactions", Geochimica Et Cosmochimica Acta, **67**, A325-A325, (2003).

[76] Y. Kebukawa, C. M. O. D. Alexander, and G. D. Cody, "Compositional diversity in insoluble organic matter in type 1, 2 and 3 chondrites as detected by infrared spectroscopy", Geochimica et Cosmochimica Acta, **75**, 3530-3541, (2011).

[77] R. T. Morrison and R. N. Boyd, "Organic Chemistry", 3rd ed. Allyn and Bacon, Inc., (1973)

[78] Y. J. Pendleton and L. J. Allamandola, "The organic refractory material in the diffuse interstellar medium: Mid-infrared spectroscopic constraints", The Astrophysical Journal Supplement Series, **138**, 75, (2002).

[79] Y. Kebukawa, S. Nakashima, and M. E. Zolensky, "Kinetics of organic matter degradation in the Murchison meteorite for the evaluation of parent-body temperature history", Meteoritics & Planetary Science, **45**, 99-113, (2010).

[80] K. D. Hopkins, "Basic statistics for the behavioral sciences", Englewood Cliffs, N.J.: Prentice-Hall, Inc., (1978)

[81] M. Igisu, Y. Ueno, M. Shimojima, S. Nakashima, S. M. Awramik, H. Ohta, and S. Maruyama, "Micro-FTIR spectroscopic signatures of bacterial lipids in proterozoic microfossils", Precambrian Research, **173**, 19-26, (2009).

[82] C. P. Marshall, E. J. Javaux, A. H. Knoll, and M. R. Walter, "Combined micro-Fourier transform infrared (FTIR) spectroscopy and micro-Raman spectroscopy of proterozoic

acritarchs: a new approach to palaeobiology", Precambrian Research, **138**, 208-224, (2005).

[83] G. J. Flynn, L. P. Keller, M. Feser, S. Wirick, and C. Jacobsen, "The origin of organic matter in the solar system: evidence from the interplanetary dust particles", Geochimica et Cosmochimica Acta, **67**, 4791-4806, (2003).

[84] S. A. Sandford, L. J. Allamandola, A. G. G. M. Tielens, K. Sellgren, M. Tapia, and Y. Pendleton, "The interstellar CH stretching band near 3.4 microns-Constraints on the composition of organic material in the diffuse interstellar medium", The Astrophysical Journal, **371**, 607-620, (1991).

[85] Y. J. Pendleton, S. A. Sandford, L. J. Allamandola, A. G. G. M. Tielens, and K. Sellgren, "Near-infrared absorption spectroscopy of interstellar hydrocarbon grains", The Astrophysical Journal, **437**, 683-696, (1994).

[86] H. Busemann, C. M. O. D. Alexander, and L. R. Nittler, "Characterization of insoluble organic matter in primitive meteorites by microRaman spectroscopy", Meteoritics and Planetary Science, **42**, 1387-1416, (2007).

[87] C. Floss, F. Stadermann, "High abundances of circumstellar and interstellar C-anomalous phases in the primitive CR3 chondrites QUE 99177 and MET 00426", The Astrophysical Journal, **697,** 1242-1255, (2009)

[88] G. Matrajt, G. J. Flynn, D. Brownlee, D. Joswiak, and S. Bajt, "The origin of the 3.4 μm feature in Wild 2 cometary particles and in ultracarbonaceous interplanetary dust particles", The Astrophysical Journal, **765**, 145, (2013)

[89] G. J. Flynn, S. Wirick, L. P., Keller, and C. Jacobsen, "Modification of the Murchison insoluble organic matter (IOM) by acid extraction", LPI Contributions, **1538**, 5162, (2010).

[90] G. Matrajt, G. M. Muñoz Caro, E. Dartois, L. d'Hendecourt, D. Deboffle, and J. Borg, "FTIR analysis of the organics in IDPs: Comparison with the IR spectra of the diffuse interstellar medium", Astronomy and Astrophysics, **433**, 979-995, (2005).

[91] S. A. Sandford, "Infrared transmission spectra from 2.5 to 25 μm of various meteorite classes", Icarus, **60**, 115-126, (1984).

[92] Z. Martins, J. S. Watson, M. A. Sephton, O. Botta, P. Ehrenfreund, and I. Gilmour, "Free dicarboxylic and aromatic acids in the carbonaceous chondrites Murchison and Orgueil", Meteoritics and Planetary Science, **41**, 1073-1080, (2006).

[93] M. Zolensky, T. Mikouchi, M. Fries, R. Bodnar, P. Jenniskens, Q-Z. Yin, K. Hagiya, K. Ohsumi, M. Komatsu, M. Colbert, T. Nakamura, M. Matsuoka, S. Sasaki, A. Tsuchiyama, M. Gounelle, L. Le, J. Martinez, and K. Ross, "Mineralogy and petrography of C asteroid regolith: The Sutter's Mill", Meteoritics and Planetary Science, **49**, (2014).

[94] G. D. Cody, C. M. O. D. Alexander, H. Yabuta, A. L. D. Kilcoyne, T. Araki, H. Ade, P. Dera, M. Fogel, B. Militzer, and B. O. Mysen, "Organic thermometry for chondritic parent bodies", E&PSL, **272**, 446–455, (2008).

[95] M. Nuevo, S. A. Sandford, G. J. Flynn, and S. Wirick, "Mid-IR study of stones from the Sutter's Mill meteorite", Meteoritics and Planetary Science, 49, (2014).

[96] S. A. Sandford, M. Nuevo, G. J. Flynn, and S. Wirick, "Mid-Infrared Study of Samples from Several Stones from the Sutter's Mill Meteorite", LPI Contributions, **1719**, 1663, (2013).

[97] A. S. Burton, D. P. Glavin, J. E. Elsila, J. P. Dworkin, P. Jenniskens, and Q-Z. Yin, "The amino acid composition of the Sutter's Mill CM2 carbonaceous chondrite", Meteoritics & Planetary Science, **49**, (2014).

[98] A. Suzuki, Y. Yamanoi, T. Nakamura, and S. Nakashima, "Micro-spectroscopic characterization of organic and hydrous components in weathered Antarctic micrometeorites", Earth Planets and Space, **62**, 33–46, (2010).

[99] M. Fries, R. Matson, J. Schaefer, J. Fries, V. Reddy, L. Lecorre, and M. Hankey, "Detection and rapid recovery of the Sutter's Mill meteorite as a model for future recoveries worldwide", Meteoritics & Planetary Science, **49**, (2014).

[100] J. W. Salisbury, L. S. Walter, N. Vergo, and D. M. D'Aria, "Infrared (2.1-25 μm) spectra of minerals", Baltimore:John Hopkins University Press, 267 pp, (1991).

[101] T. Osawa, H. Kagi, T. Nakamura, and T. Noguchi, "Infrared spectroscopic taxonomy for carbonaceous chondrites from speciation of hydrous components", Meteoritics and Planetary Science, **40**, 71–86, (2005).

[102] Y. Kebukawa, S. Nakashima, K. Nakamura-Messenger, and M. E. Zolensky, "Submicron distribution of organic matter of carbonaceous chondrite using near-field infrared microspectroscopy", Chemistry Letters, **38**, 22–23, (2009b).

[103] T. Nakamura, "Post-hydration thermal metamorphism of carbonaceous chondrites", J. Mineral. Petrol. Sci., **100**, 260–272, (2005).

[104] A. Nakato, T. Nakamura, F. Kitajima, and T. Noguchi, "Evaluation of dehydration

mechanism during heating of hydrous asteroids based on mineralogical and chemical analysis of naturally and experimentally heated CM chondrites", Earth Planets Space, **60**, 855–864, (2008).

[105] D. Takir, J. P. Emery, H. Y. McSween, C. A. Hibbitts, R. N. Clark, N. Pearson, and A. Wang, "Nature and degree of aqueous alteration in CM and CI carbonaceous chondrites", Meteoritics and Planetary Science, **48,** 1618-1637, (2013).

[106] G. J. Flynn, S. Wirick, S. A. Sandford, and M. Nuevo, "Infrared analyses of minerals and organics in the Sutter's Mill meteorite", 44th Lunar and Planetary Science Conference, . (abstract #1595), (2013).

[107] V. K. Pearson, A. T. Kearsley, M. A. Sephton, and I. Gilmour, "The labelling of meteoritic organic material using osmium tetroxide vapour impregnation", Planetary and Space Science, **55**, 1310–1318, (2007).

[108] S. A. Sandford, J. Aléon, C. M. O. D. Alexander, T. Araki, S. A. Bajt, G. A. Baratta, J. Borg, J. P. Bradley, D. E. Brownlee, and J. R. Brucato, "Organics captured from comet 81P/Wild 2 by the Stardust spacecraft", Science, **314**, 1720–1724, (2006).

[109] S. Pizzarello, S. K. Davidowski, G. P. Holland, and L. B. Williams, "Processing of meteoritic organic materials as a possible analog of early molecular evolution in planetary environments", Proceedings of the National Academy of Sciences, **110**, 15614-15619, (2013).

[110] H. Haack, R. Michelsen, G. Stober, D. Keuer, and W. Singer, "The Maribo CM2 fall: Radar based orbit determination of an unusually fast fireball", Meteoritics and Planetary Science, **73**, 5085, (2010).

[111] J. M. Trigo-Rodriguez and J. Blum, "The Effect of Aqueous Alteration and

Metamorphism in the Survival of Presolar Silicate Grains in Chondrites", Publications of the Astronomical Society of Australia, **26**, 289-296, (2009).

[112] P. Ehrenfreund, F. Robert, L. d'Hendecourt, and F. Behar, "Comparison of interstellar and meteoritic organic matter at 3.4 microns", Astronomy and Astrophysics, **252**, 712-717, (1991).

[113] J. Akai, "T-T-T diagram of serpentine and saponite, and estimation of metamorphic heating degree of Antarctic carbonaceous chondrites", Proceedings of the NIPR Symposium on Antarctic Meteorites, **5**: 120-135, (1992).

[114] G. R. Huss, A. E. Rubin, and J. N. Grossman, "Thermal metamorphism in chondrites", In Meteorites and the early solar system II, edited by D. S. Lauretta, L. A. Leshin, and H. Y. McSween, Tucson, AZ: The University of Arizona Press, pp. 567–586, (2006).

[115] C. M. O. D. Alexander, G. D. Cody, Y. Kebukawa, R. Bowden, M. L. Fogel, A. L. D. Kilcoyne, L. R. Nittler, and C. D. K. Herd, "Elemental, isotopic, and structural changes in Tagish Lake insoluble organic matter produced by parent body processes", Meteoritics & Planetary Science, **49**:503-525, (2014).

[116] M. Yesiltas, Y. Kebukawa, R. E. Peale, E. Mattson, C. J. Hirschmugl, and P. Jenniskens, "Infrared imaging spectroscopy with micron resolution of Sutter's Mill meteorite grains", Meteoritics & Planetary Science, **49**:2027-2037, (2014).

[117] S. S. Russell, J. Zipfel, J. N. Grossman, and M. M. Grady, Meteoritics and Planetary Science, **37**, A157, (2002).

[118] S. Messenger, L. P. Keller, F. J. Stadermann, R. M. Walker, and E. Zinner, "Samples of Stars Beyond the Solar System: Silicate Grains in Interplanetary Dust", Science,

300:105-108, (2003).

[119] X. Zhao, C. Floss, Y. Lin, and M. Bose, "Stardust Investigation into the CR Chondrite Grove Mountain 021710", The Astrophysical Journal, **769**:49, (2013).

[120] A. Brearley, "The action of water", In Meteorites and the Early Solar System II (Eds Dante Lauretta, H.Y. McSween Jr), Arizona University Press, pp. 587-624, (2006).

[121] M. R. M. Izawa, M. A. Craig, and E. A. Cloutis, "Spectral variations in the Tagish Lake carbonaceous chondrite in the ultraviolet, visible, and near-infrared", 44th LPSC 2013, 3019.pdf